Helical Magnetorotational Instability in MHD Taylor-Couette Flow

Jacek T. Szklarski

Thesis submitted in Partial Fulfillment
of the Requirements for the Degree of
Doctor of Philosophy in Physics

University of Potsdam
Astrophysikalisches Institut Potsdam
Helmholtz Institute for Supercomputational Physics

August 2007

Elektronisch veröffentlicht auf dem
Publikationsserver der Universität Potsdam:
http://opus.kobv.de/ubp/volltexte/2008/1600/
urn:nbn:de:kobv:517-opus-16002
[http://nbn-resolving.de/urn:nbn:de:kobv:517-opus-16002]

In memory of Marek Szklarski

Abstract

Magnetorotational instability (MRI) is one of the most important and most common instabilities in astrophysics. Today it is widely accepted that it serves as a major source of turbulent viscosity in accretion disks, the most energy efficient objects in the universe.

The importance of the MRI for astrophysics has been realized only in recent fifteen years. However, originally it was discovered much earlier, in 1959, in a very different context. Theoretical flow of a conducting liquid confined between differentially rotating cylinders in the presence of an external magnetic field was analyzed. The central conclusion is that the additional magnetic field parallel to the axis of rotation can destabilize otherwise stable flow. Theory of non-magnetized fluid motion between rotating cylinders has much longer history, though. It has been studied already in 1888 and today such setup is usually referred as a Taylor-Couette flow.

To prove experimentally the existence of MRI in a magnetized Taylor-Couette flow is a demanding task and different MHD groups around the world try to achieve it. The main problem lies in the fact that laboratory liquid metals which are used in such experiments are characterized by small magnetic Prandtl number. Consequently rotation rates of the cylinders must be extremely large and vast amount of technical problems emerge. One of the most important difficulties is an influence of plates enclosing the cylinders in any experiment. For fast rotation the plates tend to dominate the whole flow and the MRI can not be observed.

In this thesis we discuss a special helical configuration of the applied magnetic field which allows the critical rotation rates to be much smaller. If only the axial magnetic field is present, the cylinders must rotate with angular velocities corresponding to Reynolds numbers of order $\mathrm{Re} \approx 10^6$. With the helical field this number is dramatically reduced to $\mathrm{Re} \approx 10^3$. The azimuthal component of the magnetic field can be easily generated by letting an electric current through the axis of rotation,

In a Taylor-Couette flow the (primary) instability manifests itself as Taylor vortices. The specific geometry of the helical magnetic field leads to a traveling wave solution and the vortices are drifting in a direction determined by rotation and the magnetic field. In an idealized study for infinitely long cylinders this is not a problem. However, if the cylinders have finite length and are bounded vertically by the plates the situation is different.

In this dissertation it is shown, with use of numerical methods, that the traveling wave solution also exists for MHD Taylor-Couette flow at finite aspect ratio H/D, H being height of the cylinders, D width of the gap between them. The nonlinear simulations provide amplitudes of fluid velocity which are helpful in designing an experiment. Although the plates disturb the flow, parameters like the drift velocity indicate that the helical MRI operates in this case.

The idea of the helical MRI was implemented in a very recent experiment PROMISE. The results provided, for the first time, an evidence that the (helical) MRI indeed exists. Nevertheless, the influence of the vertical endplates was evident and the experiment can be, in principle, improved. Exemplary methods of reduction of the end-effect are here proposed.

Near the vertical boundaries develops an Ekman-Hartmann layer. Study of this layer for the MHD Taylor-Couette system as well as its impact on the global flow properties is presented. It is shown that the plates, especially if they are conducting, can disturb the flow far more then previously thought also for relatively slow rotation rates.

Zusammenfassung

Die magnetische Scherinstabilitaet (engl. MRI) ist eine sehr häufig in der Astrophysik anzutreffende Instabilität. Es wird heute weithin angenommen, dass sie die Ursache für die turbulente Viskosität in Akkretionsscheiben ist, den Objekten mit der höchsten Energieeffizienz im Kosmos.

Die Bedeutung der MRI ist erst in den letzten fünfzehn Jahren klargeworden. Entdeckt wurde sie jedoch schon viel früher, im Jahre 1959 in einem völlig anderen physikalischen Kontext. Die Strömung in einer leitfähigen Flüssigkeit zwischen differentiell rotierenden Zylindern unter dem Einfluss eines externen Magnetfeldes wurde theoretisch untersucht. Die Schlussfolgerung war, dass das zugesetzte Magnetfeld eine sonst stabile Strömung destabilisieren kann. Die Geschichte der Theorie von Strömungen zwischen Zylindern reicht bis ins Jahr 1888 zurück. Heute wird ein solcher Aufbau üblicherweise als Taylor-Couette-Strömung bezeichnet.

Ein System rotierender Zylinder, zwischen denen sich flüssiges Metall befindet, war Gegenstand des kürzlich durchgeführten Experiments PROMISE. Die Ergebnisse belegen zum ersten Mal experimentell die Existenz der MRI. Um die notwendigen Drehzahlen gering zu halten, wurde ein spezielles, helikales Magnetfeld angelegt.

Gegenstand dieser Dissertation ist die theoretische Behandlung der magnetohydrodynamischen Taylor-Couette-Strömung, ähnlich der des Experiments PROMISE. Insbesondere der Einfluss der vertikalen Ränder (Deckel) wird untersucht. Es wird gezeigt, dass die MRI auch in Zylindern mit endlicher Höhe und mit begrenzenden Deckeln einsetzt.

In der Nähe der vertikalen Ränder bildet sich eine Ekman-Hartmann-Schicht. Die Untersuchung dieser Schicht im Zusammenhang mit dem MHD-Taylor-Couette-System sowie ihr Einfluss auf die globalen Strömungseigenschaften werden vorgestellt. Es wird gezeigt, dass die Deckel - insbesondere wenn sie elektrisch leitend sind - die Strömung stärker beeinflussen können als bisher angenommen, selbst bei den geringen Drehzahlen. Es werden Methoden zur Verringerung dieser unerwünschten Effekte vorgeschlagen.

Contents

Chapter 1

Introduction

The remoteness and scale of astronomical systems preclude the possibility of any attempt to control them. For most types of astrophysical objects long timescales make theirs evolution unobservable. Therefore, unlike a classical physicist, an astronomer usually is forced to work with a ,,snap-shot" of reality. Consequently astrophysicists must have developed a research strategy which significantly differs from strategies used by, for example, atomic physicists or biochemists. Based on physical assumptions, a model is created and then its predictions are compared with the observed ,,snap-shot" reflecting complex features of our universe. Therefore it is not common but very exiting when a fundamental astrophysical process can be directly observed in action under controlled laboratory conditions down on the Earth.

Naturally in order to model such process one has to design a proper experimental setup which resembles physics involved on astrophysical scales. An interesting example is a recent ,,Riga dynamo experiment" (Gailitis et al., 2000, 2001) which demonstrated a phenomena well known in theory as cosmic dynamo (Ponomarenko, 1973; Krause and Rädler, 1980; Dobler et al., 2002). Using a facility which was able to spirally rotate liquid sodium at temperature about $250\,^{\circ}\mathrm{C}$ with velocity of order of 15 m/s, it has been shown that initially weak magnetic field is amplified and the expected exponential growth of non-axisymmetric mode $m = 1$ has been reported.

The subject of this thesis is theory connected with an another recent experiment, PROMISE – Potsdam-ROssendorf Magnetic InStability Experiment. As stated in the acronym, the aim of the experiment was to model an astrophysical process known as MagnetoRotational Instability – MRI. It is widely accepted that MRI plays a crucial role in large class of astrophysical objects. In particular it serves as a source of turbulent viscosity in accretion disks – the most energy efficient objects in the universe.

1.1 Accretion disks and the MRI

Let us consider cloud of gas surrounding a compact, massive object. Since any gas particle certainly possesses some angular momentum it will not free-fall onto the central body but instead eventually it will settle on a circular orbit around the object. It will stay there unless energy and angular momentum will be extracted in which case it will spiral inwards. The spiraling matter tends to form an accretion[1] disk.

The accretion disk arise in variety of astrophysical conditions, along the most important classes are binary star systems or active galactic nuclei. Most of the stars are found in binary (or multiple) systems and it is common that they are both of different types. In such a binary system the star with higher mass will evolve faster and will eventually become a compact object,

[1] lat. *accretio* refers to the accumulation of matter onto a massive central body.

e.g. a neutron star or a black hole. The other companion can later expand so that its outer atmosphere reaches so called Roche lobe and its matter falls onto the compact object forming a disk.

Active galactic nuclei (AGN) and quasars (active nuclei of young galaxies) are the most spectacular forms of accretion disks. AGN is a compact region at the center of a galaxy which is characterized by enormous rate of emitted energy and it is the most luminous persistent sources in the universe. These objects are thought to be accretion disks formed around supermassive black holes.

Another important example are protoplanetary disks which surround T Tauri stars. These disks, formed from an interstellar medium (from which the central star was also formed), are the precursors of planetary systems.

Common feature for all the accretion disks is that theirs circular differential rotational profile is Keplerian[2]:

$$\Omega(r) = \sqrt{\frac{GM_*}{r^3}}, \tag{1.1}$$

r being distance from the central body with mass M_*. The amount of energy which can be emitted by an accretion disk from a gas with mass m is equal to the binding energy of the innermost orbit

$$E_{\rm accr} = \frac{GM_*m}{R_*}. \tag{1.2}$$

If the central object is more compact, i.e., has larger mass and smaller radius R_* then more energy can be extracted from any gas particle. We notice that this mechanism is far more efficient than, for example, nuclear burning. For a typical neutron star with $R_* \approx 10$ km and with solar mass $M_* = M_\odot$ from each gram of the infalling matter the generated energy is of order of 10^{20} erg. The typical nuclear burning hydrogen into helium gives $E_{\rm nuc} = 0.007mc^2$, so that each gram provides about 6×10^{18} erg of the radiated energy. On the other hand, for a less compact object like a white dwarf with solar mass, the efficiency of accretion is much less than from the burning.

A seminal work in the disk accretion theory has been performed by Shakura and Sunyaev (1973). The authors have developed equations governing a flow in a thin, steady, subsonic accretion disk surrounding a black hole. One of the most fruitful assumptions was to describe any physical mechanism responsible for extraction of the angular momentum form the infalling matter by a single dimensionless parameter α. There must exist a viscous process which allows the angular momentum to be transported outwards. Let us assume that the viscosity ν in such process is due to the turbulent motions of some kind

$$\nu \sim \mathcal{L}\,\mathcal{U}, \tag{1.3}$$

where $\mathcal{L}$ is the length scale of turbulent eddies, $\mathcal{U}$ the velocity scale. For accretion disks we may assume that those scales are smaller than height of the disk H and sound speed in the disk $c_{\rm s}$ respectively, so that

$$\nu = \alpha\, c_{\rm s}\, H, \qquad \alpha \leq 1. \tag{1.4}$$

[2]At least in regions where general relativity does not play significant role. At the inner edge of a disk around a black hole these effects become crucial. A simple treatment of the problem can be realized by applying so called pseudo-Newtonian potential. The simplest example of such potential is $\Phi = -GM/(r - r_g)$ where $r_g = GM/c^2$ is the Schwarzschild radius. It correctly resembles marginally stable and marginally bound orbits. A more exact solution, also for rotating black holes, has been proposed by e.g. Mukhopadhyay (2002)

Having this defined one can derive all important parameters (like thickness, time scale of evolution or emitted spectrum) characterizing the disk with given α and with given accretion rate $\dot{M}$. Nevertheless one can not make any quantitative predictions unless there is provided a physical explanation for nature of the turbulent, or any other, viscosity and therefore the α parameter.

In the first place the molecular viscosity, undoubtedly existing, is much too small to allow construction of an accretion disk with reasonable parameters and accretion rates.[3] The linear hydrodynamical instability can not operate since Rayleigh criterion (local)

$$\partial_r(r^2\Omega) \geq 0 \qquad \text{for stability} \tag{1.5}$$

is always fulfilled for the Keplerian rotation. The criterion states that the specific angular momentum $l = r^2\Omega$ must increase outwards for hydrodynamically stable flows.

Various other possible explanation for the apparent viscosity have been proposed, including transfer of angular momentum by magnetic stresses (already suggested by Shakura and Sunyaev, 1973), convective instability (Livio and Shaviv, 1977) or spiral waves. However, none of those propositions was widely accepted as a major, efficient mechanism providing the necessary viscosity and the subject became a long-standing challenge to the theory of accretion disks.

The explanation has been given in a work by Balbus and Hawley (1991). They have shown that for accretion disks there exists a very powerful, local shearing instability mediated by a weak magnetic field. The importance of magnetic fields has been recognized before but stability analyses were usually in gasdynamical character. Balbus & Hawley argued that even very small magnetic seed field cannot be ignored when considering linear disturbances and that the underlying instability is generally applicable and very effective.

The derived criterion for stability can be stated as

$$\partial_r\Omega^2 \geq 0 \qquad \text{for stability,} \tag{1.6}$$

so that if there exists a weak poloidal magnetic field component (not too strong though) and angular velocity decreases outwards the flow can become unstable. Since the above criterion is easily violated in astrophysical disks we expect that the MRI arise. The fastest growing wavenumbers have huge growth rates of order of 0.75Ω independently of the strength of the magnetic field. The wavelengths are much smaller then the height of the disk and therefore one expects turbulence to be developed.

The most important consequence of this instability is that it provides a convincing explanation for the transport of angular momentum in a differentially rotating medium. A simple quantitative picture of the phenomenon can be given as follows: consider an outwardly displaced fluid element in a disk embedded in a vertical magnetic field. There is a tendency that the magnetic field tries to enforce solid body rotation by resisting shearing, consequently the displaced element is forced to rotate too fast in its new position. When the restoring forces are unable to overcome this effect, the fluid element is driven away and the angular momentum is transported.

When considering what happens in nonlinear fully saturated state one has to perform numerical calculations. Local box simulations of the nonlinear development of the MRI reach state of magnetohydrodynamical turbulence (see e.g. Hawley et al., 1995; Brandenburg et al., 1995). It is characterized by anisotropic Reynolds and Maxwell stress tensors and the angular momentum is indeed transported outwards, while the turbulence is supported by shearing in the disk. More complex physics in the disks also have been studied, including radiation, stratification, Hall ef-

[3] For more details on basics of accretion disk theory and nature of the viscosity, the reader can refer to work by Pringle (1981).

fect or non-uniform conductivity. Global models of the disks also have been studied (e.g. Kersalé et al., 2004). For more information about transporting the angular momentum in accretion disks the reader can refer to reviews, Balbus and Hawley (1998); Balbus (2003).

It is not to be forgotten that the interaction of the gaseous medium with magnetic fields requires that the gas is a good conductor. Usually this condition is easily fulfilled since the gas is hot and well ionized. However, for cold protostellar disks it may not be the case since the conductivity is very small, of order 10^{-9} S/m (Brandenburg and Subramanian, 2005). Therefore one should consider other mechanisms governing such disks, for example Hall conductivity may be critical in this regime. Other, quite new and convincing explanation, is non-axisymmetric hydrodynamical instability for stratified disks (Dubrulle et al., 2005).

We also shall mention that the accretion disks are not the only astrophysical objects which are subject to MRI. The differential rotation and magnetic fields, two essential components necessary for MRI also exist for example in stars. It is possible for a star, unlike for a disk, to rotate as a solid body but, depending on the type of the star, it is likely that there exists a region with differential rotation. For example in the sun the solar interior rotates uniformly up to radius of $0.7R_{\odot}$. At this distance there exist a region called tachocline where the solid body rotation changes to a differential one which is characteristic for the solar outer envelope.

1.2 The MRI Experiment

It is surprising that while astrophysicists have been looking for the explanation of the mechanism for the angular momentum transport, thirty years before work by Balbus & Hawley a corresponding phenomenon has been already discussed. However, in a different contest.

Consider two concentric, independently rotating cylinders with the gap between them filled with a liquid, see Fig. 1.1. This setup has been experimentally studied by Couette (1888) and Mallock (1888). Although the system is conceptually very simple it provides amazingly reach variety of complex solutions and become a classical case for fluid dynamics.[4] In magnetohydrodynamics (MHD) there exists analogously defined problem where the fluid is assumed to be conducting and the cylinders are placed in an external magnetic field.

The stability of the classical Couette flow (or Taylor-Couette flow as it is often named) has been subject to intensive study, highlighted by landmark work by Taylor (1923). Prior to Taylor's results, Rayleigh (1917) has defined criterion (1.5) according to which the inviscid flow is always hydrodynamically stable if the cylinders rotate in such a way that the angular momentum increases with distance r from the axis of rotation.[5] For the MHD case it was work by Velikhov (1959) and later, with more general treatment, by Chandrasekhar (1960). They have shown that a conducting fluid with zero resistivity undergoing Couette flow with externally applied, vanishingly small magnetic field obeys precisely the criterion (1.6). Therefore in this limit a sufficient condition for stability is that angular velocity increases with r. The magnetized flow can be unstable whereas the purely hydrodynamical one is stable. However, even the unstable flow can be always stabilized with sufficiently strong magnetic field.

It is remarkable that the Rayleigh criterion is not recovered in the limit of small applied magnetic field. The origin of the instability lies in fact that in fluid with zero resistivity the lines of magnetic forces are permanently attached to the fluid (freezed-in), independently of strength of the applied field. The criterion is connected with presence of the field only, not its strength.

[4] This complexity is reflected in the number of papers concerning the subject. For example search for on-line issues of „Physics of Fluids" with the word „Couette" in abstract gives about 20.000 papers. Similarly the matter is popular among astrophysicists, Nasa's ADS system returns about 3.000 abstracts with the „Couette" word.

[5] More details on stability of the Couette flow will be presented in Chapter 2 of this thesis.

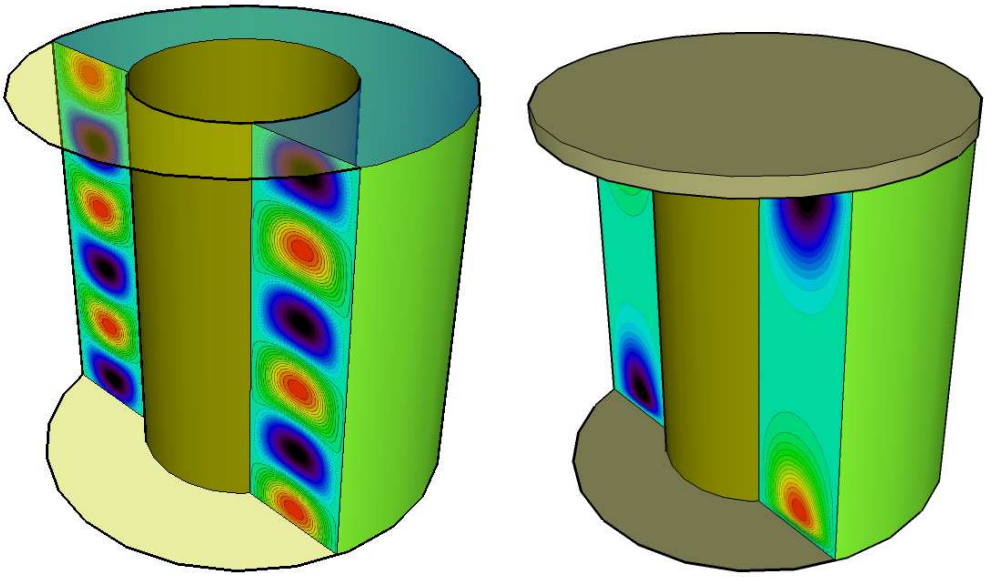

Figure 1.1: *Sketch of the Taylor-Couette flow. On the left side we see part of concentric, infinitely long cylinders filed with liquid in the gap between them. If rotation velocity of the both cylinders lies in a certain range, i.e., exceeds a critical value which depends on the problem geometry then* Taylor vortices *develop. Here these vortices are represented by contour lines of stream function ψ and a color map associated with value of ψ. In the incompressible flow the fluid tends to move along those contour lines, for reddish colors the movement is clockwise, for the bluish ones counter-clockwise. On the right side the cylinders are covered with rotating plates. The cylinder rotation rates do not exceed the critical value and therefore there are no Taylor vortices. However, due to imbalance in pressure close to the endplates there exists a circular motion – two Ekman vortices can be seen.*

The flow can be stabilized by applying magnetic field, its minimum strength for given conditions can be determined by considering an explicit solution and will be discussed later.

Only after Balbus & Hawley showed that a related process plays crucial role on astrophysical scales the Couette flow has gained significant attention among astrophysical community.[6] A clear link between MHD astrophysics and MHD experiment has been created. Proving in a laboratory that such very basic instability exists and directly study its properties become a challenge for different MHD groups along the world (see e.g. Rosner et al., 2004). In the last years interest of theoretical and experimental fluid dynamicists in MHD Taylor-Couette flow was somewhat renewed, it turned out that there exists new territory in the field to be explored. Doubtless a connection between the astrophysical theories and the laboratory experiments is very much appreciated.

Beside proving a physical theory there is one more, important point connected with such experiments which cannot be underestimated. Astrophysics is very complex, operates usually in highly nonlinear regime and on very broad range of length scales and time scales. It is understood that most of the modern results ultimately come from numerical simulations. Much of our understanding concerning astrophysical objects relies on accuracy of such calculations, proper treatment of boundary conditions, etc. There exists a need for testing astrophysical codes, used numerical methods and validating them against data collected from the experiments. Therefore

[6] However Balbus & Hawley were not the first ones to realize that the stability of MHD Couette flow can be considered in astrophysical theories. For example Fricke (1969) has investigated local stability of differential rotation in stars in the presence of magnetic fields. He realized that there exists a connection with Chandrasekhar's work but his results have gone unappreciated and in any way were not so directly related to angular momentum transport like in the work by Balbus & Hawley.

such laboratory experiments can assure us that the codes and the methods used to solve, for example, MHD equations are reasonable and one can trust that the calculated results indeed correspond to real physical mechanisms.

We should stress that, obviously, there exist considerable limitations in computational techniques. It is not possible to perform, e.g., fully nonlinear simulations of a global turbulent MHD Couette flow of a liquid with small conductivity. The different scales which are involved prohibit such calculations. Therefore the experiments are the only way to obtain certain classes of results, for example scaling of Reynolds stresses in turbulent flow for broad range of the rotation rates.

The magnetized Taylor-Couette flow is still considered as a good prototype for an MRI experiment. The main difficulty is that laboratory liquids have such conductivity and viscosity that it is difficult to excite MRI modes. Different groups have incorporated various approaches to the problem. For example a group from Princeton Plasma Physics Laboratory has constructed two cylinders with radii 7 cm and 20.3 cm with height of 28 cm, the cylinders can rotate with 4000 rpm and 533 rpm respectively, a vertical external magnetic field is applied (Ji et al., 2001). When such large rotation rates are involved there is a need for special treatment of the plates enclosing the rotating cylinders which is an engineering challenge, perhaps very difficult to overcome (this matter will be discussed later in the thesis). A different group works on dynamo and MRI experiment in New Mexico Institute of Mining and Technology (Noguchi et al., 2002). Theirs device is a bit larger but also must rotate very fast.

A novel configuration of an externally applied magnetic field was suggested by Hollerbach and Rüdiger (2005) and it led to a different experimental setup. It has been shown that if the axial field is replaced by a helical one the necessary rotation rates are much smaller, so it is much easier to built an appropriate device. Accordingly, the undesired effects generated by the plates covering the cylinders are less important however not negligible. Moreover there exists an additional frequency associated with this type of instability. This frequency can be easily measured and can serve as an important quantity parameter indicating the phenomena.

On these basis the PROMISE experiment has been proposed. The major theoretical part of the project has been done in AIP – Astrophysikalisches Institut Potsdam (Potsdam Institute for Astrophysics) and the experiment has been built and conducted in Forschungszentrum Dresden-Rossendorf (Research Center Dresden-Rossendorf). The PROMISE facility consists of two rotating cylinders with radii 4 cm and 8 cm, the gap between them is filed with the liquid alloy GaInSn. External coils produce the axial magnetic field of order 10 mT, an electric current let through the axis of rotation generates the azimuthal component. Two ultrasonic transducers measure vertical velocity fluctuations inside the fluid (for more information about the facility see Appendix A). The results from the first stage of the experiment, which have confirmed the existence of the magnetorotational instability with spiral magnetic fields, have been published in Stefani et al. (2006); Rüdiger et al. (2006); Stefani et al. (2007).

Results presented in thesis help to understand what is the influence of the plates covering the rotating cylinders. The plates are undoubtedly present in any real experiment. It also has been shown, for the first time, what are velocity amplitudes in a fully saturated nonlinear state, and how the developed traveling wave interacts with the vertical boundaries. The detailed study of the vertical hydromagnetic boundary layer has been presented.

1.3 Structure of the thesis

In this dissertation we will focus on solving incompressible MHD equations under specific boundary conditions relevant to a magnetized Couette flow with an externally applied spiral magnetic

field. Let us start with the Maxwell equations in SI units:

$$\partial_t \boldsymbol{B} = -\operatorname{rot} \boldsymbol{E}, \tag{1.7a}$$
$$\operatorname{div} \boldsymbol{B} = 0, \tag{1.7b}$$
$$\frac{1}{c^2}\partial_t \boldsymbol{E} = \operatorname{rot} \boldsymbol{B} - \mu_0 \boldsymbol{J}, \tag{1.7c}$$
$$\operatorname{div} \boldsymbol{E} = \rho_e \mu_0 c^2, \tag{1.7d}$$

where μ_0 is the magnetic permeability, ρ_e the electric charge density. The Ohm's law with the electric conductivity σ

$$\boldsymbol{J} = \sigma(\boldsymbol{E} + \boldsymbol{U} \times \boldsymbol{B}). \tag{1.8}$$

Assuming that time scale on which the electric field varies exceeds the Faraday time $\tau_\mathrm{f} = \eta/c^2$, $\eta \equiv 1/\mu_0\sigma$ being the magnetic diffusivity, we can safely neglect the displacement current (the condition is always met in the field of our interest). Therefore instead of (1.7c) we use the classical Ampère's law $\boldsymbol{J} = \operatorname{rot} \boldsymbol{B}/\mu_0$ and insert it into (1.7a) so we obtain (using the Ohm's law and the fact that $\operatorname{div} \boldsymbol{B} = 0$) the induction equation, Eq. (1.9c).

The dynamical equation for the velocity $\boldsymbol{u}$ is a typical Navier-Stokes equation supplemented by the Lorentz force, $\boldsymbol{J} \times \boldsymbol{B}$. From the assumption of incompressibility (which is fulfilled for laboratory liquid metals) and the equation of continuity $\partial_t \rho = -\operatorname{div}(\rho \boldsymbol{u})$ we obtain additional requirement that $\boldsymbol{u}$ is divergence free. So the full set of MHD equations to be solved can be written as

$$\partial_t \boldsymbol{u} + (\boldsymbol{u} \cdot \nabla)\boldsymbol{u} = -\frac{1}{\rho}\nabla p + \nu \nabla^2 \boldsymbol{u} + \frac{1}{\rho}\boldsymbol{J} \times \boldsymbol{B}, \tag{1.9a}$$
$$\operatorname{div} \boldsymbol{u} = 0, \tag{1.9b}$$
$$\partial_t \boldsymbol{B} = \eta \nabla^2 \boldsymbol{B} + \operatorname{rot}(\boldsymbol{u} \times \boldsymbol{B}), \tag{1.9c}$$
$$\operatorname{div} \boldsymbol{B} = 0, \tag{1.9d}$$

where ρ is the density, ν the kinematic viscosity. The set of Eqs. (1.9) together with boundary conditions related to Taylor-Couette setup fully define problem of our interest.

In Chapter 2 we discuss the stability of MHD Taylor-Couette flows and present a numerical method used to solve the above set of equations in the limit of highly resistive flows. The method is capable of solving axisymmetric flows with periodic vertical boundary conditions (i.e., analogously to infinitely long cylinders which is a usual assumption in a linear analysis) or finite ones (which corresponds to cylinders enclosed by endplates; the plates can have different mechanical and magnetic properties).

Chapter 3 discusses in more details the case when an external spiral magnetic field is applied to the flow for both periodic and finite cylinders. We present study of the traveling wave in the nonlinearly saturated state. It is also shown that the torque at the walls is increased so that the angular momentum is indeed transported outwards. The problems due to endplates are pointed out.

In the PROMISE experiment the both endplates had different rotational and magnetic properties. This led to additional problems which are addressed in Chapters 3 and 4. In Chapter 4 we propose a simple method of reducing the influence of the plates and present how this would improve the experiment.

More detailed study of the vertical boundary layers for the flow with the external axial magnetic field is presented in Chapter 5. It is shown that there exists an electric Hartmann current which interacts with the magnetic field which leads to a different class of flows, namely Taylor-Dean flows. Linear stability of this flow is also analyzed.

Results presented in this thesis were used in the following, published papers: Stefani et al. (2006); Szklarski and Rüdiger (2006); Stefani et al. (2007); Szklarski (2007) and one submitted: Szklarski and Rüdiger (2007).

Chapter 2

MHD Taylor-Couette flow Numerical formulation

2.1 Introduction

Motion of an incompressible, viscous fluid confined between two rotating, coaxial cylinders has been originally investigated by Couette (1888) and Mallock (1888). This system has been subject of a seminal paper by Taylor (1923). Prior to the Taylor's work many attempts were made to predict instability of a solution to the equations of hydrodynamics of viscous fluids. However, none of them succeeded which lead to confusion concerning applicability of Navier-Stokes equations. Taylor has shown that the methods for stability calculations as well as the assumed boundary conditions give results which exactly match experimental data. His work was extraordinary from the theoretical as well as the experimental point of view.

The system of rotating cylinders very well suits for a quantitative comparison between the theory and the experiment. Slow and slight increase in rotation rates gives rise to more complex fluid states. The first transition, primary instability, occurs when the homogeneous flow with zero z, r components of velocity and ϕ component matching parabolic Couette solution breaks down into Taylor vortices. Then, depending on the rotation rates of the both cylinders, one can observe various flow stages: traveling, modulated waves, dominating non-axisymmetric disturbances, spiral or featureless turbulence and more, see Fig. 2.1, for a review see e.g. Tagg (1994).

The Taylor-Couette flow can also be realized in short cylinders, i.e., when ratio of the gap width D to the height H becomes an additional parameter $\Gamma \equiv H/D$ and endplates which enclose cylinders drive secondary flow. The enclosed system is characterized by multiplicity of solution and is an excellent subject to the bifurcation theory – there exist non-unique solutions for the same boundary conditions, so which state sets in depends on history of the parameters. One of the peculiar solutions are anomalous modes. In this state one large vortex filling almost the entire gap can be observed and four counter rotating to it, smaller ones, placed in the corners (Youd and Barenghi, 2006).

When the liquid is replaced by a conducting fluid and an external magnetic field is applied additional body force acting on the fluid arises. This leads to a new family of problems – magnetohydrodynamical Taylor-Couette flows. Properties of such flows depend on strength and geometry of the applied field, magnetic properties of the cylinders and the endplates and, naturally, magnetic properties of the liquid (e.g. Willis and Barenghi, 2002a).

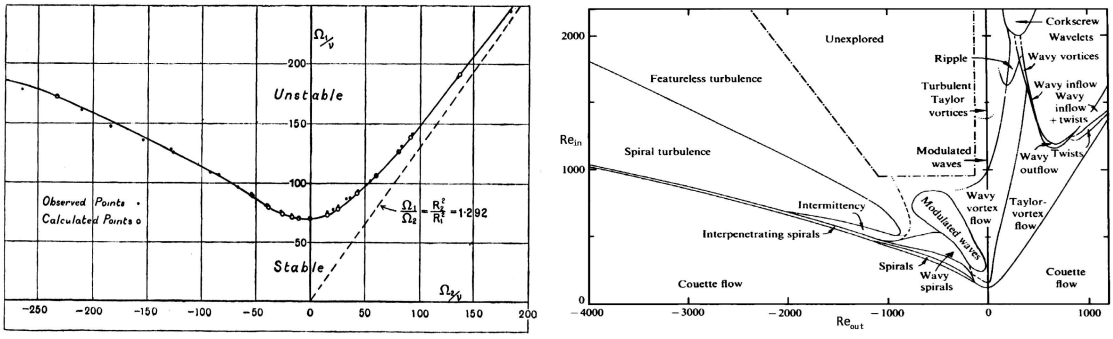

Figure 2.1: Left: *line indicating onset of stability, after Taylor (1923). Horizontal/vertical axis represent rotation rates of the outer/inner cylinder, open points represent experimental results, filled points theoretical calculation, the dashed line is the Rayleigh criterion. We notice that there are more experimental than theoretical data which is unusual in today's physics. However, back in 1923 computing values of all the integrals was very time consuming.* Right: *Phase diagram for experimental setup with $\hat{\eta} = 0.883, \Gamma = 30$, after Andereck et al. (1986).*

In this chapter we will discuss equations governing the MHD Taylor-Couette flow along with the appropriate boundary conditions and a brief description of numerical methods which are used to solve them. Important features concerning stability of such flows are pointed out.

2.2 The equations

A sketch of the Taylor-Couette flow is depicted in Fig. 2.2. Two concentric cylinders have radii $R_{\rm in}, R_{\rm out}$ and they rotate with $\Omega_{\rm in}, \Omega_{\rm out}$, the rotation ratio is defined as

$$\hat{\mu} \equiv \Omega_{\rm out}/\Omega_{\rm in}. \tag{2.1}$$

We will consider two distinct classes of the problem: infinite cylinders $\Gamma = H/D \to \infty$ and finite ones $\Gamma = 10$ (unless explicitly stated otherwise), for the latter different rotational properties of the endplates will be applied. The gap ratio is

$$\hat{\eta} \equiv R_{\rm in}/R_{\rm out}, \tag{2.2}$$

through this work we use $\hat{\eta} = 1/2$.

The fluid confined between the cylinders is a liquid metal and is assumed to be incompressible, conducting, with the kinematic viscosity ν, the density ρ, the magnetic diffusivity η, μ_0 is the magnetic permeability.

We now start with classical equations of magnetohydrodynamics (for complete derivation see e.g. Chandrasekhar, 1961). The momentum equation with the Lorentz force:

$$\partial_t \boldsymbol{u} + (\boldsymbol{u}\cdot\nabla)\boldsymbol{u} = -\frac{1}{\rho}\nabla p + \nu\nabla^2\boldsymbol{u} + \frac{1}{\mu_0\rho}(\mathrm{rot}\,\boldsymbol{B})\times\boldsymbol{B}, \tag{2.3a}$$

the induction equation

$$\partial_t \boldsymbol{B} = \eta\nabla^2\boldsymbol{B} + \mathrm{rot}(\boldsymbol{u}\times\boldsymbol{B}), \tag{2.3b}$$

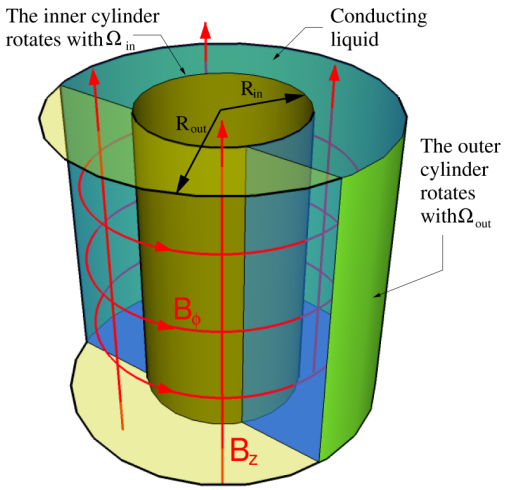

Figure 2.2: *The geometry of the problem – two concentric cylinders with radii $R_{\rm in} = 4$ cm, $R_{\rm out} = 8$ cm rotating with $\Omega_{\rm in}$, $\Omega_{\rm out}$. B_z and B_ϕ are the external magnetic fields. B_ϕ is induced by an axial current flowing through a rod placed along the axis of rotation. In the PROMISE experiment cylinders have length of H =40cm (Γ=10) and are covered with endplates. The liquid is a mixture of gallium, indium and tin.*

from the equation of continuity for an incompressible flow it follows that the velocity field $\boldsymbol{u}$ must be solenoidal as is, of course, the magnetic field $\boldsymbol{B}$

$$\begin{aligned} \operatorname{div} \boldsymbol{u} &= 0, && \text{(2.3c)} \\ \operatorname{div} \boldsymbol{B} &= 0. && \text{(2.3d)} \end{aligned}$$

The cylinders are embedded in an externally applied magnetic filed $\boldsymbol{B_0}$. We work in the cylindrical coordinates (r, ϕ, z) with the unit vectors $\hat{\mathbf{e}}_r, \hat{\mathbf{e}}_\phi, \hat{\mathbf{e}}_z$. The most general form of the field, which is steady and current free, considered in this thesis is

$$\boldsymbol{B_0} = B_0 \left(\frac{\beta R_{\rm in}}{r} \hat{\mathbf{e}}_\phi + \hat{\mathbf{e}}_z \right), \tag{2.4}$$

where the parameter β denotes ratio of the azimuthal field to the constant axial field $B_0 \hat{\mathbf{e}}_z$ at the inner cylinder.

We transform the equations (2.3) to theirs non-dimensional form with use of the following scales: $D \equiv R_{\rm out} - R_{\rm in}$ as the unit of length, ν/D as the unit of velocity, D^2/ν as the unit of time and B_0 as the unit of magnetic field. This is done by multiplying (2.3a) by D^3/ν^2 and (2.3b) by $D^2/B_0\nu$.

Let $\boldsymbol{B} = \boldsymbol{B'} + \boldsymbol{B_0}$, since $\operatorname{rot} \boldsymbol{B_0} = 0$, $\nabla^2 \boldsymbol{B_0} = 0$ we obtain the dimensionless MHD equations for the problem of our interest. After omitting the primes:

$$\begin{aligned} \partial_t \boldsymbol{u} + (\boldsymbol{u} \cdot \nabla)\boldsymbol{u} &= -\nabla p + \nabla^2 \boldsymbol{u} + \frac{\mathrm{Ha}^2}{\mathrm{Pm}} \left[(\operatorname{rot} \boldsymbol{B}) \times \boldsymbol{B} + (\operatorname{rot} \boldsymbol{B}) \times \boldsymbol{B_0}/B_0 \right], && \text{(2.5a)} \\ \partial_t \boldsymbol{B} &= \frac{1}{\mathrm{Pm}} \nabla^2 \boldsymbol{B} + \operatorname{rot}(\boldsymbol{u} \times \boldsymbol{B}) + \operatorname{rot}(\boldsymbol{u} \times \boldsymbol{B_0}/B_0), && \text{(2.5b)} \\ \operatorname{div} \boldsymbol{u} &= 0, && \text{(2.5c)} \\ \operatorname{div} \boldsymbol{B} &= 0, && \text{(2.5d)} \end{aligned}$$

with

$$\mathrm{Ha} \equiv B_0 \sqrt{\frac{D^2}{\mu_0 \rho \nu \eta}}, \quad \mathrm{Pm} \equiv \frac{\nu}{\eta}, \tag{2.6}$$

where Ha is the Hartmann number, Pm is the magnetic Prandtl number.

The basic, undisturbed rotational profile for the MHD Taylor-Couette flow between *infinitely long* cylinders governed by equations (2.5) is (see e.g. Chandrasekhar, 1961)

$$\Omega_0(r) = a + \frac{b}{r^2}, \tag{2.7}$$

where

$$a = \Omega_{\mathrm{in}} \frac{\hat{\mu} - \hat{\eta}^2}{1 - \hat{\eta}^2} \qquad b = \frac{1 - \hat{\mu}}{1 - \hat{\eta}^2} R_{\mathrm{in}}^2 \Omega_{\mathrm{in}}, \tag{2.8}$$

and $u_r = u_z = 0$ everywhere. Sometimes we will refer to field $\boldsymbol{\Omega}_0 \equiv \Omega_0 \hat{\mathbf{e}}_\phi$.

We will introduce another dimensionless parameter associated with the problem, namely the Reynolds number Re which is defined as

$$\mathrm{Re} \equiv \frac{\Omega_{\mathrm{in}} R_{\mathrm{in}} D}{\nu}. \tag{2.9}$$

The Reynolds number measures ratio of the inertial to the viscous forces. Notice that Re is prescribed by the boundary conditions, i.e., the rotational speed of the inner cylinder, and in our non-dimensional formulation if $R_{\mathrm{in}} = D$ (i.e. $\hat{\eta} = 0.5$) then it is equal to Ω_{in}. Sometimes it may be convenient to analogously define another Reynolds number related to the rotation of the outer cylinder.

For laboratory liquids conductivity σ is very small so that the magnetic diffusivity $\eta \equiv 1/\mu_0\sigma$ is very large (compared to the viscosity) and therefore the corresponding magnetic Prandtl number Pm is small, see Table 2.1. Consequently the time scale for magnetic diffusion is much shorter than other time scales. We consider the limit $\eta \to \infty$, however it must be supposed that Ha tends to a finite value. Let

$$\boldsymbol{B} = \boldsymbol{B_0} + \boldsymbol{b}, \tag{2.10}$$

perturbations $\boldsymbol{b}$ of the externally applied field induced by the motion of the fluid are Pm times smaller than $\boldsymbol{B_0}$, although theirs effect on the Lorentz force can not be neglected since $\mathrm{Ha}^2/\mathrm{Pm}[(\mathrm{rot}\,\boldsymbol{b}) \times \boldsymbol{B_0}/B_0]$ is already of order of Ha. Nevertheless the interactions $(\mathrm{rot}\,\boldsymbol{b}) \times \boldsymbol{b}$ are vanishingly small.

Similarly in the induction equation we may apply a quasi-static approximation, so that the electromagnetic field proceeds along a sequence of steady-state solutions of the Maxwell equations to conditions described by $\boldsymbol{u}$. Therefore $\boldsymbol{b}$ in each moment adjusts instantaneously to the velocity $\boldsymbol{u}$. Consequently in the small Prandtl limit $\mathrm{Pm} \to 0$, the system (2.5) for the perturbations $\boldsymbol{b}$ of the external field $\boldsymbol{B_0}$ (2.4) can be written as

Table 2.1: *Physical properties of liquid metals which are suitable for the MRI experiment. The star * denotes the PROMISE mixture.*

	ρ [g/cm^3]	ν [cm^2/s]	η [cm^2/s]	Pm
sodium	0.9	$7.1\ 10^{-3}$	$0.8\ 10^{3}$	$0.9\ 10^{-5}$
gallium	6.0	$3.2\ 10^{-3}$	$2.1\ 10^{3}$	$1.5\ 10^{-6}$
GaInSn*	6.4	$3.4\ 10^{-3}$	$2.4\ 10^{3}$	$1.4\ 10^{-6}$

$$\partial_t \boldsymbol{u} + (\boldsymbol{u}\cdot\nabla)\boldsymbol{u} = -\nabla p + \nabla^2\boldsymbol{u} + \mathrm{Ha}^2(\nabla\times\boldsymbol{b})\times\boldsymbol{B_0}/B_0, \tag{2.11a}$$

$$\nabla^2\boldsymbol{b} = -\nabla\times(\boldsymbol{u}\times\boldsymbol{B_0}/B_0), \tag{2.11b}$$

$$\mathrm{div}\,\boldsymbol{u} = 0, \tag{2.11c}$$

$$\mathrm{div}\,\boldsymbol{b} = 0. \tag{2.11d}$$

The MHD Taylor-Couette flow governed by the above system is the main subject of this thesis and will be numerically solved with method described in Section 2.4. However, solutions of the equations in theirs more general form (2.5) will be also discussed (for more information about the small Prandtl number limit the reader can refer to e.g. Roberts, 1967; Zikanov and Thess, 1998; Youd and Barenghi, 2006).

All the numerical calculations are done using the dimensionless equations and consequently all the figures presented in the thesis reflect non-dimensional quantities, unless the physical units are explicitly mentioned. If the physical units are present, the equations has been scaled according to the physical properties of the PROMISE facility, for the length scale, the viscosity, the magnetic diffusivity, etc.

2.3 Stability of the Taylor-Couette flow

In this section we will shortly discuss stability of the classical and the MHD Taylor-Couette flow with assumption of infinitely long cylinders. Purely hydrodynamical flow is obtained simply by neglecting the Lorentz force in the momentum equation, i.e., setting $\mathrm{Ha} = 0$ and omitting the equations involving the magnetic field.

2.3.1 Hydrodynamics

First we will consider a stability criterion for inviscid flow, i.e., $\nu = 0$ in the momentum equation. Assume that two rings of fluid at $r_1 < r_2$ have velocity u_1, u_2 and centripetal acceleration u_1^2/r_1, u_2^2/r_2. If the inner ring acquires velocity u_1' it will be pushed back to its position unless $u_1'^2/r_2 > u_2^2/r_2$. From the conservation of angular momentum we have $u_1' = u_1 r_1/r_2$ so the ring will move outwards if $(r_1u_1)^2/r_2^3 > u_2^2/r_2$. From this the condition for stability of such flow (i.e., case when the inner ring will be pushed back to the original location) can be written as

$$\partial_r\left(\Omega r^2\right)^2 \geq 0 \qquad \text{for stability.} \tag{2.12}$$

This criterion, although with use of different arguments, has been first formulated by Rayleigh (1917). It separates flow with increasing and decreasing angular momentum.

When viscous effects are taken into account and no-slip boundary conditions are applied at the walls of the cylinders, it can be showed from angular momentum conservation that the rotational profile of the fluid $\Omega_0(r)$ is given by (2.7). Generally one should expect that the effect

of viscosity is to postpone the onset of the instability, therefore from (2.12) follows conclusion that the flow between cylinders is always hydrodynamically stable for $\hat{\mu} > \hat{\eta}^2$, i.e., $\hat{\mu} > 0.25$ for our geometry, see Fig. 2.3. In the centrifugal instability indeed viscosity plays only stabilizing role. However, for other types of flows, for example parallel shear flows, it is possible that viscosity plays the dual roles of stabilizer and destabilizer (Drazin and Reid, 1981).

Nonlinear hydrodynamic instability often occur in linearly stable flows when the corresponding Reynolds number is very large (for example in pipe flows). It is not clear whether linearly stable Taylor-Couette flow would be eventually destabilized for sufficiently high rotation rates. In a recent experiments Ji et al. (2006) have claimed that non-magnetic quasi-Keplerian $\Omega \propto r^{-3/2}$ (and therefore satisfying Rayleigh stability criterion) flows are essentially steady up to Reynolds number of order of millions (in order to minimize effects induced by endplates covering the cylinders the lids were divided into four independently rotating rings).

However, accretion disks are characterized by Re of order $10^7 - 10^{12}$, so perhaps the shear flows become unstable for higher Re? In the absence of magnetic field, turbulent angular momentum transport is realized by correlated velocity fluctuations, so that the angular momentum flux in radial direction is $\rho r \left\langle u'_\phi u'_r \right\rangle$. Let $\mathrm{Re}_{\mathrm{cturb}}$ denote a critical Reynolds number at which linearly stable flow becomes turbulent. Results of the experiment Ji et al. (2006) indicate that the correlations are negligible up to $\mathrm{Re} \lesssim 2 \times 10^6$ and even if transition $\mathrm{Re} > \mathrm{Re}_{\mathrm{cturb}}$ has occurred, the angular momentum transport was too small to be detected.

Let ν_{turb} be the viscosity associated with the turbulent transport. Empirical observations of, e.g., pipe flows, show that after transition $\mathrm{Re} > \mathrm{Re}_{\mathrm{cturb}}$ the value of this viscosity is approximately independent of Re, so that $\nu \approx \mathcal{LU}/\mathrm{Re}_{\mathrm{cturb}}$. If, relaying on these results, one assumes that this is true also for the shear flow, ν_{turb} is smaller than molecular viscosity also for $\mathrm{Re} > \mathrm{Re}_{\mathrm{cturb}}$. Therefore even if the transition has occurred in the experiment, it turns out that purely hydrodynamical turbulent viscosity can not efficiently drive angular momentum transport in the disks.

It should be noticed that the above discussion concerns only incompressible flows. If a fluid with stable axial density stratification is studied, the sufficient condition for (non-axisymmetric) instability can become $\partial_r \Omega^2 < 0$, (Molemaker et al., 2001). This is identical to the Velikhov criterion for magnetorotational instability, Eq. 1.6. Since the astrophysical disks are vertically stratified it is likely that this type of instability plays role, especially in weakly ionized disks (Dubrulle et al., 2005). However, when the stratification is too large it can have also stabilizing effect.

2.3.2 Magnetohydrodynamics

Decades ago Velikhov (1959) and then, more generally, Chandrasekhar (1960) have shown that even very weak axial magnetic field applied to a Taylor-Couette flow with fluid possessing zero resistivity can alter the stability criterion dramatically. Firstly the flow is always stable when $\hat{\mu} > 1$, moreover it can be destabilized by the magnetic field even if the Rayleigh criterion is fulfilled. We notice that line $\hat{\mu} = 1$ distinguishes between flow with increasing and decreasing angular velocity.

It has been more than thirty years later when, after work by Balbus and Hawley (1991), astrophysical community realized that this type of instability can play crucial role in wide range of astrophysical objects. In particular it can serve as a mechanism of transporting angular momentum in accretion disks. It is worth noting that there is virtually no references in astrophysical literature to Velikhov (1959) or Chandrasekhar (1960) prior to the work by Balbus & Hawley.

Accretion disks are mostly Keplerian, which means that theirs rotational profile scales like $\Omega \propto r^{-3/2}$ so that $|\Omega|$ decreases radially outward but specific angular momentum $|\Omega r^2|$ increases radially. We will call Taylor-Couette flows quasi-Keplerian if $\Omega \propto r^{-3/2}$ is fulfilled so, for our

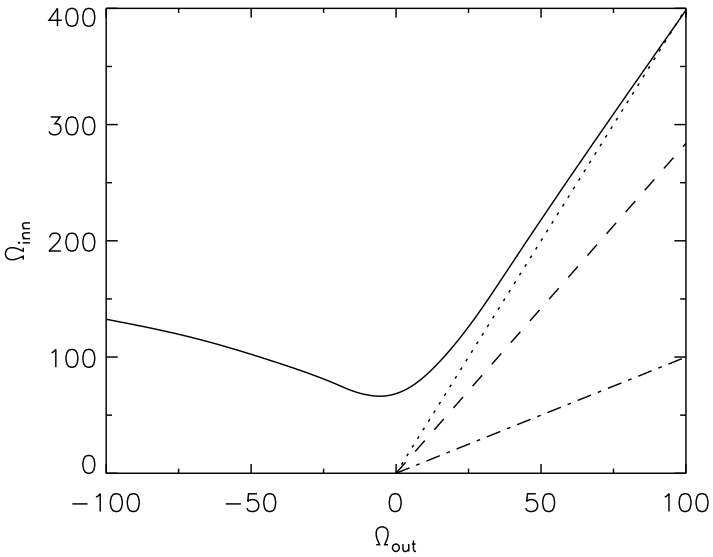

Figure 2.3: *Marginal stability diagram for Taylor-Couette flow for radius ratio $R_{\rm in}/R_{\rm out} = 1/2$ in non-dimensional formulation according to equations* (2.5)*. (——) viscous flow. (· · · · ·) Rayleigh line $\hat{\mu} = 0.25$: flow is hydrodynamically stable below this line. (·–·–·) $\hat{\mu} = 1.00$ below the line the flow is always stable. (– – –) quasi-Keplerian flow, $\Omega_{\rm in}/\Omega_{\rm out} = (R_{\rm out}/R_{\rm in})^{3/2}$ which implies $\hat{\mu} = 0.3535$. The most interesting region lies between (· · · · ·) and (·–·–·), where magnetic field can destabilize flow. For counter-rotation of the cylinders the inviscid flow is always unstable.*

geometry, $\hat{\mu} = 0.3535$. We notice that the magnetorotational instability can exist for range $0.25 < \hat{\mu} < 1$, see Fig. 2.3.

The main differences between astrophysical and experimental MRI are physical properties of the rotating medium – on astrophysical scales it is usually hot, well ionized plasma whereas down on the Earth the most convenient approach consists of the Taylor-Couette flow with a liquid metal. Experiments with fast rotation of plasma also have been proposed (Noguchi and Pariev, 2003) but they undergo lots of technical problems and are still in development stage.

One of the most important parameters characterizing laboratory liquid metals is the magnetic Prandtl number Pm which is ratio of the kinematic viscosity ν to the magnetic diffusivity η. For such liquids this ratio is very small, of order of 10^{-5}-10^{-6}. For astrophysical objects ionized plasma can have Pm ranged from 10^{-8} for protostellar disks, 10^{-6} for cataclysmic variables and disks around compact objects such as neutron stars, to 10^{4} for active galactic nuclei (Brandenburg and Subramanian, 2005). However, Reynolds numbers for such disks can easily be of order 10^{7} - 10^{10}. Also density can vary significantly whereas laboratory liquids are essentially incompressible.

The axial magnetic field

Velikhov (1959) has shown that for the ideal MHD the applied axial field can destabilize hydrodynamically stable flow. Later Kurzweg (1963) demonstrated that also for non-ideal MHD, for small gap approximation and weak fields, the critical Reynolds number $\mathrm{Re_c}$ can become even smaller than for the corresponding purely hydrodynamical flow, provided that the magnetic Prandtl number is sufficiently large. From Fig. 2.4 we see that for the magnetic flow with $\mathrm{Pm} = 1$ (the left panel) subcritical excitations exist and it is possible to obtain smaller $\mathrm{Re_c}$ when compared to the hydrodynamical flow. Moreover, the flow remains unstable even if the Rayleigh

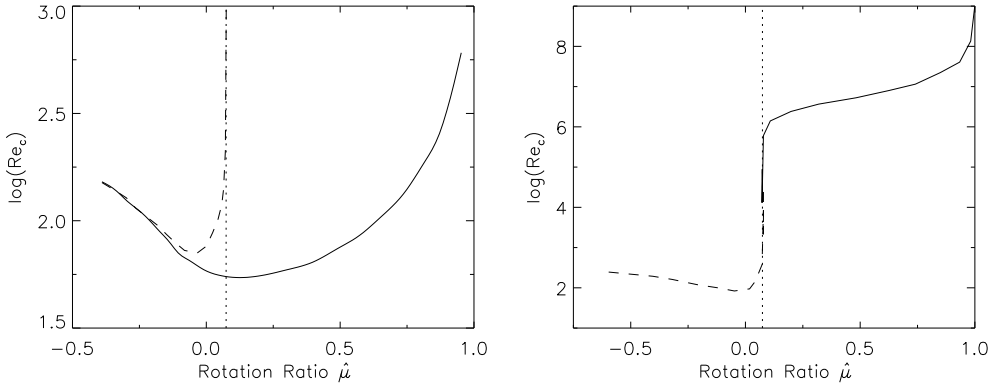

Figure 2.4: *Critical Reynolds number* $\mathrm{Re_c}$ *as a function of the rotation ratio* $\hat{\mu}$ *for the Taylor-Couette flow with* $\hat{\eta} = 0.27$*. Left:* $\mathrm{Pm} = 1$*, right:* $\mathrm{Pm} = 10^{-5}$*. (– – –) is for purely hydrodynamical flow* $\mathrm{Ha} = 0$*, (——) represents minimal* $\mathrm{Re_c}$ *for non-zero magnetic field,* $\mathrm{Ha} > 0$*. The dotted vertical line denotes Rayleigh stability criterion.*

criterion for stability is fulfilled, i.e., on the right side of the vertical line. This remains true also for small $\mathrm{Pm} = 10^{-5}$, however the required $\mathrm{Re_c}$ is much larger, at least of order 10^6.

Already Velikhov found that a critical vertical wavenumber k_c corresponding to such instability fulfills

$$k_c \leq \hat{\eta}\frac{2\Omega_{\mathrm{in}}}{V_a}, \tag{2.13}$$

where V_a is the Alfvén velocity

$$V_a = \frac{B_0}{\sqrt{\mu_0 \rho}}. \tag{2.14}$$

However the applied magnetic field can not be too strong, the instability can arise only if

$$V_a < -r^2 \partial_r \Omega, \tag{2.15}$$

i.e., when the Alfvén velocity is smaller than the shear. When magnetic field is too strong the MRI ceases to exists.

For hydrodynamically stable flows there is a significant difference between $\mathrm{Pm} \gtrsim 1$ and $\mathrm{Pm} \ll 1$. In the former case the additional axial field can reduce the critical Reynolds number, this is more evident for larger Pm, however this effect vanishes if Ha is large enough. In the latter case, $\mathrm{Pm} \ll 1$, the magnetic field plays only stabilizing role, i.e., increases $\mathrm{Re_c}$. However when the rotation is sufficiently fast it can bring hydrodynamically stable flow into unstable regime, Fig. 2.4 (right).

On the Rayleigh line, $\hat{\mu} = \hat{\eta}^2$ and hence $a = 0$ in (2.7) from which follows (see e.g. Rüdiger, 2004) that for axisymmetric case the quantities u_r, u_z, b_r, b_z scale as $\mathrm{Pm}^{-1/2}$ while $u_\phi, b_\phi, k, \mathrm{Ha}$ scale as Pm^0. Therefore for $\hat{\mu} = \hat{\eta}^2$, the critical Reynolds number (for axisymmetric modes which are preferred over non-axisymmetric ones for that instability) scales as

$$\mathrm{Re_c} \propto \mathrm{Pm}^{-1/2}. \tag{2.16}$$

Willis and Barenghi (2002b) have demonstrated, with use of numerical methods, that this scaling holds independently of the radial magnetic boundary conditions (i.e., conducting or insulating).

On the other hand, if the Rayleigh line is crossed $\hat{\mu} > \hat{\eta}^2$, quickly much steeper scaling sets in (see e.g. Rüdiger et al., 2003):

$$\mathrm{Re_c} \propto \mathrm{Pm}^{-1}, \tag{2.17}$$

and the corresponding strength of the magnetic field

$$\mathrm{Ha}\sqrt{\mathrm{Pm}} \propto \mathrm{const.} \tag{2.18}$$

This leads to a conclusion that $\mathrm{Re_c}$ undergoes a sudden change when $\hat{\mu}$ is very slightly increased over $\hat{\eta}^2$ and small Pm is used. Naturally this transition is not so important when $\mathrm{Pm} \approx 1$. We shall notice that for $\hat{\mu} > \hat{\eta}^2$ from the above relations and Eq. (2.13) it follows that the critical vertical wavenumber is independent of Pm.

From (2.16), (2.17) we conclude that for $\mathrm{Pm} = 10^{-6}$ the critical $\mathrm{Re_c}$ changes two orders of magnitude from $\hat{\mu} = \hat{\eta}^2$ to $\hat{\mu} > \hat{\eta}^2$. Since it is undoubtedly easier to perform an experiment with smaller Re, i.e., slower rotation, one would prefer to perform the experiment exactly at the Rayleigh line. However, even smallest deviation from the line would dramatically alter excitation conditions and the results would be unclear.

We now introduce the magnetic Reynolds number

$$\mathrm{Rm} \equiv \frac{\Omega_{\mathrm{in}} R_{\mathrm{in}} D}{\eta} = \mathrm{RePm}, \tag{2.19}$$

and from (2.17) we conclude that in the region of our interest $\hat{\eta}^2 < \hat{\mu} < 1$, MRI operates for $\mathrm{Rm} \propto \mathrm{const}$. The MRI exists if Rm is of order of $O(10)$ so that for $\mathrm{Pm} = 10^{-6}$ the critical $\mathrm{Re_c} = 10^5$.

Let us now consider an experiment consisting of two cylinders with radii $R_{\mathrm{in}} = 5$cm, $R_{\mathrm{out}} = 10$cm ($\hat{\eta}^2 = 0.25$) filled with gallium, so that $\mathrm{Pm} = 10^{-6}$. For, say, $\hat{\mu} = 0.27$ the critical $\mathrm{Re_c}$ is then 10^7, this corresponds to rotation of the inner cylinder with frequency 200Hz! Moreover the required magnetic field is $\mathrm{Ha} = 1700$, i.e. $B_z = 7500G$ and huge currents in a coil surrounding the cylinders are necessary to generate it. Such vast rotation rates and strong fields are technically extremely, or even forbiddenly, challenging and this is also the reason why MRI has never been observed ,,by chance" as it often in physics is.

Besides the purely technical problems there is an additional issue which must be addressed when so fast rotation is considered. In the linear theory cylinders are assumed to be infinitely long or periodic, whereas in reality they are enclosed by plates. From Taylor-Proudman theorem, which states that fluid tends to align itself along axis of rotation, follows that such relatively rotating plates would significantly alter the background flow. Indeed Hollerbach and Fournier (2004) have shown that for large $\mathrm{Re} \gtrsim 10^6$ the plates can easily dominate the whole flow, and even if they are divided into differentially rotating rings problems arise.

Axial and azimuthal magnetic field

In order for the MRI to operate when there is only the axial external magnetic field applied, an azimuthal component of the field must be produced by the rotation. Rüdiger et al. (2005) have shown that externally imposing the additional azimuthal component dramatically reduces critical characteristic values, and makes it possible to find that type of MRI experimentally. The applied field has the form (2.4) and is current-free (except along the axis of rotation) so that the only source of energy to drive the instability is still the imposed differential rotation. The

azimuthal component can be easily generated by letting an electric current through a rod placed in the axis of rotation.

Due to the specific configuration of the imposed field this type of MRI is usually referred as ,,spiral" or ,,helical", also the acronym HMRI is used, in contrast to SMRI – Standard MRI.

The main finding is that for the spiral MRI critical Reynolds number necessary to excite instability are dramatically reduced – from $O(10^6)$ to $O(10^3)$, for $\beta \approx 4$.

This specific form of the external magnetic field breaks the reflectional symmetry of the problem and consequently the instability takes the form of a traveling wave. The direction of the wave propagation is defined by signs of $\Omega_{\rm in}$, β and B_z – for all three being positive the wave moves downwards. The frequency of the traveling wave and its velocity can be derived from the linear analysis of the problem and then becomes an important, easy to measure parameter indicating this type of instability. For more detailed discussion on breaking symmetry in MHD rotating flows see Knobloch (1996).

Chapters 3 and 4 of this thesis will cover the subject of spiral MRI in more details, especially focusing on the experimental point of view with geometry of the PROMISE facility.

2.4 Numerical method and the boundary conditions

We now formulate the problem in a way suitable for solving with numerical methods. The system (2.11) will be solved in its fully nonlinear form with the method described below, however in Chapter 5 of this work we will also consider linear stability of the Eqs. (2.5). We assume that $R_{\rm in}, R_{\rm out}, H$ are provided here in the non-dimensional form, i.e., $R_{\rm in}/D \to R_{\rm in}, R_{\rm out}/D \to R_{\rm out}, H/D \to H$.

The vorticity is defined as

$$\boldsymbol{\omega} = \mathrm{rot}\, \boldsymbol{u}. \tag{2.20}$$

Taking curl of (2.11a), (2.11b) and using the Ampère's law without the displacement current we obtain equations for the vorticity $\boldsymbol{\omega}$ and the perturbation current $\boldsymbol{j}$. Assuming that the flow is *axisymmetric* we neglect all ϕ derivatives and find a set of equations in a stream function-vorticity formulation, i.e.,

$$\partial_t u_\phi = (\nabla^2 - r^{-2})u_\phi + [\boldsymbol{u} \times (\mathrm{rot}\, \boldsymbol{u})]_\phi + \mathrm{Ha}^2 \partial_z b_\phi, \tag{2.21a}$$
$$\partial_t \omega_\phi = (\nabla^2 - r^{-2})\omega_\phi - [\mathrm{rot}(\boldsymbol{\omega} \times \boldsymbol{u})]_\phi + \mathrm{Ha}^2 [\mathrm{rot}(\boldsymbol{j} \times \boldsymbol{B_0})]_\phi, \tag{2.21b}$$

with elliptic equations for the stream function, the perturbed magnetic field and the current:

$$\left[-r^{-1}(\partial_{zz} + \partial_{rr}) + r^{-2}\partial_r\right]\psi = \omega_\phi, \tag{2.22a}$$
$$(\nabla^2 \boldsymbol{b})_\phi = -\partial_z \left(u_\phi - \frac{u_z \beta B_0 R_{\rm in}}{r}\right) + \partial_r \frac{u_r \beta B_0 R_{\rm in}}{r}, \tag{2.22b}$$
$$(\nabla^2 \boldsymbol{j})_\phi = -\partial_{zz}(u_r) + \partial_r r^{-1} \partial_r (r u_r), \tag{2.22c}$$

where the stream function ψ is defined as

$$u_r = -\frac{1}{r}\partial_z \psi, \tag{2.23}$$
$$u_z = \frac{1}{r}\partial_r \psi. \tag{2.24}$$

The above equations are solved with a finite-difference method in the r-z plane.

No-slip boundary conditions for the velocity on the walls and the endplates are used, so that

$$u_r = 0 \qquad \text{at} \qquad r = R_{\text{in}}, r = R_{\text{out}}, \tag{2.25}$$
$$u_z = 0 \qquad \text{at} \qquad z = 0, z = H, \tag{2.26}$$

hence, after setting the arbitrary constant to zero,

$$\psi = 0 \qquad \text{at} \qquad r = R_{\text{in}}, r = R_{\text{out}}, \tag{2.27}$$
$$\psi = 0 \qquad \text{at} \qquad z = 0, z = H. \tag{2.28}$$

Boundary conditions for u_ϕ at the walls are determined by Re and $\hat{\mu}$

$$u_\phi = \mathrm{Re} \qquad \text{at} \qquad r = R_{\text{in}}, \tag{2.29}$$
$$u_\phi = \frac{\hat{\mu}}{\hat{\eta}}\mathrm{Re} \qquad \text{at} \qquad r = R_{\text{out}}, \tag{2.30}$$

and at the endplates by their rotation properties

$$u_\phi(r) = r\Omega_{\text{bot}}(r) \quad \text{at} \quad z = 0, \tag{2.31}$$
$$u_\phi(r) = r\Omega_{\text{top}}(r) \quad \text{at} \quad z = H. \tag{2.32}$$

For example for the both endplates rigidly rotating with the outer cylinder we have $\Omega_{\text{top}} = \Omega_{\text{bot}} = \Omega_{\text{end}} = \Omega_{\text{out}}$.

Using (2.22a) we obtain

$$\omega_\phi = -(1/r)\partial_{rr}\psi \qquad \text{at} \qquad r = R_{\text{in}}, r = R_{\text{out}}, \tag{2.33}$$
$$\omega_\phi = -(1/r)\partial_{zz}\psi \qquad \text{at} \qquad z = 0, z = H. \tag{2.34}$$

The magnetic boundary conditions depend on electrical properties of the walls. For perfectly conducting cylinders we assume infinite conductivity so that with $\boldsymbol{J} = \sigma(\boldsymbol{E} + \boldsymbol{u} \times \boldsymbol{b})$ and $E_\phi = E_z = 0$ for the walls we get

$$r^{-1}b_\phi + \partial_r b_\phi = 0 \qquad \text{at} \qquad r = R_{\text{in}}, r = R_{\text{out}}, \tag{2.35}$$
$$j_\phi = 0 \qquad \text{at} \qquad r = R_{\text{in}}, r = R_{\text{out}}, \tag{2.36}$$

and $E_r = E_\phi = 0$ for the perfectly conducting end-plates

$$\partial_z b_\phi = 0 \qquad \text{at} \qquad z = 0, z = H, \tag{2.37}$$
$$j_\phi = 0 \qquad \text{at} \qquad z = 0, z = H. \tag{2.38}$$

For insulating endplates the boundary conditions for magnetic field are obtained by applying the so-called pseudo-vacuum approximation for which $b_r = b_\phi = \partial_z b_z = 0$. Then

$$b_\phi = 0 \qquad \text{at} \qquad z = 0, z = H, \tag{2.39}$$
$$\partial_z j_\phi = 0 \qquad \text{at} \qquad z = 0, z = H. \tag{2.40}$$

We also use magnetic boundary conditions which are intermediate between a perfect conductor and a perfect insulator. In this case the endplate consists of thin layer with thickness ε and conductivity σ_w below which (below for the bottom and above for the top endplate) there is an

insulator (see e.g. Loper, 1970). Then this layer can be characterized with the parameter κ

$$\kappa = \varepsilon \frac{\sigma_{\mathrm{w}}}{\sigma_{\mathrm{f}}}, \tag{2.41}$$

where σ_{f} is conductivity of the fluid. The vertical boundary conditions become

$$b_\phi = \kappa \partial_z b_\phi \qquad \text{at} \qquad z = 0, \tag{2.42}$$
$$b_\phi = -\kappa \partial_z b_\phi \qquad \text{at} \qquad z = H, \tag{2.43}$$
$$\partial_z j_\phi = 0 \qquad \text{at} \qquad z = 0, z = H. \tag{2.44}$$

For $\kappa \to 0$ we obtain the pseudo-vacuum boundary conditions, for $\kappa \to \infty$ the perfectly conducting ones.

To get b_r and b_z components we introduce scalar field a such

$$\boldsymbol{b} = b_\phi \hat{\mathbf{e}}_\phi + \mathrm{rot}(a \hat{\mathbf{e}}_\phi), \tag{2.45}$$

since $\boldsymbol{j} = \mathrm{rot}\, \boldsymbol{b}$ we obtain a by solving the elliptic equation:

$$\left(\nabla^2 - \frac{1}{r^2} \right) a = -j_\phi, \tag{2.46}$$

and then

$$b_r = -\partial_z a \qquad b_z = \frac{1}{r} \partial_r (ra). \tag{2.47}$$

The boundary conditions for a follow from these for $\boldsymbol{b}$ and $\boldsymbol{j}$

$$a = 0 \quad \text{at} \quad r = R_{\mathrm{in}}, r = R_{\mathrm{out}}, \tag{2.48}$$

and

$$\partial_z a = 0 \qquad \text{at} \qquad z = 0, z = H \quad \text{for insulating endplates,} \tag{2.49}$$
$$a = 0 \qquad \text{at} \qquad z = 0, z = H \quad \text{for perfectly conducting endplates.} \tag{2.50}$$

For periodic cylinders the boundary conditions are straightforward: all the quantities are copied to appropriate cells in the vertical direction. However this leads to different matrices in the Poisson solvers, so that bands which appear are in larger distance from the diagonals and the computation time is slowed down when compared to the finite cylinders approach.

We simulate the axisymmetric two-dimensional flow described by Eqs. (2.21), (2.22) in cylindrical coordinates (r, ϕ, z) with a numerical code adapted for our purposes. The original version of the code was provided by A. Youd (see Youd and Barenghi, 2006; Youd, 2005, for details and tests). The assumption of axisymmetry is justified in this case since $m = 0$ modes are preferred over non-axisymmetric in the type of instability which is under study. The code has been significantly modified in order to handle periodic boundary conditions in a way suitable for our needs, the toroidal field was added and different magnetic and hydrodynamic boundary conditions at the endplates were applied, also solvers for b_r, b_z were introduced.

Variables from Eqs. (2.21) - (2.22) are approximated on a grid with resolution $N_r \times N_z = 80 \times \Gamma 80$ with second order finite-differences (resolution $40 \times \Gamma 40$ is also used for comparison, the difference in obtained results is always less than couple of percent). The dynamic variables u_ϕ, ω_ϕ from Eq. (2.21) are forwarded in time with the second order implicit Crank-Nicolson scheme for

linear terms and the third order explicit Adams-Bashforth for the nonlinear terms. The time-step is constant with $\mathrm{d}t = 10^{-5}$ or $\mathrm{d}t = 10^{-4}$ for comparison. RHS for system (2.21) are obtained by solving the elliptic Eqs. (2.22) with the appropriate boundary conditions. This is done by solving an adequate matrix equation with use of SCALAPACK library. This library makes it possible to use parallel computation facility – Sansoussi and Octopus clusters from AIP have been used to perform the calculations. The form of the matrix depends on the boundary conditions and takes the form of a tridiagonal matrix with bands. The code can handle flows with Reynolds numbers up to ≈ 2500, higher rotation rates require significantly finer resolution and smaller time-steps.

2.4.1 Sample solution I – Hydrodynamics

We now demonstrate some general features of a solution of the MHD Taylor-Couette problem formulated in the way described above.

Figure 2.5 refers to a non-magnetic case when the cylinders are infinitely long, i.e., the periodic vertical boundary conditions are used. For the given gap ratio $\hat{\eta} = 0.5$, the critical Reynolds number has well known value $\mathrm{Re}_\mathrm{c} = 68.9$, and the vertical wavenumber is $k = 3.14$. Therefore the vertical wavelength $\lambda = 2D$ and the Taylor cells, arising when Re_c is reached, are almost square. This is not instantly seen from the figure since the axes r, z are not drawn at scale.

Fluid circulates along contour lines of stream function ψ clockwise where it is positive (solid lines) and counter-clockwise where ψ is negative. We also notice that the rotational profile u_ϕ is clearly z-dependent. When scaled to physical properties of viscosity of gallium, the maximum velocity u_z is of order up to 1.0 mm/s for these conditions. This velocity scales linearly with Reynolds numbers. However, this scaling holds only up to a certain point when next mode of instability sets in, or eventually turbulent state is reached.

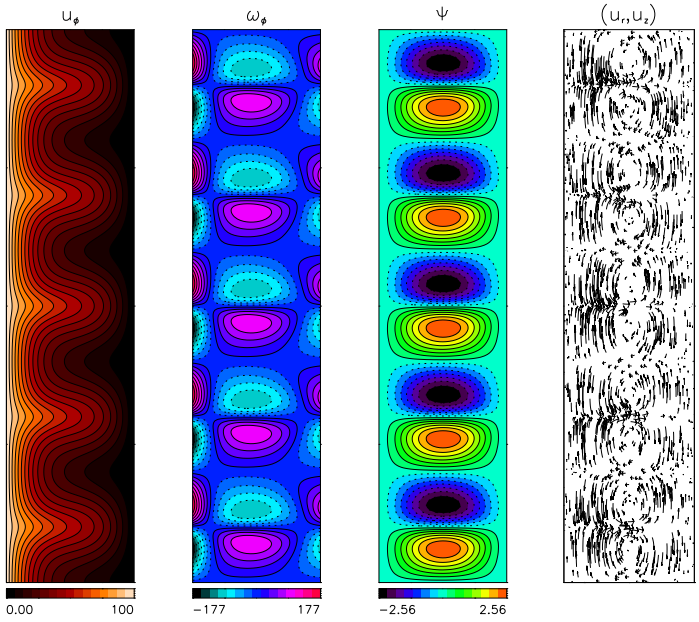

Figure 2.5: *Contour lines of dynamical variables u_ϕ, ω_ϕ and corresponding solution of the elliptic Eqs.* (2.22) *for ψ for cross section in the $r - z$ plane. Cylinders have height $H = 10D$ and periodic boundary conditions in the vertical direction are used. Rotation of the inner cylinder (the left edge of each panel) corresponds to $\mathrm{Re} = 100$ thus $\Omega_\mathrm{in} = 100$, the outer cylinder (the right edge of each panel) is at rest $\Omega_\mathrm{out} = 0$ so that $\hat{\mu} = 0$. There is no axial magnetic field, $\mathrm{Ha} = 0$. The plot is not at scale.*

A situation where the cylinders are enclosed by rigidly rotating endplates is shown in Fig. 2.6. In this case the outer cylinder rotates sufficiently fast so that the Rayleigh criterion is fulfilled and the flow is essentially hydrodynamically stable. Nevertheless we notice two large Ekman vortices nearby each endplate.

The mechanism generating the vortices is due to the vertical no-slip boundary conditions. In the bulk of the container the pressure gradient is balanced so that $\frac{u_\phi^2}{r} \approx \frac{\nabla p}{\rho}$, whereas at the boundaries we have $u_\phi = r\Omega_{\mathrm{out}}$. Consequently, the resulting imbalanced pressure gradient drives a radial flow which, due to the conservation of mass, turns into axial direction close to the radial boundaries. This secondary flow is usually considered as an analog to the geophysical Ekman flow. Eventually in our incompressible fluid a global meridional circulation is induced.

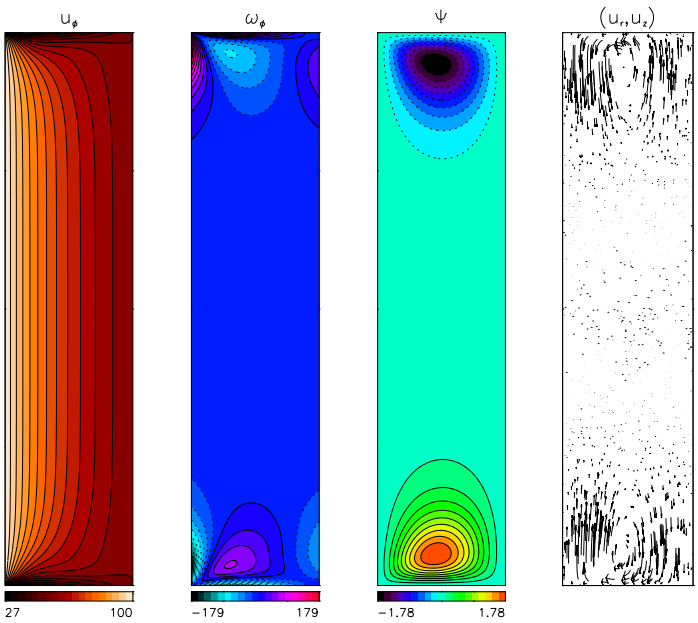

Figure 2.6: *Contour lines of dynamical variables u_ϕ, ω_ϕ and the stream function ψ for cross section in $r-z$ plane. Cylinders have height $H = 10D$ and boundary conditions corresponding the endplates rotating with the outer cylinder were applied $\Omega_{\mathrm{end}} = \Omega_{\mathrm{out}}$. The endplates are represented by the top and the bottom edge of each panel. The inner cylinder rotates with $\Omega_{\mathrm{in}} = 100$, hence $\mathrm{Re} = 100$ and the outer one rotates with $\Omega_{\mathrm{out}} = \hat{\mu}\Omega_{\mathrm{in}}$, where $\hat{\mu} = 0.27$. Since the Rayleigh criterion for stability is fulfilled, the flow is hydrodynamically stable. Nevertheless the endplates induce global circulation – the Ekman vortices. No magnetic field is applied,* $\mathrm{Ha} = 0$.

2.4.2 Sample solution II – Magnetohydrodynamics

Flow for finite cylinders covered with stationary lids but with a weak external axial magnetic field applied is depicted in Fig. 2.7. Since $\mathrm{Re} = 100$ and $\hat{\mu} = 0$, the flow is hydrodynamically unstable and Taylor vortices are clearly visible. Since aspect ratio is $\Gamma = 10$ there are 5 pairs of them. Two, a bit larger, vortices near boundaries correspond to the Ekman vortices.

As it has been mentioned before, when the external axial magnetic field is strong enough it can suppress the hydrodynamical instability. This situation is presented in Fig. 2.8, the Taylor vortices disappeared, there exists clear interaction between Ekman circulation and the field in vicinity of the plates. Two new vortices are generated close to the outer cylinder, strong currents are localized in the boundary layer. Yet still the rotational profile is somewhat similar to Ω_0.

Imposing perfectly conducting boundary conditions on the magnetic fields has drastic influence for properties of this type of MHD flows. In that case even a weak external magnetic field alters the flow profoundly, see Fig. 2.9. The induced azimuthal magnetic field is almost order of magnitude larger than for the insulating plates, Taylor vortices nearly vanished and there exists counter-rotation $u_\phi < 0$. The assumption of a perfectly conducting material is a very strong one and in reality, even for good conductors like copper, is not fulfilled. Instead intermediate conditions can be applied, see Eq. (2.41).

A detailed discussion of the complex situation which arise near vertical boundary layer and associated global effects for MHD Taylor-Couette flow will be subject of Chapter 5.

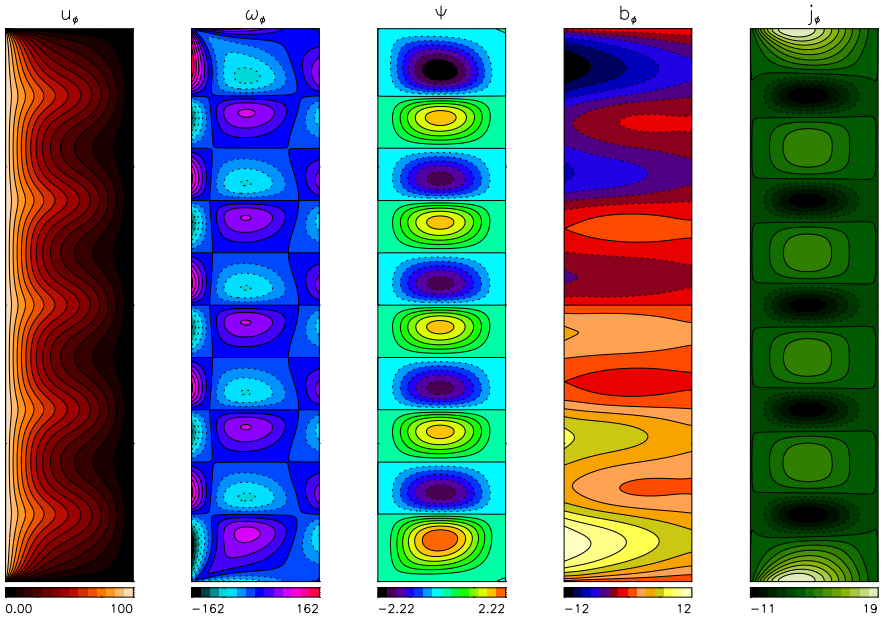

Figure 2.7: *The solution for finite cylinders with a weak axial magnetic field is presented,* $\mathrm{Re} = 100, \hat{\mu} = 0.0, \Gamma = 10$. *The plates are at rest,* $\Omega_{\mathrm{end}} = \Omega_{\mathrm{out}} = 0$. *The applied axial field is very weak,* $\mathrm{Ha} = 3$ *so its influence on the flow is small. Pseudo-vacuum, i.e., insulating like, magnetic boundary conditions are used.*

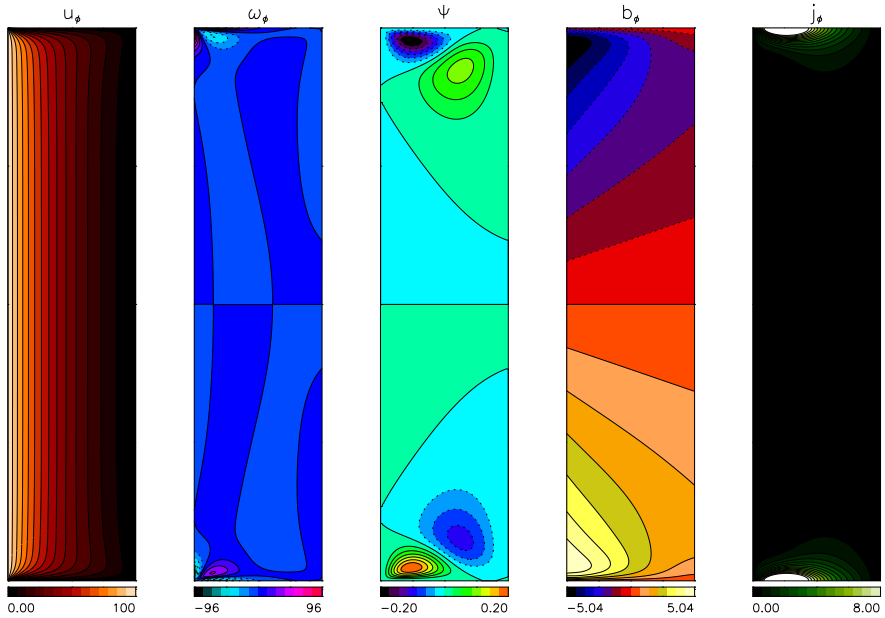

Figure 2.8: *Figure is analogous to Fig. 2.7 but here much stronger magnetic field is applied,* $\mathrm{Ha} = 10$*. Strong field suppresses Taylor vortices and situations close to vertical boundaries is more complicated – Ekman vortices are smaller, larger counter rotating vortices in theirs vicinity are generated, azimuthal currents concentrate very close to the plates.*

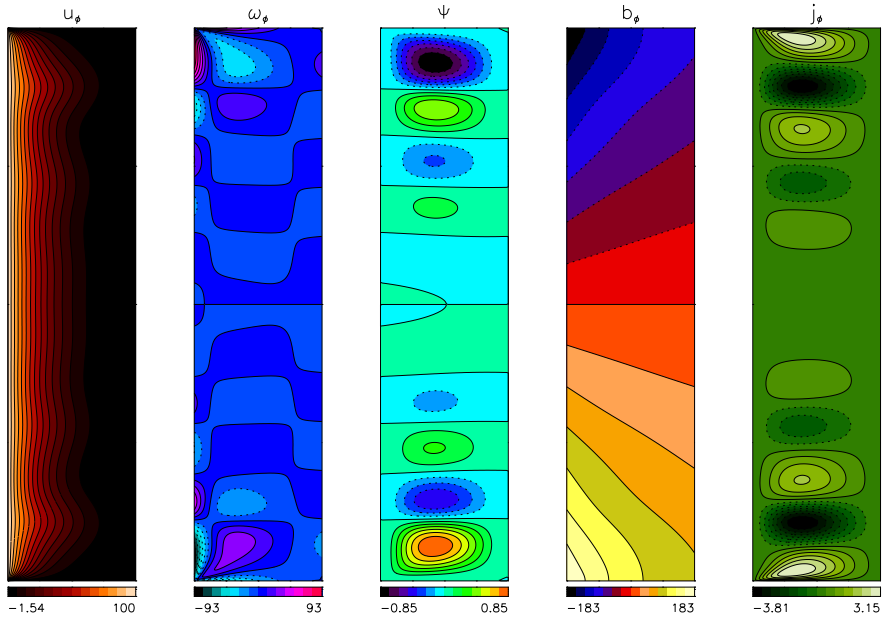

Figure 2.9: *Figure is analogous to Fig. 2.7 but here plates enclosing the cylinders are assumed to be perfectly conducting, magnetic field is weak,* $\mathrm{Ha} = 3$*. Those specific magnetic boundary conditions result in the very strong induced magnetic field. Remnants of Taylor vortices can be seen, rotational profile* u_ϕ *is significantly changed and even counter-rotation exists.*

Chapter 3

Helical magnetic field

3.1 Introduction

In the Section 2.3 the question of stability of magnetized Taylor-Couette flow has been addressed. We have seen that for liquids possessing small Prandtl number the rotation rates must be very large when the externally applied magnetic field consists only of the axial component. Moreover this instability does not exist to the right of the Rayleigh line in the $\mathrm{Pm} \to 0$ limit. Due to the vast rotation rates technical problems arise when constructing an experiment. There is also a need for careful treatment of the vertical boundaries since the flow is strongly constrained by the Taylor-Proudman theorem and as a result it is controlled almost entirely by the endplates, especially if they are rotating rigidly (Hollerbach and Fournier, 2004).

When an azimuthal component is added to the external magnetic field, the critical Reynolds numbers $\mathrm{Re_c}$ associated with the rotation rates is dramatically reduced. This firstly has been shown by Hollerbach and Rüdiger (2005). The motivation for such field geometry is quite simple: it is uncomplicated modification to the pure axial field, it is also current-free and it is very easy to realize it in an experiment – just by running a sufficiently large electric current through the axis of rotation. It should be stressed that the magnetic field is current-free and itself it does not exert any forces on the fluid, so the instability ultimately is driven by the rotation.

In Fig. 3.1 we see the dependence of the critical Reynolds number $\mathrm{Re_c}$ on the rotation ratio $\hat{\mu}$ for different strengths of the azimuthal magnetic field, i.e., for different β. The dotted line denotes hydrodynamical stability, it reaches asymptotic value $+\infty$ for $\hat{\mu} = 0.25$, i.e., where the flow is stable according to the Rayleigh criterion. The solid and dashed lines are for magnetic case, $\mathrm{Pm} = 10^{-6}$, $\mathrm{Pm} = 10^{-5}$ respectively. When there is only an axial field applied, i.e., $\beta = 0$, we see that $\mathrm{Re_c}$ rises very rapidly in vicinity of $\hat{\mu} = 0.25$ and ends up with very large value, proportional to Pm^{-1} and goes to infinity for $\mathrm{Pm} \to 0$. In this form MRI sets in when magnetic Reynolds number Rm is of order $O(10)$ so the resulting $\mathrm{Re_c} = \mathrm{Rm}/\mathrm{Pm} = 10^6 - 10^7$.

We now focus on non-zero β, it is evident that $\mathrm{Re_c}$ is significantly smaller also for $\hat{\mu}$ extending far beyond the Rayleigh line. Moreover with larger β the scaling becomes less and less like the previous Pm^{-1}, it becomes independent of Pm and eventually this type of instability exists also in $\mathrm{Pm} \to 0$ limit. The reason for that is that the existing meridional circulation advects the applied B_ϕ giving contribution to the induced b_ϕ so that it is possible to maintain the instability.

It has already been mentioned in the previous chapter that the up/down symmetry in the z direction is broken when the helical magnetic field is applied. Consequently the new modes are no longer stationary, as is for the classical MRI or primary hydrodynamical instability, but drift in the z-direction – downwards when product $\beta \times B_0 \times \Omega$ has positive sign, upwards otherwise (a traveling wave exists in the solution). Naturally this drift must be suppressed at vertical boundaries when the cylinders are finite and covered with plates.

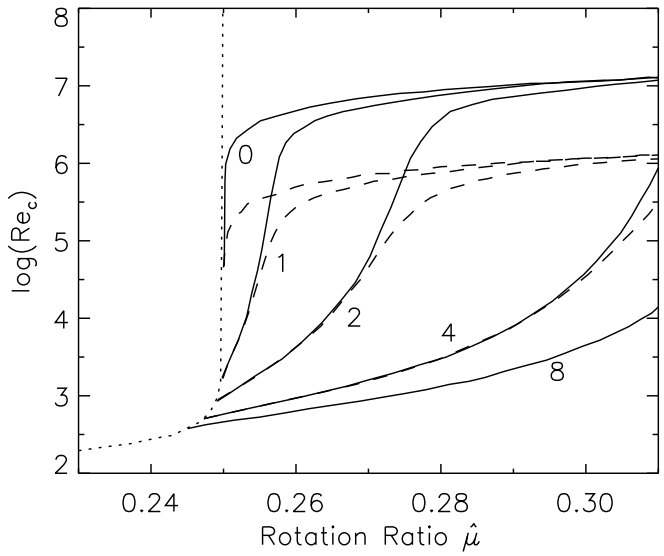

Figure 3.1: *The critical Reynolds number* $\mathrm{Re_c}$ *as function of the rotation ratio* $\hat{\mu}$. *(· · · · ·) denotes purely hydrodynamical marginal stability line. The flow is always hydrodynamically stable if the Rayleigh criterion for stability is fulfilled, i.e., on the right of* $\hat{\mu} = 0.25$. *The lines on the right of* $\hat{\mu} = 0.25$ *denote magnetohydrodynamic instability, (——)* $\mathrm{Pm} = 10^{-6}$, *(– – –)* $\mathrm{Pm} = 10^{-5}$. *The numbers indicate different values of* β. $\mathrm{Re_c}$ *is minimized over a range of values* Ha, k.

Generally it is easier to obtain instability when perfectly conducting cylinders are used unlike the insulating ones. Hereby the treatment of the magnetic boundary conditions for the walls (i.e., the radial ones) is such that the walls are assumed to be perfectly conducting. On the other hand, in this chapter the endplates (i.e., the vertical boundaries) are assumed to be insulating in order to minimize magnetic forces induces in their vicinity.

The aim of this chapter is to investigate nonlinearly saturated state of MHD Taylor-Couette flow embedded in the external helical magnetic field. We will focus on parameters resembling PROMISE facility and present results which helped to conduct the experiment. Results of the computations, with the numerical method outlined in Section 2.4, for periodic and finite cylinders are shown. It is found that the helical MRI exists also when the cylinders are finite.

3.2 Infinite container

First we have performed simulations for periodic vertical boundary conditions in order to compare the critical Reynolds numbers with results obtained from linear analysis. For this instability axisymmetric modes $m = 0$ are preferred to non-axisymmetric ones, which is usually the case both in non-magnetic Taylor-Couette flow as well as in classical $\beta = 0$ MRI. Therefore our assumption of axisymmetry in the numerical approach is valid. The method allows us also to obtain physical values of velocities in the nonlinear saturated state, which can not be found from the linear stability analysis.

For infinite cylinders and $\hat{\mu} = 0.27$ the flow is always hydrodynamically stable. With the external axial magnetic field it looses the stability for large Reynolds number of order $O(10^6)$, the additional toroidal current-free field can reduce this number to $O(10^3)$ – for $\beta = 3, 4$ the critical $\mathrm{Re_{crit}}$ is 1160 and 842, respectively. In the simulations the length of the periodic cylinders was chosen to be three times the wavelength obtained with linear analysis. The agreement between the previous and presented results is rather good, see Table 3.1.

Table 3.1: *Characteristic values for $\hat{\eta} = 0.5$ and $\hat{\mu} = 0.27$ taken from Rüdiger et al. (2005) for $\mathrm{Pm} = 10^{-5}$, $\mathrm{Re_c}$ is minimized over k, Ha for given $\mathrm{Pm}, \beta, \hat{\mu}, \hat{\eta}$. f_{cyl} represents the rotation frequency of the inner cylinder. $\mathrm{Re_c}^{b)}$ is the critical Reynolds number found with use of the code for given Ha, β, k (in the $\mathrm{Pm} \to 0$ limit). Simulations for different Re were accomplished, the presented values correspond to Re where the exponential growth rate becomes positive.*

β	Ha	k	$\mathrm{Re_c}^{a)}$	f_{cyl} [Hz]	$\mathrm{Re_c}^{b)}$
0.0	542	1.7	10^6	338	
1.0	38.4	0.6	33833	1.14	
2.0	14.6	1.3	2383	0.08	
3.0	10.7	1.6	1160	0.04	1248
4.0	9.5	2.0	842	0.028	860

3.2.1 Frequencies

Figure 3.2 shows snapshots of contour lines of the stream function for saturated state for Reynolds number just above the critical value $\mathrm{Re_c}$. Three pairs of drifting vortices can be seen, the drift direction and its velocity agrees with the previous results – it is slow, for gallium the period of the traveling wave is about 230 s for $\beta = 4$ which corresponds to $u_{\mathrm{drift}} = 0.5$ mm/s (the period of one rotation of the inner cylinder is about 35 s for $\mathrm{Re} = 900$).

From the experimental point of view it is also convenient to present traveling wave frequencies as function of $\hat{\mu}$ (Fig. 3.3). All the frequencies were obtained by taking the spectrum of the velocity component $u_z(t)$ in the middle of the gap (i.e. at $r = R_{\mathrm{in}} + D/2, z = \Gamma/2$) and then choosing the dominant frequency. Except for very small $\hat{\mu}$ the resulting frequencies are always smaller than the frequencies of the both cylinders. Beyond the Rayleigh limit (i.e., for $\hat{\mu} > 0.25$) the characteristic frequency is about 10% of the frequency of the inner cylinder. This means that beyond the timescale of rotation, another timescale exists, perhaps also in magnetic astrophysical

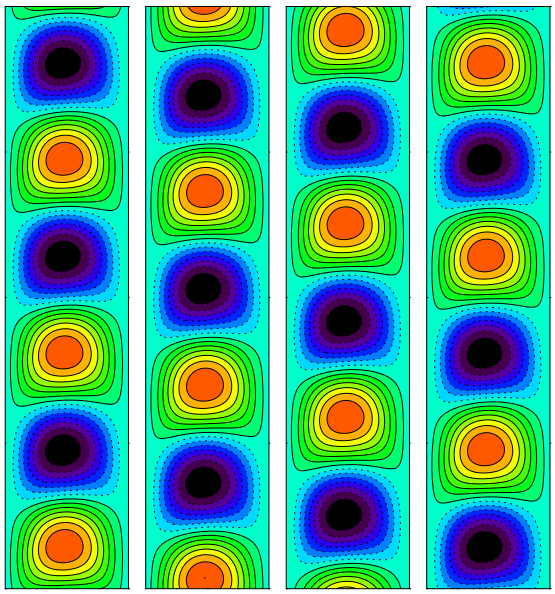

Figure 3.2: *Snapshots of contour lines of the stream function: dashed lines represent counter-clockwise rotation, solid lines clockwise rotation. $\mathrm{Ha} = 9.5, \mathrm{Re} = 900, \hat{\mu} = 0.27, \beta = 4, \Gamma = 9.4$, the time between snapshots is $\Delta t = 37$s. The fluid was initially at rest and then cylinders were suddenly accelerated to their final rotation rates. We notice drift of the fully developed Taylor vortices.*

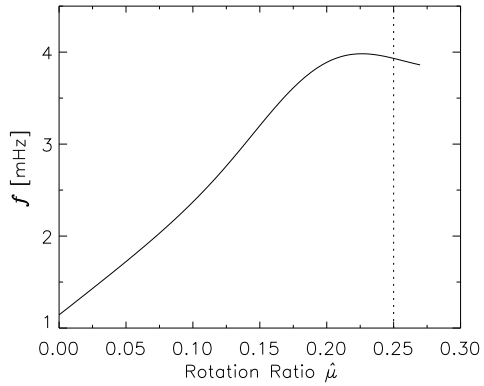

Figure 3.3: *Frequency of the traveling wave as a function of rotation ratio $\hat{\mu}$ for infinite cylinders, $\mathrm{Ha} = 9.5, \mathrm{Re} = 900, \beta = 4$. The units are scaled according to the physical properties of liquid used in the PROMISE experiment. The values were obtained by performing simulations for several different values of $\hat{\mu}$.*

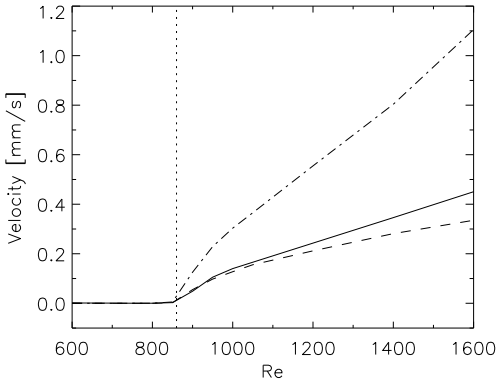

Figure 3.4: *Amplitudes of velocity (averaged in time) as a function of the Reynolds number. (——) $\max|u'_\phi|$ (deviation from the standard Couette solution Ω_0), (– – –) $\max|u_r|$, (·–·–·) $\max|u_z|$. The amplitudes increase from the critical point (vertical line) and continue to increase with* Re*. Periodic cylinders,* $\mathrm{Ha} = 9.5, \hat{\mu} = 0.27, \beta = 4$.

systems, which exceeds the rotation period by (say) a factor of ten. For the astrophysical scales it means that any phenomenon with such frequency would be difficult to observe.

It is worth to be mentioned that in the regime where the hydrodynamical instability operates the traveling wave also can be observed, so that the spiral nature of the imposed magnetic field forces the existing Taylor vortices to drift.

3.2.2 Velocity amplitudes

The solution in a nonlinear saturated regime provides information about magnitudes of physical variables which can me measured in an experiment. In a Taylor-Couette experiment the most important quantity to be observed is the fluid velocity. The PROMISE facility was equipped with two independent devices capable of measuring z component of the velocity along z axis at fixed distance $R = 6.4$ cm from the axis of rotation of the cylinders. Two such devices are necessary in order to distinguish between axisymmetric and non-axisymmetric flow (for details on the setup see Appendix A). The performed nonlinear calculations give information about magnitudes of the velocity and therefore the required accuracy of the measuring devices.

Figure 3.4 shows how maximum values of different components of the velocity depend on the Reynolds number Re. The velocities are zero up to critical point $\mathrm{Re}_{\mathrm{crit}}$ at which they start to increase with Re. We notice that the values of u_z, u_r, u'_ϕ become larger when increasing the rotation rates of the container and therefore it is easier to measure u_z for higher Re.

Naturally, if the rotation ratio $\hat{\mu}$ is smaller for fixed Ω_{in} (i.e., Ω_{out} is decreased), the magnitude of the velocity becomes larger since there are stronger shears in the radial direction. The dependence of the maximum amplitudes of velocity on $\hat{\mu}$ for constant $\mathrm{Re} = 900$[1] and $\beta = 4$ is depicted in Fig. 3.5. For any stable solution all the amplitudes should be zero just beyond the Rayleigh line, i.e., on the right of $\hat{\mu} = 0.25$. We see that with the additional toroidal field this is not the case – the velocities for $\hat{\mu} = 0.27$ are of order of 0.1 mm/s and drop to zero for $\hat{\mu} = 0.28$ for these parameters. From Fig. 3.1 it is clear that it is possible to get unstable solution also for $\hat{\mu} = 0.28, \beta = 4$ by increasing the rotation rates.

[1]We recall that in our notation Re is defined by Eq. 2.9 and depends only on Ω_{in}.

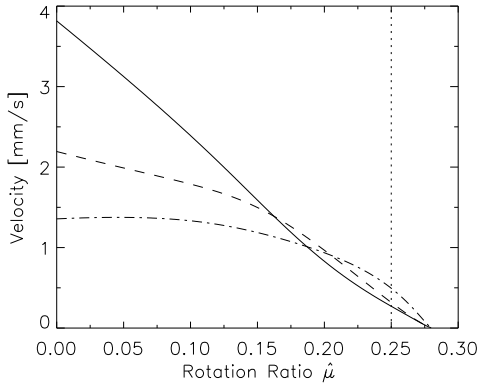

Figure 3.5: *Maximum amplitudes of the velocity (averaged in time) versus $\hat{\mu}$ for periodic cylinders,* $\mathrm{Re} = 900, \beta = 4, \mathrm{Ha} = 9.5$, *(——)* $\max|u'_\phi|$, *(– – –)* $\max|u_r|$, *(·–·–·)* $\max|u_z|$. *The vertical line denotes hydrodynamical stability threshold,* $\hat{\mu} = 0.25$.

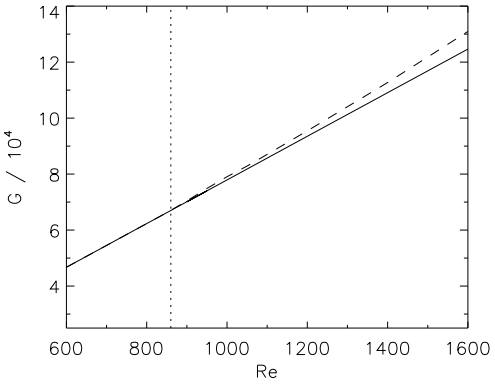

Figure 3.6: *Torque at the walls for two different β: (——) $\beta = 0$, (– – –) $\beta = 4$. Note that from the critical* $\mathrm{Re_c}$ *(the vertical line) for $\beta = 4$ the torque is larger than for the stable $\beta = 0$ case,* $\mathrm{Ha} = 9.5$, $\hat{\mu} = 0.27$.

3.2.3 The torque

From the conservation of angular momentum it follows that the change of the angular momentum is equal, in absence of any external forces, to the divergence of the stress tensor. For our axisymmetric case we can write

$$\partial_t(\rho l) = \mathrm{div}\, \boldsymbol{t}, \tag{3.1}$$

where $\boldsymbol{t}$ represents stresses acting on the fluid, l the specific angular momentum. The total torque T acting on a cylinder with radius r is

$$T(r) = \int_V \mathrm{div}(\boldsymbol{t})\mathrm{d}V, \tag{3.2}$$

the integration is done over the volume enclosing the cylinder. From the divergence theorem

$$T(r) = \oint_S \boldsymbol{t} \cdot \mathrm{d}\boldsymbol{S} \tag{3.3}$$

Therefore the total torque acting on the cylinder is equal to the angular momentum flux through its surface. The stresses which can contribute to the torque are the material, the magnetic and the viscous stress, hence (see e.g von Rekowski and Brandenburg, 2004; Liu et al., 2006b)

$$T(r) = \oint_S \left[\rho r u_r u'_\phi - \frac{r b_r b_\phi}{\mu_0} - r\rho\nu\partial_r\Omega(r)\right] \cdot \hat{n}\mathrm{d}S, \tag{3.4}$$

with $u'_\phi = u_\phi - r\Omega_0$. In a steady state the total torque is independent of r. In any case the only contribution to $T(r)$ at the walls with the no-slip boundary conditions is due to the viscous stress since the others vanish. Consequently the total torque at the outer wall R_{out} (similarly for R_{in}) for the cylinders with height H (also for the periodic cylinders with the assumed H) is

$$T(r = R_{\mathrm{out}}) = -2\pi \int_0^H (R_{\mathrm{out}})^3 \rho\nu\partial_r\Omega(r)|_{r=R_{\mathrm{out}}}\mathrm{d}z. \tag{3.5}$$

Usually it is presented as a non-dimensional quantity G

$$G = \frac{T}{\nu^2 H}. \tag{3.6}$$

For the unstable flow we expect the angular momentum to be transported outwards and therefore to increase the torque (3.5). From Fig. 3.6 we clearly see that indeed the torque is increased when the helical field with $\beta = 4$ is applied when compared to $\beta = 0$. The difference starts at the critical Reynolds number, i.e., when the Taylor vortices are formed.[2] The change of the torque is rather small and would be difficult to measure in an experiment, nevertheless in the computations for helical MRI the angular momentum is shown to be transported outwards.

3.3 Finite container

In any real Taylor-Couette experiment finite cylinders must be enclosed by endplates (when the upper one is missing a free-surface boundary conditions must be applied and the problem is changed significantly). It has been pointed out that the endplates can have significant impact on the flow, especially for short cylinders or for fast rotation rates (Hollerbach and Fournier, 2004; Kageyama et al., 2004). Consequently different methods for reduction of the endplates effect have been proposed (e.g. Burin et al., 2006). Here we are mainly interested in answering a question if the endplates, i.e., theirs mechanical and magnetic properties, influence the velocity amplitudes and frequencies for slow rotating finite cylinders with aspect ratio of $\Gamma = H/D = 10$ under the helical external magnetic field. In particular it is important to know whether the traveling wave solutions is not suppressed by the vertical boundaries.

3.3.1 Influence of the Ekman layer

The existence of the endplates results in developing an Ekman layer close to the vertical boundaries since the fluid is forced to match the corresponding boundary conditions. Two localized vortices, so-called Ekman vortices, arise in the vicinity of the endplates. In the vortices velocity differs from $\mathbf{\Omega}_0$ and they drive a global meridional flow: the Ekman circulation. The velocity in this region (which can dominate the fluid in the whole container) depends on the Reynolds number and the velocity of the endplates themselves. For non-rotating endplates (or rotating as a solid body with Ω_{out}) there is a radial inflow close to the boundaries and for solid-body rotation with Ω_{in} there is a radial outflow.

In the Rayleigh-stable regime the flow is hydrodynamically stable for both the infinite and finite containers, whereas for the latter two Ekman vortices are always present. We confirmed it with the numerical method that it is used here.

A simple estimate of the thickness of the Ekman layer for endplates rigidly rotating with Ω_{out} gives

$$\delta \approx \sqrt{\frac{\nu}{\bar{\Omega}}}, \tag{3.7}$$

where $\bar{\Omega} = \sqrt{\Omega_{\mathrm{in}}\Omega_{\mathrm{out}}}$. For the $\beta = 4$ critical transition, $\mathrm{Re_c} \approx 850$ and $\delta \approx 0.13\ \mathrm{cm}$, this is much larger value when compared to other experiments dealing with faster rotation rates (like

[2] The general scaling of G with Re in Taylor-Couette flow for large Re is a complicated issue. For more information, especially in turbulent regime, the reader can refer to e.g. Dubrulle and Hersant (2002). For example for moderate Re as of order up to $O(10^4)$ $G \propto \mathrm{Re}^{3/2}$, whereas for faster rotation it switches to different scalings.

$\mathrm{Re} \approx 10^6$; for example for the already mentioned New Mexico experiment $\delta \approx 0.1$mm). We can estimate the Reynolds number in the Ekman layer

$$\mathrm{Re}_\delta \approx \frac{D\bar{\Omega}\delta}{\nu} = \frac{D}{\delta}, \tag{3.8}$$

for the rotation rates of our interests Re_δ is of order $O(10)$. For other experiments with much larger Re, apart problems concerning domination the whole rotational profile by the plates, Re_δ can easily reach $O(10^3)$ (e.g. $\mathrm{Re}_\delta \approx 3000$ for the New Mexico device). Therefore, since Re_δ is in a region when one can expect transition from a laminar into a turbulent flow, it is likely that the layer, and consequently the whole flow in the container, will become turbulent. Naturally this is an undesirable effect and should be avoided.

The typical velocity in the bulk of the fluid due to the Ekman circulation can be approximated by

$$\bar{u_\delta} = \sqrt{\hat{\mu}\bar{\Omega}}, \tag{3.9}$$

which for $\mathrm{Re} = 900$ gives 0.02 cm/s. This is of the same order as velocities for the unstable case presented for infinite cylinders (see Fig. 3.5). For $\mathrm{Re} = 900$ the maximum value of u_z (in the corners of the container) is above 0.1 cm s^{-1} which is ten times more than the values computed for infinite cylinders. Therefore we should conclude that endplates, giving rise to velocities of that order, can significantly alter the flow.

In the computations it turns out that in the presence of an external axial field, the Ekman flow induces significant z-gradients and an electric Hartman current is generated. This can result in a magnetic instability even for small Reynolds number. Such undesirable effects can be significantly suppressed when insulating plates are used, therefore here we present results only for pseudo-vacuum boundary conditions. Full discussion concerning impact of the vertical boundaries on the Taylor-Couette flow in the presence of axial magnetic field is presented in the Chapter 5.

3.3.2 Amplitudes and frequencies

We have considered two different cases in terms of mechanical properties of the endplates: i) both plates rotate with angular velocity equal to that of the outer cylinder $\Omega_{\mathrm{top}} = \Omega_{\mathrm{bot}} = \Omega_{\mathrm{out}}$, ii) the bottom endplate is fixed $\Omega_{\mathrm{bot}} = 0$ while the upper rotates with $\Omega_{\mathrm{top}} = \Omega_{\mathrm{out}}$. The latter case is analogous to the PROMISE setup. However, here the both plates were assumed to be insulating whereas in the real experiment one of the ends was made from copper, the other from plexiglas. Although copper is considered as a good conductor it is significantly different, in terms of constrains on the boundary conditions, from a perfect conductor. Still, using plates made of material with different magnetic characteristic in reality introduced an additional asymmetry in the problem.

Figure 3.7 displays snapshots of contour line of stream function ψ for parameters which closely resemble the first run of the PROMISE (Stefani et al., 2006). We notice that the flow is complicated, the vortices deformed and highly irregular. The asymmetry of the vertical boundaries for the velocity is clearly seen – the Ekman pumping mechanism works differently at the bottom and at the top. Nevertheless one can observe that vortices develop and they move downwards as expected for the helical MRI instability.

Although the flow is at the first glance very irregular, still by investigating changes of, say, $u_z(r, z)$ (or any other dynamical variable) in time we can get a spectrum with a clear peak corresponding to a dominant frequency of the vertical traveling wave. Unlike for the case with infinite (periodic) cylinders, here the choice of the measurement position (r, z) makes difference

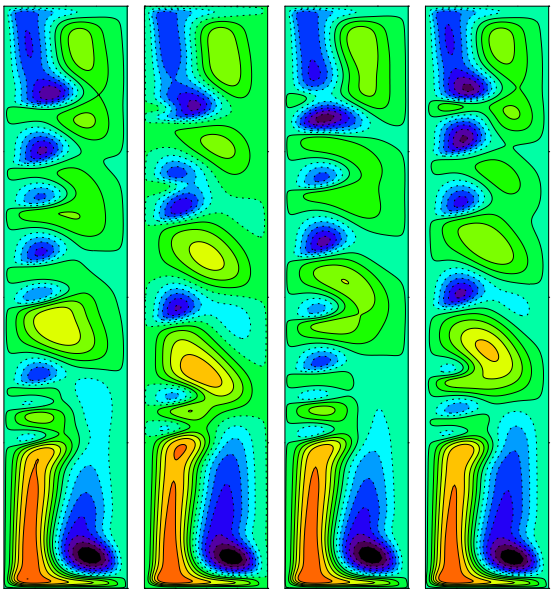

Figure 3.7: *Snapshots of contour lines of the stream function analog to Fig. 3.2 but for finite cylinders.* $\mathrm{Re} = 1480, \beta = 6, \mathrm{Ha} = 9.5, \hat{\mu} = 0.27$*, the time between snapshots is* $\Delta t = 47$*s. Insulating endplates, the bottom one is fixed, the upper one is rotating with* Ω_{out}.

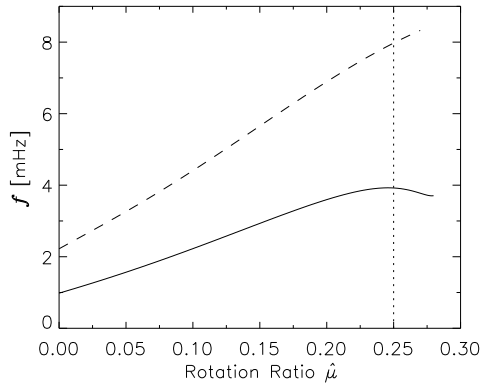

Figure 3.8: *Frequency as a function of the rotation ratio* $\hat{\mu}$ *for finite cylinders. a) (——)* $\beta = 4, \mathrm{Re} = 900, \mathrm{Ha} = 9.5$*, insulating endplates both rotating with* $\Omega_{\mathrm{bot}} = \Omega_{\mathrm{top}} = \Omega_{\mathrm{out}}$*. b) (– – –)* $\beta = 6, \mathrm{Re} = 1480, \mathrm{Ha} = 9.52$*, insulating endplates, bottom: fixed* $\Omega_{\mathrm{bot}} = 0$*, upper: rotating* $\Omega_{\mathrm{top}} = \Omega_{\mathrm{out}}$.

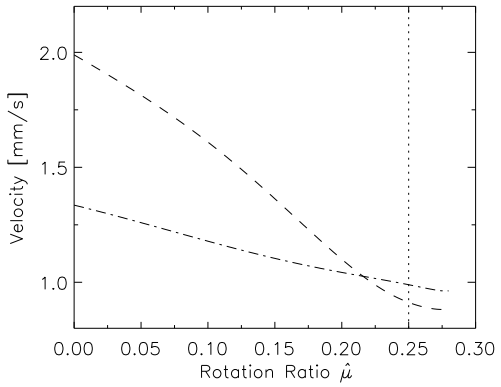

Figure 3.9: *Amplitudes of the velocity for finite cylinders, cf. Fig. 3.5, (– – –)* $\max|u_r|$*, (·–·–·)* $\max|u_z|$*,* $\mathrm{Re} = 900, \beta = 4, \mathrm{Ha} = 9.5$*, Insulating endplates (the pseudo-vacuum boundary conditions) rotating with the outer cylinder* $\Omega_{\mathrm{end}} = \Omega_{\mathrm{out}}$.

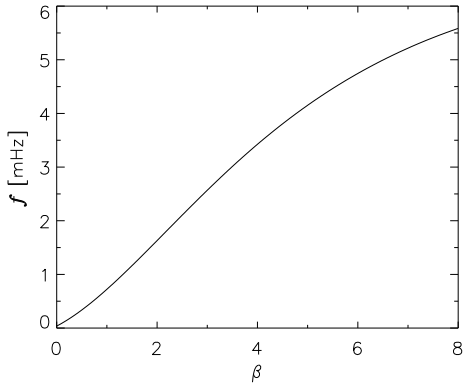

Figure 3.10: *Frequencies of the traveling wave in the middle of the gap for finite cylinders as function of* β. $\mathrm{Re} = 900, \hat{\mu} = 0.27, \mathrm{Ha} = 9.5$*, insulating endplates rotating with* Ω_{out}.

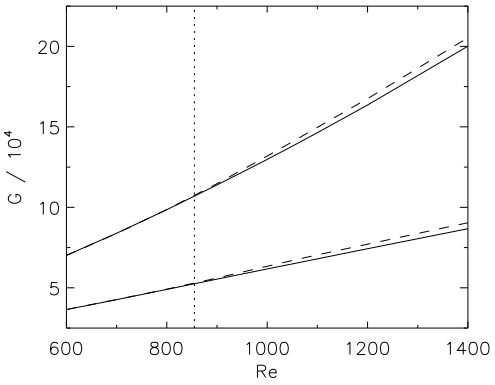

Figure 3.11: *Torque at the walls for finite cylinders for different values of* β*: (——)* $\beta = 0$*, (– – –)* $\beta = 4$. $\mathrm{Re} = 900, \mathrm{Ha} = 9.5, \hat{\mu} = 0.27$. *The upper lines correspond to the inner cylinder, the lower ones to the outer. The vertical line denotes critical Reynolds number* $\mathrm{Re_c}$.

since the flow is completely suppressed at the boundaries and u_z close to them would give wrong results. Bearing in mind that the flow near the middle of the container is least affected by the boundaries we chose straightforward $u_z(r = 6.4$ cm, $z = H/2)$, where the value of radius $r = 6.4$ cm is used accordingly to placement of the measuring devices in the PROMISE facility.

The dependence of the traveling wave frequency f on the rotation ratio $\hat{\mu}$ is shown in Fig. 3.8. Two different cases are presented: a) symmetrically rotating plates with parameters analogous to that from Fig. 3.3, b) faster rotation, higher β and plates rotating with different Ω, similar like in the PROMISE setup. We notice that the observed frequency in the case a) closely resembles results for the periodic cylinders so that it is evident that helical MRI produces the traveling wave also for the enclosed system.

The results for the case b) show that also for the asymmetric mechanical boundary conditions the traveling wave can be easily identified. The higher frequency is due to different parameters, especially β. The dependence of the frequency on strength of the imposed azimuthal component of the magnetic field is presented in Fig. 3.10. We notice that this frequency can also be obtained when β is small, i.e., in case when the flow is in stable regime for the periodic cylinders. The reason for such behavior is that for the flow with endplates, there exist some vortices even if there is only axial field imposed (which is obviously not true for the periodic case). Due to the spiral nature of the applied magnetic field the vortices are drifting. This matter will be discussed in more details in Chapter 4.

The velocity amplitudes for finite cylinders just above the critical Reynolds number are shown in Fig. 3.9. We notice that due to the Ekman circulation those velocities do *not* drop to zero even for $\hat{\mu} = 0.28$, which was true for the periodic cylinders. In the middle of the container, far from the boundaries the z component of the velocity reaches value up to about 0.7 mm/s, see Fig 3.12. This is enough to be detected by the devices used in the experiment.

Similarly like for the infinite case one can also observe the increase of the torque in comparison with $\beta = 0$ case (Fig. 3.11). When the plates are present the torque is also transferred due to theirs influence (like the Ekman pumping) and consequently there is the difference in a value for the inner and outer cylinder. We notice that the torque at the both walls increases from the critical point $\mathrm{Re_c}$ computed for the infinite (or periodic) cylinders.

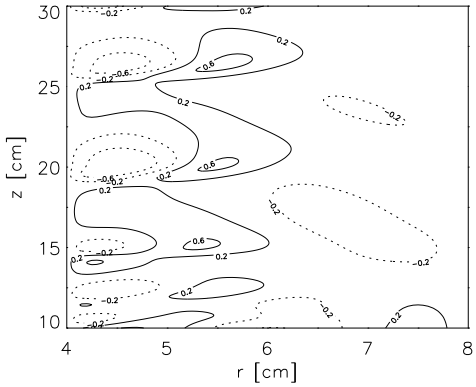

Figure 3.12: *Contour lines of u_z corresponding to the state presented in the last snapshot in Fig. 3.7. The lines are drawn for values of u_z: -0.6, -0.2, 0.2, 0.6 mm s^{-1}, only the middle part of the cylinders is shown, the drawing is not at scale.*

3.4 Keplerian rotation

We have shown that the MHD Taylor-Couette flow becomes unstable in the hydrodynamically stable regime when a helical magnetic field is applied. This instability works for small Reynolds number and can also be observed for a finite aspect ratio Γ. In particular the traveling wave is not suppressed for the parameters characterizing the PROMISE experiment, i.e., $\Gamma = 10$.

However from astrophysical point of view it is interesting to see if this type of MRI operates for much flatter rotation profiles, especially for Keplerian (like in accretion disks). In the geometry of our interest the Keplerian profile corresponds to $\hat{\mu} = 0.3535$, from Fig. 3.1 we notice that the critical Reynolds number becomes significantly larger with $\hat{\mu}$, yet the figure does not show what happens for $\hat{\mu} > 0.31$.

An important question arise: does the helical MRI exist for the Keplerian rotation? If yes, does it operate in the small $\mathrm{Pm} \to 0$ limit? Former results indicate that for flatter profiles scaling Re with Pm becomes more alike the scaling for the classical MRI with axial magnetic field only (recall that this classical MRI does not exist for $\mathrm{Pm} \to 0$).

Liu et al. (2006a) argued that from WKB analysis it follows that the helical MRI does not work for the Keplerian rotation (more precisely they did this for profiles $\Omega \propto r^n$, and concluded that the necessary conditions is $n < -1.66$, whereas the Keplerian profile yields $n = -1.5$). However the WKB analysis is local so it does not take into account the global problem and associated boundary conditions. Rüdiger and Hollerbach (2007) have shown that, in the $\mathrm{Pm} \to 0$ limit (which assures that the instability is of the helical type) it is possible to get unstable flow for Keplerian rotation provided that the radial boundaries are taken into consideration and one of them is at least somewhat conducting. In particular it is enough that the conductance of the inner boundary is only half of that of the fluid. Solely when the both boundaries are insulating the helical instability ceases to exist for quasi-Keplerian Couette flows.

Figure 3.13 displays how the critical Reynolds number depends on $\hat{\mu}$ and β for two cases: the inner boundary conducting, the outer insulating and the both boundaries insulating. We notice that in the former case the flow for $\hat{\mu} = 0.3535$ is unstable when Re_c is of order $O(10^4 - 10^5)$ and the imposed azimuthal field is not too strong. Although for both conducting cylinders Re_c is smaller it is still necessary to apply rotation rates corresponding to $\mathrm{Re}_\mathrm{c} \approx 10^4$ to get the unstable flow. Such high Reynolds numbers are beyond reach of the numerical method used here due to constrains on time step and grid size (we have reported simulations up to $\mathrm{Re} \approx 2500$). Consequently flows with Keplerian rotational profiles can not be here directly studied in the nonlinear regime.

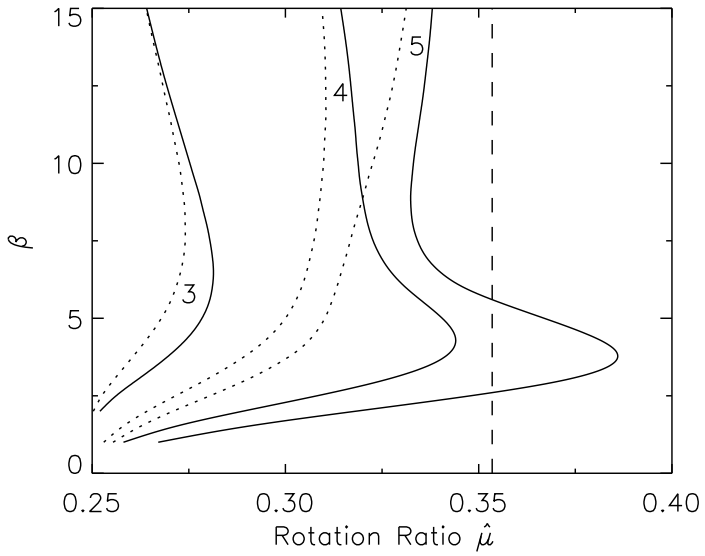

Figure 3.13: *Contours of* $\log(\mathrm{Re_c})$ *as a function of rotation rate* $\hat{\mu}$ *and* β. $\mathrm{Re_c}$ *is minimized over* Ha, k, $\mathrm{Pm} \to 0$ *is assumed, the cylinders are infinitely long. (——) the inner cylinder is perfectly conducting, the outer insulating. (· · · · ·) both the cylinders are insulating. The vertical line indicates quasi-Keplerian rotation,* $\hat{\mu} = (R_{\mathrm{in}}/R_{\mathrm{out}})^{3/2}$.

3.5 Summary

Hollerbach and Rüdiger (2005) have proposed a novel configuration of external magnetic field that could be applied to the magnetized Taylor-Couette flow. Due to the additional azimuthal component of the field it is possible to bring rotation rates to much smaller, by three to four orders of magnitude, values when compared to the classical MRI with axial magnetic field only. Therefore the helical MRI is suitable for an experiment with liquid metals. Moreover, it operates also for $\mathrm{Pm} \to 0$.

We have shown above that our quasi-static approximation (2.11) for axisymmetric flow yields very similar critical values for the critical Reynolds number as the linear analysis for finite Pm for conducting, periodic cylinders. The expected traveling wave is also observed and the Taylor vortices undergo a slow, yet easily measurable, drift. When the cylinders are enclosed by endplates the drift still can be observed and the helical MRI is not suppressed.

The fluid velocity amplitudes u_r, u_z, u'_ϕ, which were not known until now, are small: 0.1-1 mm/s, still it is not very difficult to measure them experimentally. We shall also mention that increasing Reynolds numbers result in linear (at least to some point) increase of velocity amplitudes therefore it is easier to detect them for higher Re. However, for too high rotation rates the assumption of axisymmetry may not be valid.

The drift velocity of the vortices can easily be detected by investigating changes of the velocity field. The drift itself is quite slow. The frequency of the traveling wave is about 10% of the rotation so and consequently the drift velocity is about 0.5 mm/s.

For finite aspect ratio calculations the velocities induced by Ekman pumping are of similar order as those resulting from the instability. Therefore one should not neglect the influence of the endplates in such experiments, clearly they alter the flow when compared to the periodic boundary conditions. In the next chapter we propose simple and inexpensive methods of reducing influence of the plates.

The helical MRI also operates for quasi-Keplerian rotation rates if at least one of the radial boundaries is somewhat conducting. In our treatment of the boundary conditions the both cylin-

ders are assumed to be perfectly conducting. However, for flat profiles like $\hat{\mu} = 0.35$ the rotation rates are beyond reach of the numerical method which is used to solved the nonlinear equations (2.11). For example for $\beta = 4$ and $\hat{\mu} = 0.35$, Reynolds number of order 2×10^4 is required for instability to grow.

Chapter 4
Reduction of boundary effects

4.1 Introduction

In the previous chapter we have shown that an MHD Taylor-Couette flow under an external magnetic field with both an axial and an azimuthal component becomes unstable for relatively small Reynolds number. Moreover, vertical boundary conditions associated with plates enclosing finite container do not destroy such instability.

In reality the idea of the additional azimuthal field was successfully implemented in the PROMISE experiment by Stefani et al. (2006) where modes corresponding to helical MRI were observed for the first time (see also Stefani et al., 2007). Results of this experiment also show that in the basic stable state, without any toroidal field, there exists a non-zero axial velocity field which arises due to presence of the rigid endplates enclosing the cylinders. These plates, undoubtedly present in any real experiment, are responsible for additional effects which do not take place for an idealized infinitely long container.

The boundary layer which exists in the vicinity of the endplates consists of an Ekman layer which is a result of the rotation of a rigid surface, and a Hartmann layer which develops when a conducting fluid is used and an external axial magnetic field is applied (see e.g. Ekman, 1905; Roberts, 1967). Consequently, the global properties of the flow change when compared to the idealized case of infinitely long cylinders: a secondary flow, i.e. two large Ekman vortices appear, and the Hartmann current is drawn into the bulk of the fluid. All these effects depend on the mechanical and magnetic properties of the lids. In the PROMISE experiment one of the lids is made of copper and is attached to the outer cylinder, the other one is a stationary plexiglass plate.

In this chapter we review simple improvements which can reduce undesired effects induced by the lids and provide therefore the possibility to distinguish more clearly between stable and unstable states of the MRI.

4.2 Periodic cylinders

From the point of view of the MRI experiment we are interested in obtaining a stable rotation profile which for subcritical characteristic parameters is as close as possible to the idealized basic state Ω_0. On the other hand we expect a clear pattern of traveling vortices for supercritical conditions. For infinite cylinders with an external axial magnetic field and liquids with Pm of our interest the basic Couette profile Ω_0 is not altered until a critical Reynolds number of order $O(10^6$–$10^7)$ is reached (corresponding to a rotation frequency $f \gtrsim 100$ Hz). For an instability due to the additional toroidal field with $\beta = 4$ we expect Re to be of order $O(10^3)$ (implying

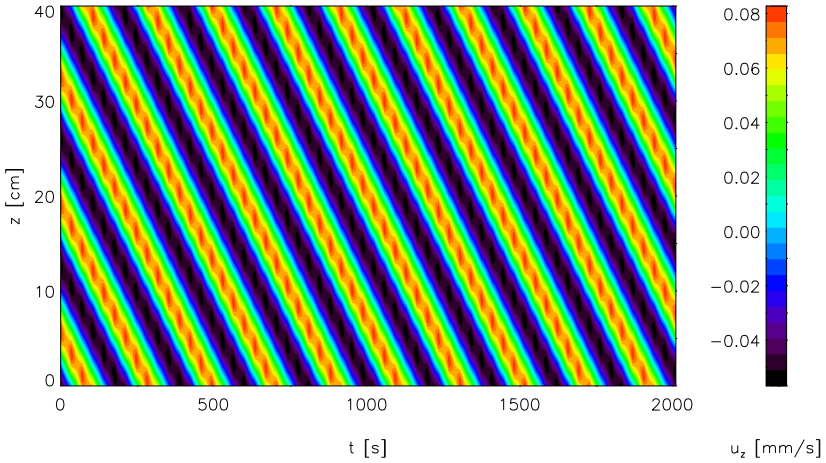

Figure 4.1: *Profiles of $u_z(z,t)$ at $r = R_{\rm in} + 0.6\,D$ for periodic cylinders just above the critical characteristic values:* $\mathrm{Re} = 1000, \mathrm{Ha} = 9.5, \beta = 4$. *The critical Reynolds number in this case is* $\mathrm{Re}_c = 842$.

$f \approx 0.1$ Hz), Ha of order $O(10)$, and therefore we search for conditions for which the flow is closest to the Ω_0 profile for these parameters.

Figure 4.1 displays values of the velocity component u_z measured along the z axis at $r = R_{\rm in} + 0.6D$ for supercritical values of rotation and magnetic fields.[1] $R_{\rm in} = 4$ cm, $R_{\rm out} = 8$ cm, and the physical properties of gallium for the viscosity and the magnetic diffusivity are used in order to obtain values in physical scales comparable with those of the PROMISE experiment. The results in this figure are for cylinders with periodic boundary conditions so that the profiles are not constrained by end-effects and are directly comparable with results from linear theory for infinite cylinders. We notice clear traces of the drifting Taylor vortices.

4.3 Reducing endplates effects

All undesirable effects induced by the endplates arise as a consequence of vertical shears near the boundaries. Thus we attempt to reduce the shears by using appropriate boundary conditions. Some experiments (Noguchi et al., 2002; Ji et al., 2004) must deal with vast rotation rates since the azimuthal field is not applied (i.e. $\beta = 0$) and the rigidly rotating boundaries dominate the whole flow. In this case it is necessary to split the end-plates into many independently rotating rings (Kageyama et al., 2004; Burin et al., 2006). When the rotation rates are relatively slow, so that the corresponding Reynolds number is of order $O(10^3)$, the desired result can be achieved either by allowing the endplates to rotate rigidly and independently of the cylinders (see e.g. Abshagen et al., 2004) or by splitting them into two rings which are attached to the both cylinders. From technical point of view the latter configuration is easier to implement and can be considered as a possible extension to the next spiral MRI experiment. An experiment with the independently rotating plates would require an additional driving systems for the both plates.

Firstly we consider a criterion according to which we say that the boundary conditions are more suitable. In the basic state for subcritical parameters for the case of periodic cylinders the rotational profile of the fluid is $\Omega_0(r)$ and is independent of z, and the magnetic perturbations $\boldsymbol{b}$ are zero everywhere. Introducing endplates leads to the development of z and r gradients in velocity, especially close to the vertical boundaries where $\Omega(r)$ from the bulk of the fluid must

[1] Visualizing data in such a way is straightforward since in the real experiment $u_z(z)$ is measured along the z axis at the distance $0.4D$ from the inner cylinder and sampled every $\approx$ sec.

match the imposed conditions at $z = 0,\ z = H$. Consequently two Ekman vortices, new currents and magnetic fields are generated (here we assume the lids to be insulating unless explicitly stated otherwise). Any deviation from $\mathbf{\Omega}_0$ will result in generating an azimuthal component of the magnetic field, b_ϕ, its z-gradient enters the momentum equation (and in our 2D axisymmetric formulation it is the only term which gives rise to the Lorentz force).

Vertical profiles of b_ϕ in the middle, i.e. for $r = D/2$, are shown in Fig. 4.2 for two different boundary conditions. If the endplates rotate rigidly with the outer cylinder, $\Omega_{\rm end} = \Omega_{\rm out}$, the Ekman circulation at the bottom lid has a clockwise direction, if they rotate with the inner cylinder, $\Omega_{\rm end} = \Omega_{\rm in}$, counter-clockwise: all the gradients have opposite sign. We conclude that, not surprisingly, there exists a condition with $\Omega_{\rm out} < \Omega_{\rm endmin} < \Omega_{\rm in}$ for which the shears are minimized and the generated magnetic field as well.

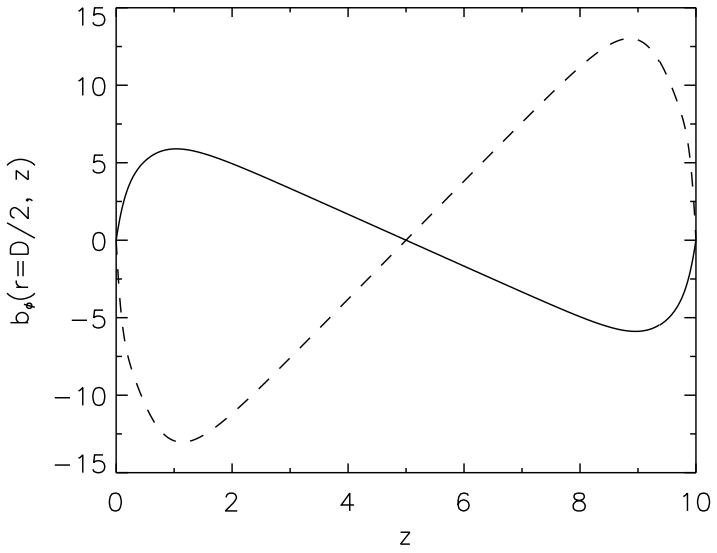

Figure 4.2: *Vertical profiles for the induced b_ϕ in the middle of the gap, $r = D/2$ for $\beta = 0, \mathrm{Re} = 100, \mathrm{Ha} = 1$ and insulating boundary conditions. (——) $\Omega_{\rm end} = \Omega_{\rm out}$, (– – –) $\Omega_{\rm end} = \Omega_{\rm in}$.*

We are interested in obtaining a rotational profile for which the energy in b_ϕ is minimized,

$$E_b = \iint b_\phi(r,z)^2 \mathrm{d}r\mathrm{d}z, \tag{4.1}$$

where the integration is done over the total volume. As a measure of the deviation from Ω_0 one could also consider, for example, the kinetic energy of the flow. However, since our aim is to obtain good rotational profiles also for Ha of order 10 (and $\beta = 0$) this is not necessarily a good approach: the axial field can inhibit the flow velocity while the rotational profile will still be significantly different from $\mathbf{\Omega}_0$.

Figure 4.3 shows how E_b depends on the rotation rates of the rigid endplates, $\Omega_{\rm in} < \Omega_{\rm end} < \Omega_{\rm out}$. We notice that a minimum of E_b occurs for $\Omega_{\rm endmin} \approx 0.3(\Omega_{\rm in} - \Omega_{\rm out}) + \Omega_{\rm out}$ which is even three orders of magnitude smaller than for $\Omega_{\rm end} = \Omega_{\rm in}$.

When considering endplates divided into two rings we assume that the ring attached to the inner cylinder has a width w_1, the other one attached to the outer cylinder has $w_2 = D - w_1$. Because it is not obvious which value for w_1 should be chosen we search for the optimal w_1, i.e. for which E_b has a minimum, by performing simulations for several different values (Wendt, 1933, for example, used $w_1/D = 0.5$), From Fig. 4.4 we see that the energy of the induced b_ϕ has a minimum for $w_1/D \approx 0.4$ which is roughly independent of the applied axial magnetic field.

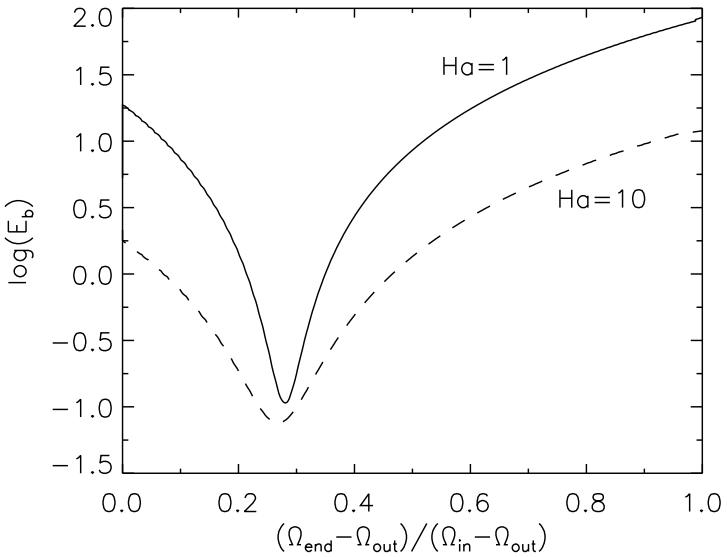

Figure 4.3: *The magnetic energy E_b as a function of angular velocity of independently rotating endplates, $\Omega_{\rm end}$, for $\beta = 0, \mathrm{Re} = 100$. (——) $\mathrm{Ha} = 1$, (– – –) $\mathrm{Ha} = 10$.*

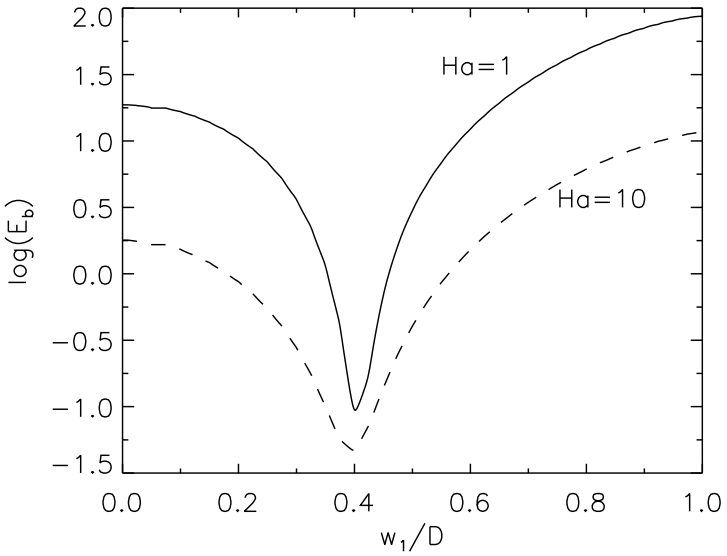

Figure 4.4: *The magnetic energy E_b as a function of radius of the inner ring for $\beta = 0, \mathrm{Re} = 100$. (——) $\mathrm{Ha} = 1$, (– – –) $\mathrm{Ha} = 10$.*

It has also been checked that the minimum holds for larger Reynolds numbers (for the Fig. 4.3 as well). Again we notice the improvement of E_b of two to three orders of magnitude when compared to one end-ring attached either to the inner ($w_1 = D$) or the outer ($w_1 = 0$) cylinder. The minimum value is very similar to that for independently rotating endplates.

A qualitative view of the resulting rotational profiles gives Fig. 4.5 which displays deviations of $\bar{\Omega}(r)$ – the angular velocity averaged in the z domain – from $\Omega_0(r)$ for different rotational properties of the endplates and for varied Re and magnetic field strength. The case with independently rotating endplates refers to boundary conditions where the both lids rotate with angular velocity $\Omega_{\rm end}$ corresponding to the minimum value of E_b. For comparison we also present the case for two rings attached to the cylinders with equal width $w_1 = w_2 = D/2$.

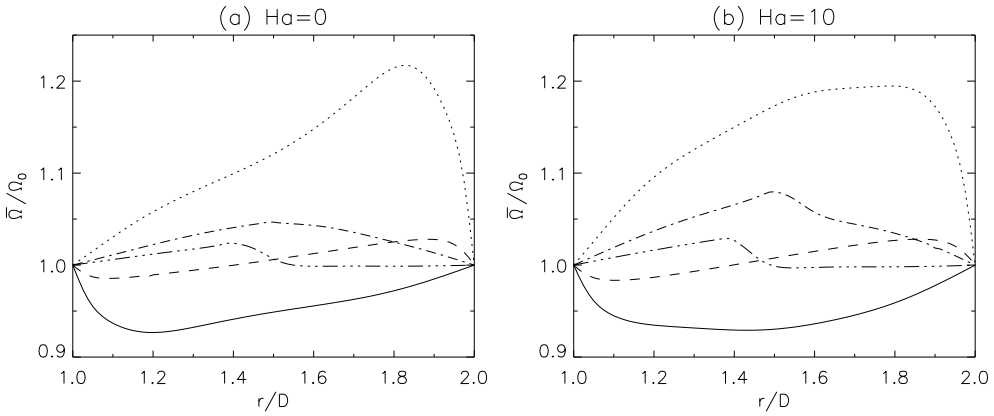

Figure 4.5: *Deviations of the averaged $\bar{\Omega}(r)$ from the basic state $\Omega_0(r)$ for different vertical boundary conditions; rigidly rotating endplates (both with $\Omega_{\rm end}$): (——) $\Omega_{\rm end} = \Omega_{\rm out}$, (· · · · · ·) $\Omega_{\rm end} = \Omega_{\rm in}$, (– – –) $\Omega_{\rm end} = \Omega_{\rm endmin}$; divided into two rings: (·—·—·) $w_1 = 0.5$, (· · · — · · ·) $w_1 = 0.4$. (a) $\mathrm{Re} = 1000,\ \mathrm{Ha} = 0$, (b) $\mathrm{Re} = 1000,\ \mathrm{Ha} = 10$.*

We see that applying independently rotating or split endplates produce significantly more suitable profiles – flatter and closer to 1. We also notice that using $w_1 = 0.4D$ gives somewhat better results than $w_1 = 0.5D$, especially for $r > R_{\rm in} + D/2$ where the former profile is almost flat.

More details about the flow for selected boundaries reveal Figs. 4.6 and 4.7, where the cross sections in r, z plane are presented for different dynamical variables u_ϕ, ψ, b_ϕ. Fig. 4.6 shows the situation without any magnetic field for the case when the plates rotate with $\Omega_{\rm end} = \Omega_{\rm out}$. We notice that u_ϕ significantly depends on z so that the rotational profile differs from $\mathbf{\Omega}_0$, two large Ekman vortices fill the whole container. If the plates are replaced by two rings, the flow looks much better: u_ϕ is almost independent of z in major part of the container, the Ekman circulation is not so dominating.

If the axial magnetic field is applied (Fig. 4.7), the situation changes importantly. For the endplates rotating rigidly $\Omega_{\rm end} = \Omega_{\rm out}$ the rotational profile becomes even worst than for non-magnetic case. Due to interaction of induced currents and the magnetic field vortices develop, moreover the flow is not steady. The second case, with two rings attached to the cylinders, looks much better: it is almost unchanged when compared to $\mathrm{Ha} = 0$ (it is even a bit improved in the sense discussed above, cf. Fig. 4.4). In this case the induced b_ϕ is about five times smaller when compared to $\Omega_{\rm end} = \Omega_{\rm out}$ and especially it is small far from the boundaries.

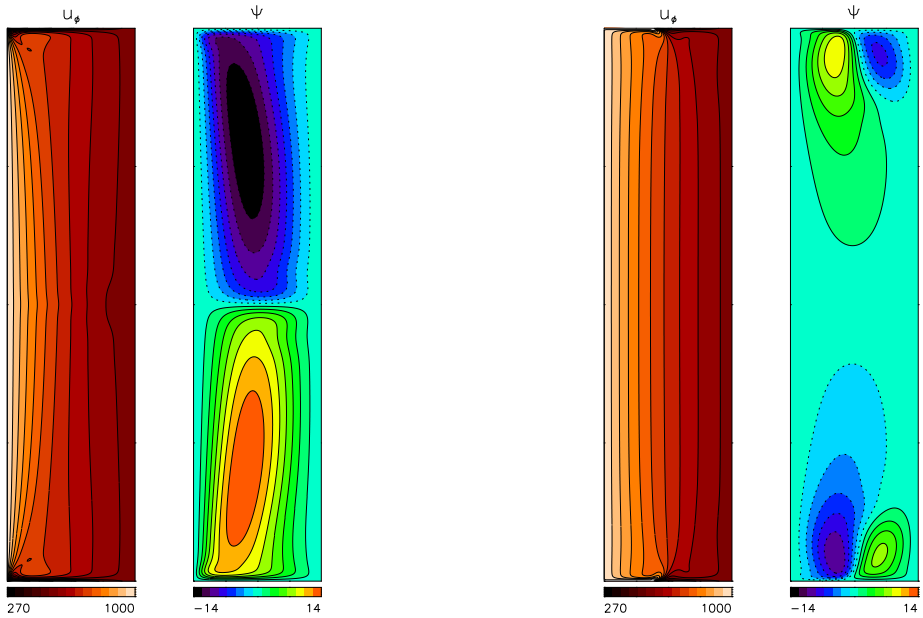

Figure 4.6: *Contour lines of u_ϕ, ψ for two different vertical boundary conditions. Left: both endplates rotate rigidly with $\Omega_{\rm end} = \Omega_{\rm out}$. Right: endplates are divided into two rings attached to the cylinders. Ratio of width of the inner ring to the gap width is 0.4. There is no magnetic field applied.* $\mathrm{Re} = 1000, \hat{\mu} = 0.27, \beta = 0$.

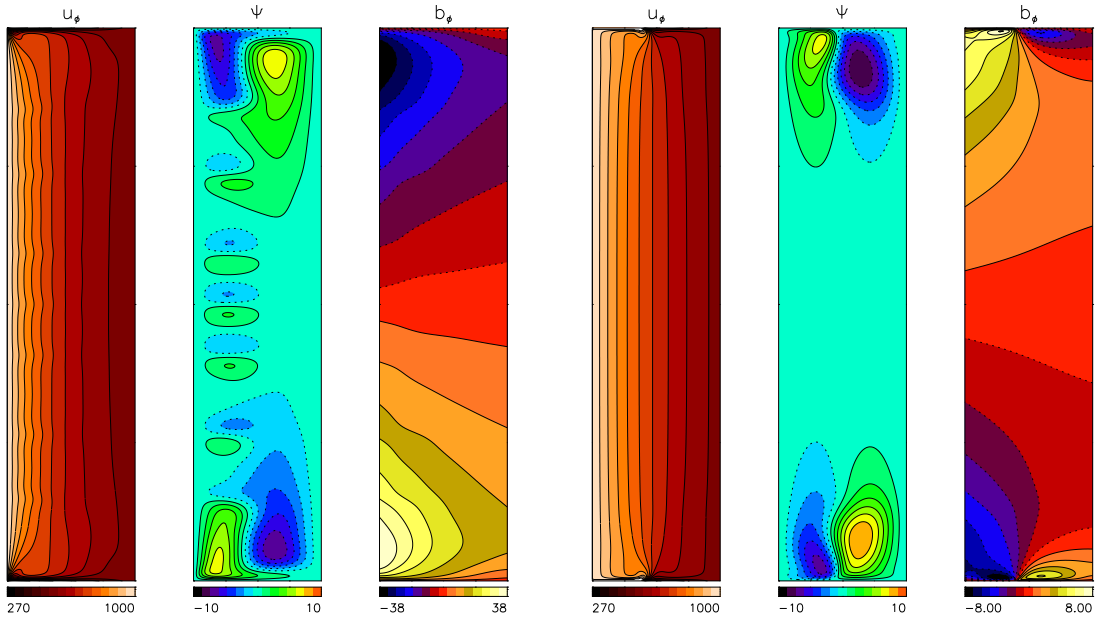

Figure 4.7: *Similar like in Fig. 4.6 but here the quite strong external axial magnetic field is applied,* $\mathrm{Ha} = 10$. *Notice significant difference in strength of the induced b_ϕ for the both cases. The vertical boundaries are insulating.*

4.4 Influence of the helical field

Figure 4.8 shows values of the velocity component u_z similarly like Fig. 4.1 but for various configurations for finite cylinders. The velocity field u_z in the basic state, i.e. $\beta = 0$ for which there is no instability, is $u_z = 0$ everywhere when considering infinite or periodic cylinders for $\mathrm{Re} \approx 10^3, \mathrm{Ha} \approx 10$. For the enclosed cylinder this is not the case. In Fig. 4.8a (left) we present results for symmetrically, rigidly rotating (with Ω_{out}), insulating endplates. We notice that u_z is quite large and, more importantly, time dependent (this is even more evident for u_z closer to the inner cylinder). The right panel in this figure displays the same flow with the toroidal field applied, $u_z(z)$ is averaged in time and subtracted in order to filter out the background. We clearly see the instability and structure of traveling vortices, the frequency of this motion agrees with the predictions based on the linear analysis.

As we have shown above, one can obtain a much better basic state for the finite cylinders by dividing endplates into two rings. The results for such conditions are presented in Fig. 4.8b. We notice that the background state quickly becomes entirely steady. Naturally the Ekman pumping mechanism is still present in this case, and traces of two Ekman vortices can be seen. The flow, however, is laminar. For $\beta = 6$ the pattern of the traveling vortices is clearly more regular (cf. Fig. 4.8b, right).

When one considers two endplates with different rotational properties, additional velocity and current gradients in the vertical direction arise and disturb further the flow. It is clearly seen in Fig. 4.8c that disturbances exist in the case where the upper endplate rotates with $\Omega_{\mathrm{top}} = \Omega_{\mathrm{out}}$, and the bottom one is fixed, $\Omega_{\mathrm{bot}} = 0$. The background flow for $\beta = 0$ is highly irregular and time-dependent, especially in the middle part of the cylinder. The circulation close to the endplates is roughly steady. Nonetheless, the additional external B_ϕ produces, again, a clear periodic motion with a frequency corresponding to that of the helical MRI.

Using conducting boundaries instead of insulating ones leads to an increase of the Ekman circulation and the Hartmann current, the latter being drawn from the plates. This current is significantly stronger than the current generated in the Ekman-Hartmann layer and therefore we expect that an experiment with conducting plates would undergo additional problems due to magnetic forces acting on the fluid. Let us consider a perfectly conducting endplates with asymmetric rotation (again at the top $\Omega_{\mathrm{top}} = \Omega_{\mathrm{out}}$ and at the bottom $\Omega_{\mathrm{bot}} = 0$), then there exists an important gradient in the radial current which, acting in concert with the axial magnetic field, is strong enough to „drag" vortices in the direction of decreasing field strength. This situation is shown in Fig. 4.8d where we see a periodic vertical motion even if $\beta = 0$. Moreover, if we introduce a toroidal field with appropriate sign (i.e. positive in this case) it will act against the force due to the current gradient and can reduce the periodic vertical motions in the flow (Fig. 4.8d, right panel). If B_ϕ would have a different sign both effects would interact resulting in a highly irregular time-dependent behavior.

We notice that in the real PROMISE experiment the bottom endplate rotating with Ω_{out} (which, after taking into account the directions of rotation and the applied magnetic field, corresponds to the top endplate in our simulations) was made of copper, and the stationary top endplate (bottom in the simulations) was made of plexiglass. Therefore an additional asymmetry in the magnetic boundary conditions was present. Although copper is a good conductor it should not be directly compared with perfectly conducting boundaries used in the simulations since the latter represent stronger assumptions and induce stronger currents. However it is clear that using insulating material on both ends would prevent additional currents from disturbing the flow.

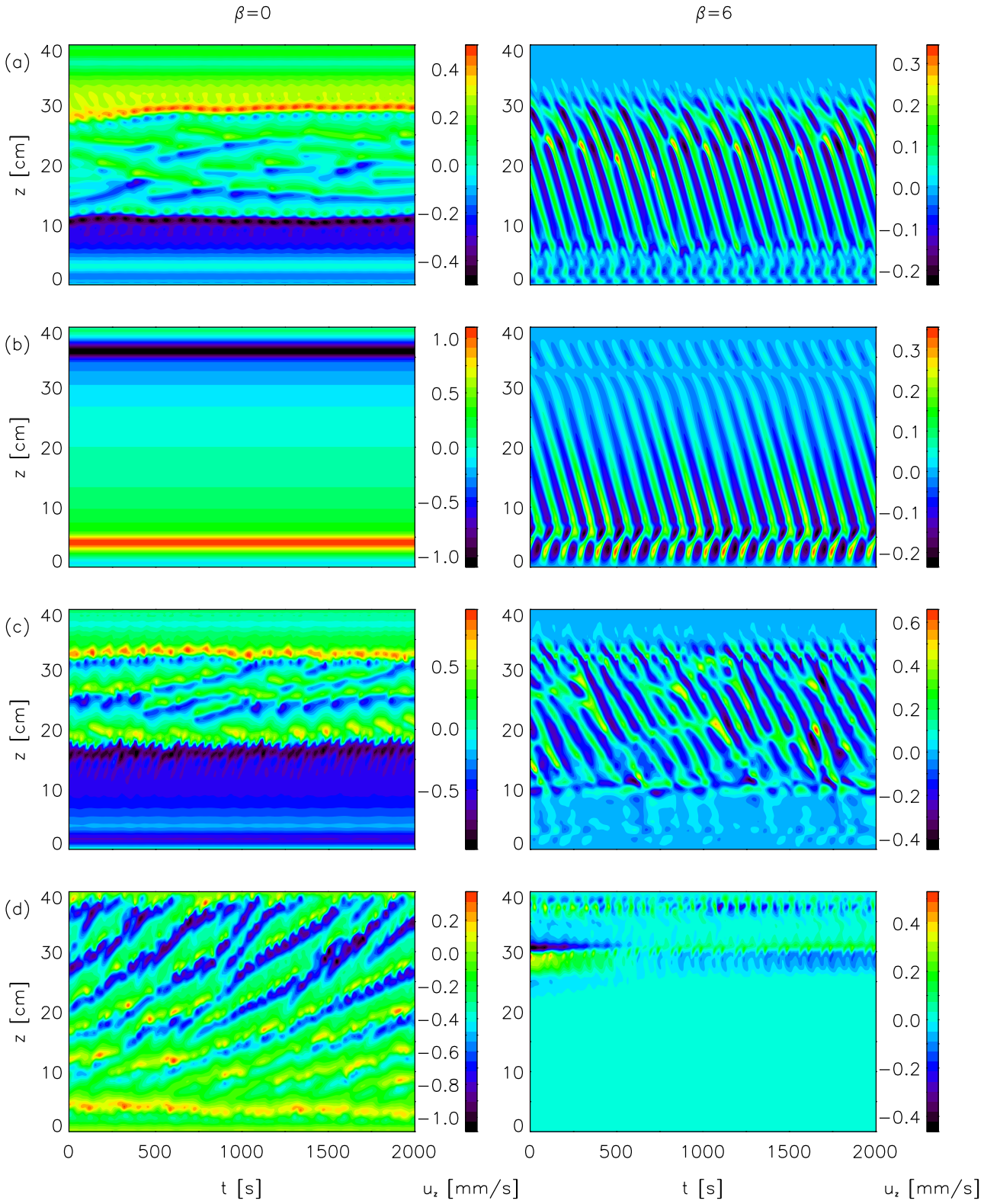

Figure 4.8: *The axial velocity $u_z(z,t)$ at $r = R_{\rm in} + 0.6D$ as a function of time t and z.* Left*: basic state $\beta = 0$.* Right*: $\beta = 6$, the averaged $u_z(t)$ is subtracted in order to eliminate the background from the velocity field, except in (d). (a): both endplates rotate rigidly with $\Omega_{\rm end} = \Omega_{\rm out}$. (b): both endplates are divided into rings attached to the cylinders; the inner ring has the width $0.4D$. (c), (d): the bottom endplate is stationary $\Omega_{\rm bot} = 0$, the upper one rotates with $\Omega_{\rm top} = \Omega_{\rm out}$. (a), (b), (c): insulating endplates, $\mathrm{Re} = 1775$ ($\Omega_{\rm in} = 0.377$ Hz), $\mathrm{Ha} = 9.5$. (d): perfectly conducting endplates, $\mathrm{Re} = 1000$, $\mathrm{Ha} = 10$. The traveling wave frequency for (a), (b), (c) is respectively $f/\Omega_{\rm in} = 0.0294,\ 0.0253,\ 0.0292$ whereas the linear stability analysis yields $f/\Omega_{\rm in} = 0.0258$.*

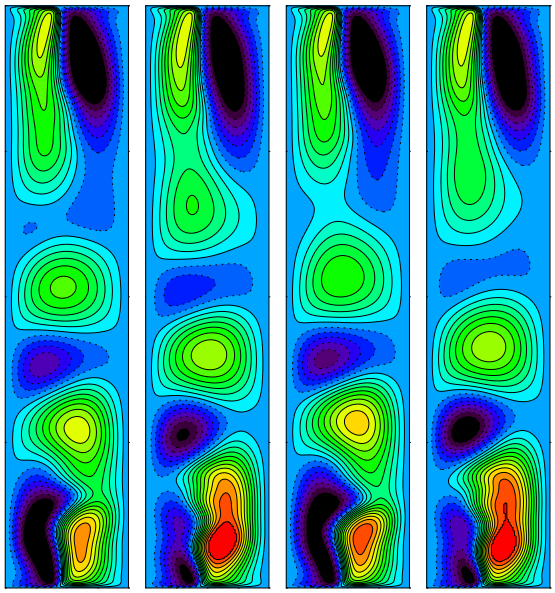

Figure 4.9: *Snapshots of contour lines of stream functions for* $\mathrm{Re} = 1775, \beta = 6, \mathrm{Ha} = 9.5$ *and for the plates divided into two rings,* $w_1 = 0.4$*. The time between consecutive drawings is* $\Delta t = 47$*s. It is evident that the traveling wave is suppressed close to the boundaries, this can be also seen in Fig. 4.8b. For the presented parameters* $\lambda = 2.5$ *so that we can expect to see two pairs of vortices in the middle of the container between the regions dominated by influence of the endplates.*

4.4.1 Critical values

Noting that the background state for sufficiently fast rotation and rigidly rotating endplates $\Omega_{\mathrm{end}} = \Omega_{\mathrm{out}}$ is not steady, it is interesting to investigate what happens when a spiral magnetic field with strength below the critical value is applied. One could expect that a viscid process (like the Ekman pumping) excites fluctuations which could then be amplified and, due to geometry of the applied magnetic field, drifting.

Figure 4.10 shows that for endplates causing strong disturbations the traveling wave can indeed be observed even for subcritical characteristic values. This is also somewhat in agreement with the experiment – traces of moving vortices were observed for states which are stable in the limit of infinite cylinders. We see that the amplitudes of the vertical component of the velocity u_z are almost unchanged when compared to the background state (Fig. 4.8a, left). Although the pattern of the vortices is not very regular, there exists a clear frequency peak for the vertical traveling wave. The frequency and the drift direction (which is reversed by a sign change of, for example, β) corresponds to results of the linear analysis for infinite cylinders. This leads to the conclusion that, although excitations do not grow due to helical MRI, still the same mechanism is responsible for the drift.

If two rings are used and the basic state is steady the situation changes since the additional excitations due to the endplates are minimized. Surprisingly, it is possible that even for super-critical parameters the traveling wave, although excited for a moment, decays (see Fig. 4.11). It is still possible to get sustained instability by increasing, for example, β (see Fig. 4.8b).

The reason for this damping is the height of the cylinders which does not match an integer value of the vertical wavenumber k. For $\mathrm{Re} = 1775$, $\beta = 5$, $\mathrm{Ha} = 9.5$ the corresponding wavelength is $\lambda = 2\pi D/2.1728$ and does not suit the assumed aspect ratio $\Gamma = H/D = 10$. If the height was changed to $\Gamma = 4\lambda = 11.57$ the observed decay of the traveling wave was significantly slower, so slow that after the sudden switching on of the external azimuthal magnetic field the

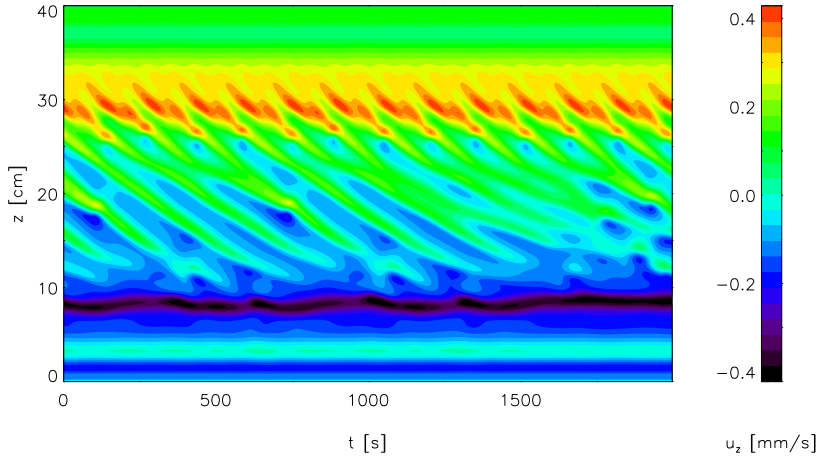

Figure 4.10: *Profiles of $u_z(z,t)$ for $\mathrm{Re} = 1775,\ \mathrm{Ha} = 9.5,\ \beta = 2$ and rigidly rotating ends with $\Omega_{\mathrm{end}} = \Omega_{\mathrm{out}}$. The critical β_c for the corresponding $\mathrm{Re},\ \mathrm{Ha}$ in the limit of infinite cylinders is $\beta_c = 2.56$, and one would expect that the traveling wave decays. This is not the case for the boundary conditions shown here where a clear periodic motion is visible. Its frequency $f/\Omega_{\mathrm{in}} = 0.0124$ agrees with the prediction of a linear analysis for marginal stability in the limit of infinite cylinders giving $f/\Omega_{\mathrm{in}} = 0.0120$. However, the latter approach yields negative growth rate.*

wave could be observed with the PROMISE facility still several hours later. Bearing in mind that wavelengths for given Reynolds numbers are longer with decreasing beta (for $\beta = 3,\ k = 1.45D^{-1},\ \beta = 1,\ k = 0.6D^{-1}$), the constant height of the cylinders ($\Gamma = 10$ in the experiment) can be an issue when looking for critical numbers. It should be noted that due to the boundary layers the effective region where the traveling wave can exists for configuration with two rings is smaller than Γ by approximately $0.5D$ (distances up to about $0.25D$ from the endplates are influenced by their presence).

Although the endplates clearly can serve as the source of viscous excitations and the axially traveling wave develops also for subcritical parameters, we shall notice that there are no peri-

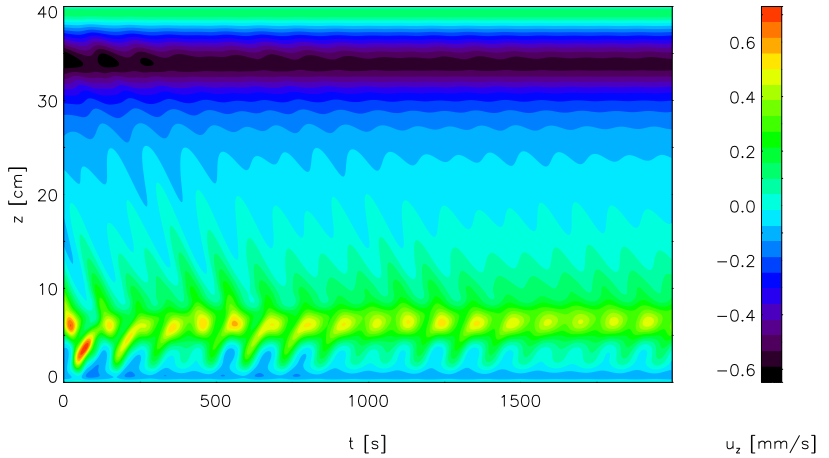

Figure 4.11: *The velocity $u_z(z,t)$ for $\mathrm{Re} = 1775,\ \mathrm{Ha} = 9.5,\ \beta = 5,\ \Gamma = 10$ and endplates divided into two rings with $w_1 = 0.4$. Although in the limit of infinite cylinders the flow is unstable, we clearly see that the disturbances (which developed after a sudden switch on of the magnetic field) decay. The frequency of the decaying wave is $f/\Omega_{\mathrm{in}} = 0.0237$ which again is in agreement with f from the result of the linear analysis, $f/\Omega_{\mathrm{in}} = 0.0232$.*

odic motions in the background state. In this sense the ,,imperfect" background state serves as a catalyst for the helical MRI instability. When the endplates are divided into rings the resulting hydrodynamic flow is laminar, and only after the magnetic field is applied the periodic fluctuations occur, and, moreover, their frequency corresponds exactly to that predicted from the linear analysis for infinite cylinders.

Liu et al. (2006a) suggested that the observed fluctuations can have theirs origin in the underlying hydrodynamical unsteady flow as reported, for example, by Ji et al. (2004). In the latter work the purely hydrodynamic flow for $\mathrm{Re} \approx 1000$ with rigidly rotating ends $\Omega_{\mathrm{end}} = \Omega_{\mathrm{out}}$ and short aspect ratio $\Gamma = 1$ was already unsteady. We confirm these results with the method used here. However, if longer cylinders are used, like $\Gamma = 10$, the flow becomes steady for $\mathrm{Re} = 1000$, and only after imposing strong enough magnetic fields (say $\mathrm{Ha} = 12,\ \beta = 6$) a traveling wave develops with a frequency that matches calculations from the linear analysis.

4.4.2 Differentially rotating ends

We have also performed simulations for differentially rotating plates with ideal Couette profile for periodic cylinders so that $\Omega_{\mathrm{end}}(r) = \Omega_0(r)$. In another recent work (Liu et al., 2007) it has been shown that for parameters corresponding to $\mathrm{Re} = 1775,\ \mathrm{Ha} \approx 10,\ \beta \approx 4$ the traveling wave decays for such boundary conditions. We confirm this result with our method, although our treatment of the magnetic boundaries is simplified compared to theirs.

The explanation for this fact is again the inappropriate height of the cylinders which is far from an integer value of the expected vertical wavelength. For these parameters $\lambda = 3.476D$ according to the linear theory so that less than three wavelengths can fit in the container. On the other hand, if $\beta = 6$ is used, $\lambda = 2.49D$ and then $\Gamma = 10$ almost exactly corresponds to 4λ. From Fig. 4.12 we see indeed that in this case persistent fluctuations exist with a frequency corresponding to the helical MRI instability. We have also made calculations for $\beta = 4$ with longer cylinders so that $H = 4\lambda = 13.90D$ and $H = 5\lambda = 17.38D$. In each case a sustained traveling wave has been observed. It should be mentioned that the vortices do not develop very close to the upper boundary so that it is convenient to take a bit longer cylinders.

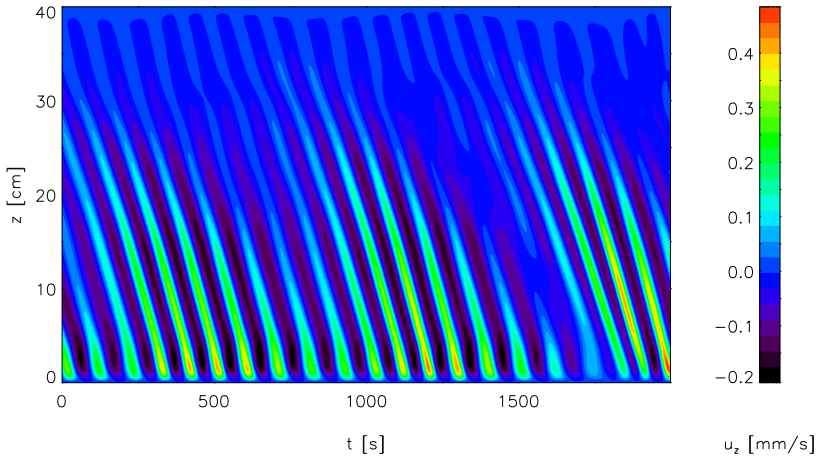

Figure 4.12: *The velocity* $u_z(z,t)$ *for* $\mathrm{Re} = 1775,\ \mathrm{Ha} = 9.5,\ \beta = 6,\ \Gamma = 10$ *and endplates rotating differentially so that* $\Omega_{\mathrm{end}} = \Omega_0$.

Table 4.1: *General features of some of the discussed flows. λ, if provided, refers to vertical wavelength obtained from linear analysis. f corresponds to highest peak in frequency in spectrum of $u_z(R_{\rm in}+D/2, H/2)$.*

Re	Ha	β	Γ	$\lambda[D]$	$f/\Omega_{\rm in}$	Vertical BCs	Flow characteristics
1000	0	0	1			$\Omega_{\rm end}=\Omega_{\rm out}$	Unsteady; flapping jet-like structure in the middle
1000	0	0	10			$\Omega_{\rm end}=\Omega_{\rm out}$	Steady meridional circulation
1775	9.5	6	∞	2.49	0.0258	periodic	traveling wave
1775	9.5	0	10			$\Omega_{\rm bot}=0, \Omega_{\rm top}=\Omega_{\rm out}$	Unsteady, irregular flow
1775	9.5	6	10		0.0294	$\Omega_{\rm bot}=0, \Omega_{\rm top}=\Omega_{\rm out}$	traveling wave can be observed, however flow is not very regular
1775	9.5	2	10		0.0120	$\Omega_{\rm bot}=0, \Omega_{\rm top}=\Omega_{\rm out}$	Subcritical excitations due to viscous pumping
1775	9.5	0	10			Two rings, $w_1=0.4D$	Steady
1775	9.5	6	10		0.0253	Two rings, $w_1=0.4D$	Regular traveling wave
1775	9.5	5	10		0.0237	Two rings, $w_1=0.4D$	Decay of the traveling wave due to $\Gamma\neq n\lambda$
1775	9.5	5	∞	2.89	0.0237	periodic	Sustained traveling wave
1775	9.5	4	10	3.48		Diff. rot. $\Omega_{\rm end}=\Omega_0$	Decay of the traveling wave due to $\Gamma\neq n\lambda$
1775	9.5	6	10		0.0255	Diff. rot. $\Omega_{\rm end}=\Omega_0$	Sustained traveling wave

4.5 Summary

It is easier to perform an experiment showing spiral MRI because much slower rotation of the cylinders is required for the instability to set in compared with MRI with an axial magnetic field only. Moreover, there exists an additional quantity, i.e., the drift frequency which is easy to measure and can serve as an important indicator for the associated phenomena. It is claimed that in the PROMISE experiment frequencies and amplitudes corresponding to the spiral MRI were observed and the results agreed with theoretical calculations of both linear and nonlinear 2D simulations. However it is still possible to improve the experiment so that the basic state is a completely steady flow.

In this chapter we have presented a relatively simple and inexpensive modification which is suitable for such an improvement. Firstly, the endplates should be both made of insulating material and both should rotate in the same way so that the system is symmetric in the z direction. Secondly, it is convenient to divide the lids into two rings which can be attached to the cylinders so that no separate driving is needed. The optimal width of the inner ring, in the sense of minimizing the induced azimuthal magnetic field, is 1.6 cm for the current experimental setup. See Table 4.1 for some general characteristics of the discussed flows.

Our calculations also show that helical MRI modes can be driven by endplate effects even for subcritical characteristic values (see Fig. 4.10). On the other side when providing a steady background flow by applying rings one has to pay more attention to the height of the cylinders and to take into account the vertical wavelengths of the traveling wave which depend on the magnetic configuration. For the current aspect ratio $\Gamma=10$ and $\mathrm{Re}=1775$ it is reasonable to consider $\mathrm{Ha}=9.5,\ \beta=6$ which almost exactly corresponds to $\Gamma=4\lambda$.

Chapter 5

The Ekman-Hartmann layer

5.1 Introduction

Bearing in mind that the aspect ratio considered in the previous chapters is $\Gamma = H/D = 10$ it may seem a bit surprising that the vertical boundaries can so profoundly alter the flow. Vast part of work in study of the Taylor-Couette system is done in a narrow gap limit, i.e., when $D/R_{\rm out} \ll 1$. The experimental part of the seminal work by Taylor (1923) was performed for the narrow gap and the aspect ratio exceeded 100 so that the role of ends enclosing the cylinders was completely negligible (also the rotation was slow). On the other hand there is also plenty of work done for small aspect ratio $\Gamma \approx 1$, where the plates play crucial role and simply introduce a new class of problems. When Γ becomes an important parameter it is possible to observe a wide family of different states (including non-axisymmetric ones) for the same parameters and the observed result depends on theirs path through the parameters space from an initial state. Therefore this system is an excellent subject to the bifurcation theory (Pfister et al., 1988; Mullin et al., 2002; Furukawa et al., 2002; Lopez and Marques, 2003; Kageyama et al., 2004). Peculiar asymmetric patterns, anomalous modes, also exists (Youd and Barenghi, 2006).

The case for $\Gamma = 10$ is an intermediate one between very short and long containers, yet in purely hydrodynamical contest the influence of the vertical boundaries is small. At least for Reynolds numbers of our interest i.e., of order $O(10^2 - 10^3)$ (see e.g. Watanabe and Furukawa, 1999; Youd and Barenghi, 2005). Naturally, if the rotation rates are large enough so that the corresponding Reynolds number is of order $O(10^5)$ and larger, the plates easily dominate the flow in the entire container. This is due to Taylor-Proudman theorem from which follows that a distance of influence of these boundaries scales as $\mathrm{Re}^{0.5}$ and for such rotations it is necessary that Γ would have to be several thousand.

If, for the rotation rates characterized by $\mathrm{Re} \approx 10^3$, the vertical boundaries should not play any important role why such problems as these depicted in the two previous chapters arise? The answer lies in magnetic forces which develop as a result of strong shears close to the boundaries in the presence of an external axial magnetic field. This can be seen when looking back to Figs. 2.7 - 2.9. From Fig. 2.7 we notice that for slow rotation, Re=100, fixed outer cylinder, $\hat{\mu} = 0.0$ and a weak axial field, $\mathrm{Ha} = 3$, for the insulating vertical boundaries the flow is very regular and influence of the endplates is negligible: five pairs of nice Taylor vortices set in. This is expected since for these parameters and $\Gamma = 10$ the vertical wavelength is $k = 3.14$ so that $\lambda = 2D$. Moreover, the Taylor vortices nicely fit into the two Ekman vortices in this particular case. When the imposed magnetic field is stronger (Fig. 2.8) or more rigorous magnetic boundary conditions are applied (i.e., the plates are perfectly conducting, Fig. 2.9) the situation changes entirely: currents induced inside the fluid interact with the axial magnetic field and alter the flow.

It seems that for MHD Taylor-Couette flow impact of the magnetic layer, unlike that of the classical Ekman layer, has been underestimated. In this chapter we argue that rotating plates together with the axial field and conducting fluid give rise to similar effects which develop for rotating infinite plate which serves as a boundary for conducting fluid. One of the most important features of such flow is the existence of an electric Hartmann current which leaves the boundary layer and then, together with the axial filed, can alter the flow significantly. In particular this becomes important for conducting plates. That was the case for the PROMISE experiment since one of the endplates was made from copper. We note that this current is absent in the conventional Hartmann problem: a flow of conducting fluid in a rectangular channel in a presence of magnetic field perpendicular to the velocity (Roberts, 1967; Krasnov et al., 2003; Andreev et al., 2006).

In this chapter we discuss properties of the Ekman-Hartmann layer for infinite, horizontally unbounded, rotating plates and relate it to the endplates enclosing the cylinders in the Taylor-Couette setup. We show that, for considered horizontal boundary conditions, the induced current turn eventually in the radial direction and acting in concert with the imposed axial magnetic field gives rise to a body force. Due to the force, the flow can be viewed as a modification of the classical Taylor-Couette problem to which a transverse pressure gradient is added. Flows of this type form a new class: Taylor-Dean flows. We analyze theirs stability and investigate how the classical MHD Taylor-Couette flow is altered focusing on aspect ratio and radius ratio of that corresponding to the PROMISE experiment (we consider only $\Gamma = 10, \hat{\eta} = 0.5$).

5.2 The Ekman-Hartmann layer

At an interface between an incompressible fluid with low viscosity and a rapidly rotating rigid surface develops an Ekman layer with thickness $d_{\mathrm{E}} \propto \sqrt{\nu/\Omega}$ where Ω is rate of uniform rotation (see e.g Ekman, 1905, also Section 2.4.1). Similarly for a flow of conducting incompressible fluid in vicinity of a rigid non-rotating boundary and under the influence of an external magnetic field perpendicular to the surface there exists a Hartmann layer with thickness $d_{\mathrm{H}} \propto \mathrm{Ha}^{-1}$ (see e.g. Acheson and Hide, 1973; Krasnov et al., 2004). When these two effects are combined the so-called Ekman-Hartmann layer develops. It can be viewed either as a modification of Ekman layer by introducing the conducting fluid and imposing the external magnetic field or a modification of the Hartmann layer by adding the uniform rotation of the bounding surface. The resulting layer (in its steady form) assures a proper transition for the velocity and the magnetic field from values inside the bulk of the fluid to the applied boundary conditions.

The linear analysis of the Ekman-Hartmann layer in its idealized case was presented by Gilman and Benton (1968). They considered an infinite insulating plate rotating with Ω_{plate} at $z = 0$ and a conducting fluid filling the space $z > 0$, the fluid far from the plain rotates with $\Omega_{\mathrm{fluid}} = \Omega_{\mathrm{plate}}(1 + \epsilon)$. The most important conclusion of this work was that in addition to the well known Ekman suction/blowing of mass flux there also exists a Hartmann current which has the same direction (or opposite when the external B_z is negative) as the velocity of the Ekman blowing[1]. This current, which is due to the vertical shears, leaves the Ekman-Hartmann layer and potentially influences the flow far away from the boundary.

Further extension of this work was performed by Loper (1970) who considered a conducting boundary was considered, Benton and Chow (1972) where nonlinear extension of Gilman and Benton (1968) study was presented and a solution for larger values of the parameter ϵ was possible. Benton and Loper (1969) studied unsteady layer and a spin-up time of the fluid as

[1]That if fluid is blown away or sucked towards the boundaries depends only on sign of ϵ. From this point on we will write only about „blowing" bearing in mind that „suction" is possible just by changing the sign.

a result of rapid increase of the plate rotation, later Loper and Benton (1970) studied similar problem but they have also taken into account the existence of a second plate within a finite distance from the first one. Stability of the layer itself was analyzed by Gilman (1971).

In the next part we will show how those results are related to effects which arise in magnetized Taylor-Couette with finite aspect ratio, i.e., the cylinders are covered with rigidly rotating endplates (insulating or conducting) in which vicinity an Ekman-Hartmann layer develops. Naturally, the influence of the vertical walls introduces additional, important effects and direct comparison with the previous work is rather not possible. Nevertheless we will show that the rotating endplates, also in this case, induce the Hartmann current which can change the global properties of the flow.

5.2.1 Insulating boundaries

We now attempt to make a general, qualitative comparison between the Ekman-Hartmann layer for infinite rotating plate and that induced by the endplates covering finite cylinders. First we restrict ourselves to consideration when the both cylinders rotate with the same angular velocity $\Omega_{\rm in} = \Omega_{\rm out}$, i.e., $\hat{\mu} = 1.0$ so that the rotational profile Ω is flat. We assume $\Gamma = 10$, and the endplates to rotate independently with velocity only slightly different $\Omega_{\rm in} = \Omega_{\rm end}(1 + \epsilon')$. The introduced ϵ' conceptually plays similar role like ϵ used as the difference between fluid and the infinite rotating plate angular velocity. In the case for Taylor-Couette flow Ω is a function of r and even „far away" from the boundaries (i.e., at $z = \Gamma/2$, in the middle of the container) is not constant in r. We also must take into account that the fluid which was ejected due to Ekman blowing mechanism must eventually get back due to the conservation of mass and finiteness of the container.

The characteristic thickness of the Ekman layer is (see e.g. Acheson and Hide, 1973, also Section 3.3.1)

$$d_{\rm E} = \sqrt{\nu/\bar{\Omega}}, \tag{5.1}$$

where $\bar{\Omega}$ measures the scale of the uniform rotation velocity, as the length scale we use D. It is clear that $\bar{\Omega} = \Omega_{\rm plate}$ when we consider rotating, unbounded, infinite plate but it is not so clear what to use for general Taylor-Couette flows when cylinders and lids can rotate independently. For example Czarny et al. (2004) as the angular velocity scale use $\bar{\Omega} = \Omega_{\rm in} - \Omega_{\rm out}$ which however is not suitable for our considerations (for example it would give $\bar{\Omega} = 0$ for any configuration with $\hat{\mu} = 1.0$ independently of the endplate rotation). Through this work we use simply $\bar{\Omega} = \Omega_{\rm out}$ which turns out to be a quite good approximation,

$$d_{\rm E} = \sqrt{\nu/\bar{\Omega}} = \sqrt{\frac{R_{\rm in} D}{{\rm Re}\hat{\mu}}} = ({\rm Re}\hat{\mu})^{-0.5}, \tag{5.2}$$

bearing in mind that the proper thickness of the layer can be different depending especially on the rotational properties of the endplates as well as on $\hat{\mu}$ (we consider only $\hat{\mu} > 0.25$).

We now introduce a parameter α which measures overall importance of the magnetic field

$$\alpha = \frac{d_{\rm E}}{\sqrt{2} d_{\rm H}} = \sqrt{\frac{{\rm Ha}^2 \nu}{2\bar{\Omega} D^2}} = (2{\rm Re}\hat{\mu})^{-0.5}{\rm Ha}, \tag{5.3}$$

where $d_{\rm H} = D{\rm Ha}^{-1}$ is the Hartmann depth. The parameter α is essentially the ratio of the Ekman depth $d_{\rm E}$ to the Hartmann depth $d_{\rm H}$. The magnetic effects start to play significant role

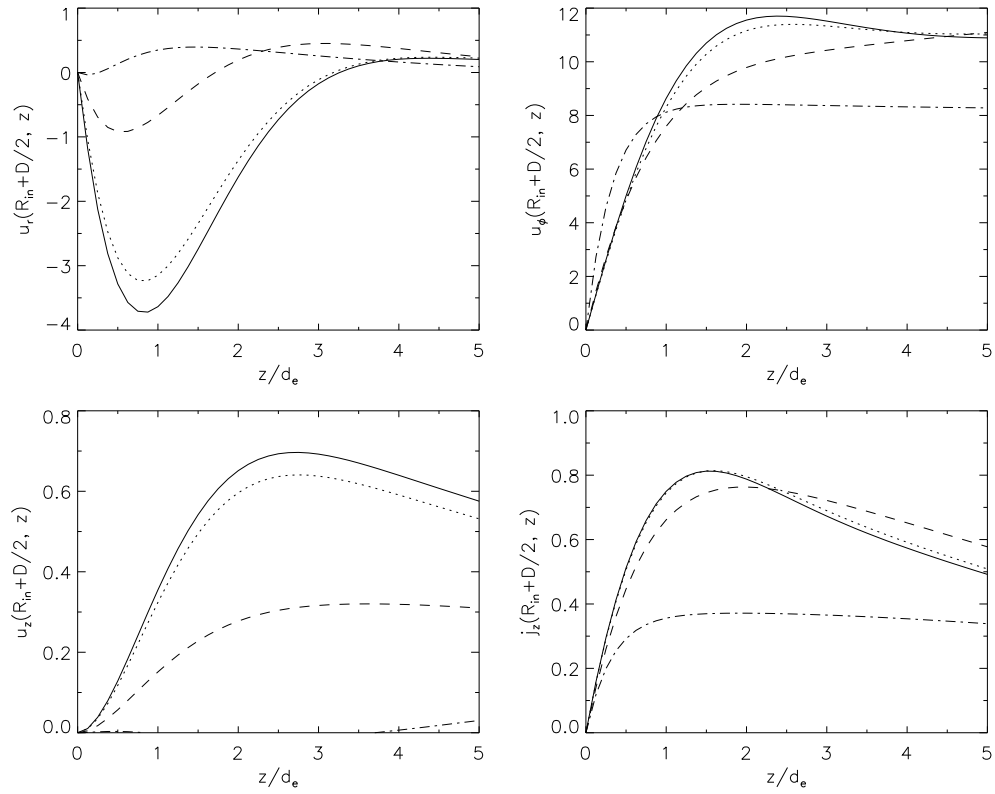

Figure 5.1: *Structure of the Ekman-Hartmann layer for nonlinear simulations of the enclosed Taylor-Couette flow. The flow profiles for u_r, u_ϕ, u_z, j_z are shown, different values of the magnetic interaction parameters correspond to: (——)* $\mathrm{Ha} \to 0.0$ $(\alpha \to 0.0)$*, (· · · · ·)* $\mathrm{Ha} = 3.0$ $(\alpha = 0.2)$*, (– – –)* $\mathrm{Ha} = 10.0$ $(\alpha = 0.7)$*, (·–·–·)* $\mathrm{Ha} = 30.0$ $(\alpha = 2.1)$*, $d_\mathrm{E} = 0.01$ is the Ekman layer thickness. The both cylinders rotate with $\Omega_\mathrm{in} = \Omega_\mathrm{out} = \mathrm{Re} = 100$, the endplates rotate with $\Omega_\mathrm{end} = 90$ thus $\epsilon' = 0.11$. The current j_z for $\alpha = 0$ is computed in $\mathrm{Ha} \to 0$ limit so that the flow is essentially non-magnetic.*

when $\alpha \gtrsim 1$, in the limit $\alpha \to 0$ we have the classical Ekman layer and for $\alpha \to \infty$ the classical Hartmann layer. We notice that for parameters of our interest α lies in range 0.3 – 1.5 and therefore we expect the magnetic fields to be important.

Figure 5.1 shows the structure of the Ekman-Hartmann layer for different values of the magnetic interaction parameter for our nonlinear simulations of the MHD Taylor-Couette flow (for $\Omega_\mathrm{in} = \Omega_\mathrm{out} = 100$, $\Omega_\mathrm{end} = 90$). Different quantities as function of the distance z from the boundary are depicted. The values of u_r, u_ϕ and j_z are taken from the middle of the gap, at $r = R_\mathrm{in} + D/2$, whereas u_z is taken close to the inner cylinder (where the suppression of u_z by the no-slip boundary conditions at the wall is still small and the blowing velocity is maximum), therefore the comparison with rotating, horizontally unbounded, infinite plate is more adequate. We notice that for the latter u_z and j_z are independent of r. The quantitative agreement with the previous linear results by Gilman and Benton (1968) for the infinite plate is very good. Also the dependence on strength of the magnetic field has essentially the same character.

The vertical shears in u_r and u_z produce currents which together with the axial field generate forces acting against the shears. Since the radial flow must vanish at the boundaries as well as it vanishes, for the basic state $\mathbf{\Omega}_0$, far away from them, the effect is to reduce the u_r and, due to the mass conservation, u_z. Therefore, what can be clearly seen in the Fig. 5.1, *the external axial magnetic field inhibits the Ekman blowing* (which is completely suppressed when $\alpha \to \infty$) and makes the boundary layer *thinner*. The azimuthal flow u_ϕ, on the other hand, is forced to have

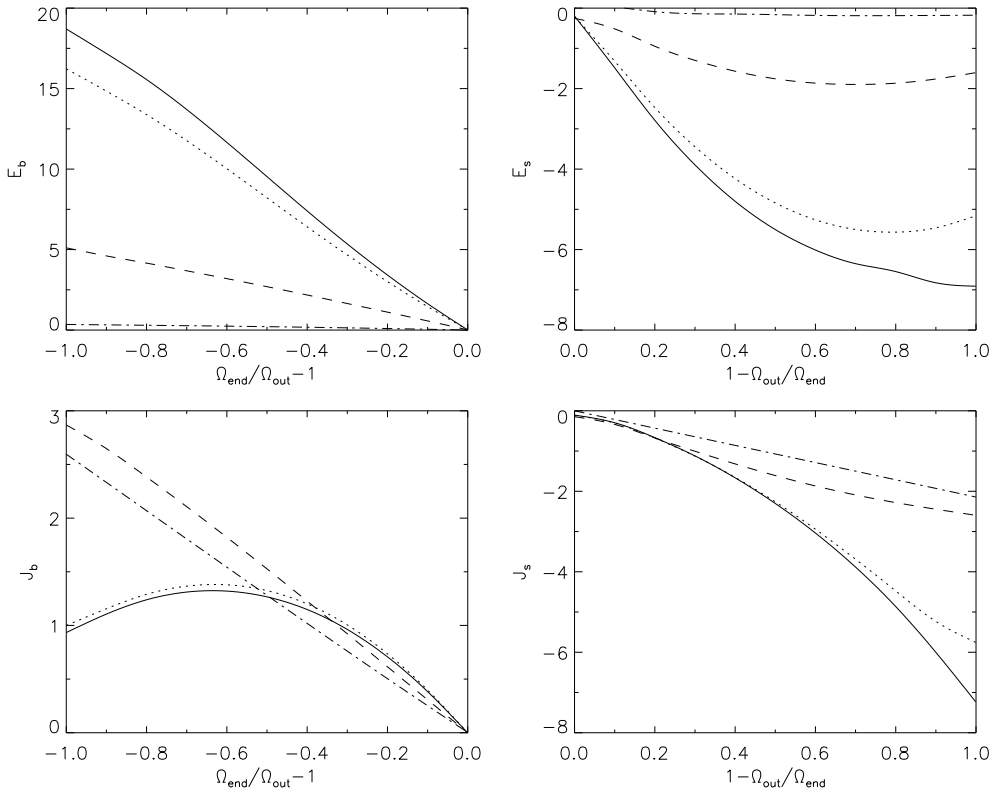

Figure 5.2: *Ekman blowing/suction (E_b/E_s) and the corresponding Hartmann current for the Taylor-Couette flow for different* Ha *numbers. The both cylinders were rotating with the same angular velocity $\hat{\mu} = 1.0$. On the left: $\Omega_{\rm in} = \Omega_{\rm out} = 100$ and the rotation of lids was varied $0 \leq \Omega_{\rm end} \leq 100$. On the right" $\Omega_{\rm end} = 100$ and the cylinder rotation was varied $0 \leq \Omega_{\rm in} = \Omega_{\rm out} \leq 100$. E_b („b" for „blowing"), E_s („s" for „suction") represents maximum/minimum velocity u_z close to the inner cylinder ; J_b, J_s reflects axial electric current in the middle of the gap at approximately 5 times the distance between the plate and maximum (minimum) of j_z (i.e., at $z \approx 10 d_{\rm E}$). (——) Ha → 0 ($\alpha \to 0$), (· · · · ·) Ha=3 ($\alpha = 0.2$), (– – –) Ha=10 ($\alpha = 0.7$), (·–·–·–) Ha=30 ($\alpha = 2.1$).*

different values at the boundaries and far away from them, thus the shear can be decreased only in the region close to the boundary.

We also notice that there exists an induced axial current j_z, the Hartmann current, outside the boundary layer (this is not the case for non-rotating Hartmann boundaries). For unbounded flow this current quickly converges to an asymptotic constant value, but for the case of flow between two plates or for finite cylinders it can not be true and currents induced by the both endplates must eventually interact. When we consider a system symmetric in the z direction, i.e., if the both plates rotate in the same manner, the induced j_z have the same strength but opposite signs and they eventually meet turning into the radial direction (and consequently $j_z = 0$ in the middle of the container for the symmetric boundary conditions).

We now turn to a situation when the angular velocity of the plates and the cylinders differs significantly, i.e., $\epsilon' \gg 0$. The Ekman blowing/suction and the corresponding Hartmann current for the flow between cylinders with independently rotating lids, for wide range of $\Omega_{\rm in}, \Omega_{\rm end}$ and different values of α is shown in Fig. 5.2. The shape of the curves is in graphical agreement with nonlinear computations for far-field values for rotating infinite plate, see Benton and Chow (1972). However, we should not attempt to make any direct comparison between those results since the quantities computed for the enclosed Taylor-Couette flow depend importantly on theirs

position. It is interesting to note that the axial current is a non-monotonic function of α – in particular the ,,blowing" current J_b increases up to $\mathrm{Ha} \approx 10$ and then is starts to decrease.

5.2.2 Magnetic diffusion region

Benton and Loper (1969, 1970) have studied a spin-up problem[2] for the Ekman-Hartmann layer, the former work concerns unsteady layer for one infinite rotating plate, the latter concerns fluid bounded by two such plates. Three essentially different regions are distinguished in the flow: the Ekman-Hartmann layer, a magnetic diffusion region (MDR) and a current-free region. The MDR arises between the boundary layer and the region far away from them. Since both the axial velocity and axial electric current leave the layer, the MDR exists to satisfy the exterior boundary conditions for the current.

In the MDR the axial Hartmann current must be reduced to zero before it reaches the current-free region and, by continuity, it is turned into radial direction. This radial perturbation current interacts with axial magnetic field and results in accelerating (for negative j_r and positive B_z) or decelerating (for positive j_r and B_z) electromagnetic body force in the magnetic diffusion region. For the spin-up problem this means that the spin-up time is not lengthened although Ekman suction is reduced by the magnetic field. In the enclosed Taylor-Couette system the rigidly rotating endplates can be viewed as planes which constantly increase (or decrease) velocity of the fluid confined between the walls therefore we expect that similar three regions can be, in principle, distinguished.

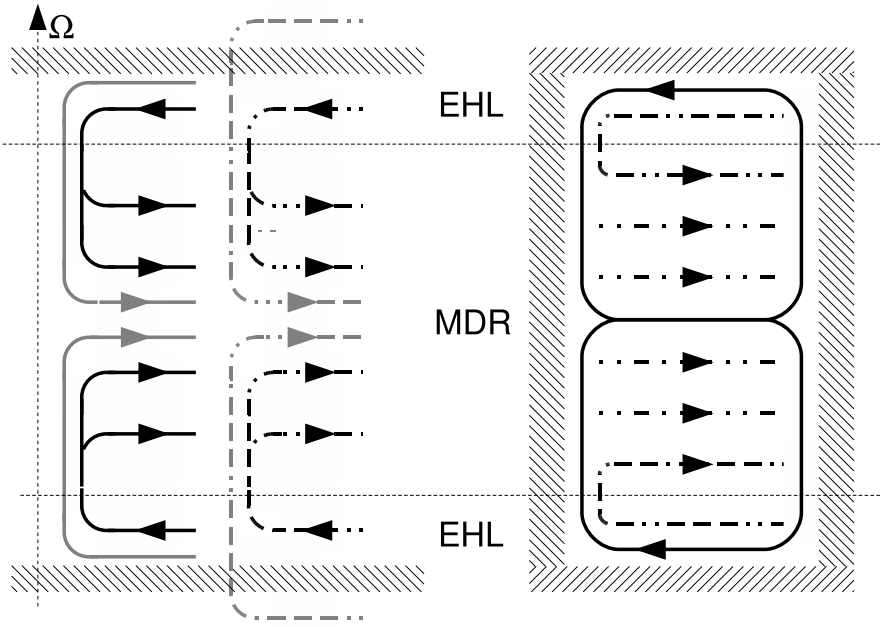

Figure 5.3: *Schematic topology of velocity (——) and electric current (· · · — · · ·). On the left: the case for an infinite plate is presented, after Loper and Benton (1970). On the right: the case for an enclosed MHD Taylor-Couette flow. (\\) denotes the perfectly conducting boundaries, (//) the insulating ones. The gray arrows on the left side correspond to additional terms due to conducting plates:* $2\alpha^2\Phi$ *for the velocity and* 2Φ *for the current. MDR – the magnetic diffusion region, EHL – the Ekman-Hartmann layer.*

[2]The spin-up problem is defined as follows: consider a rotating plate (or two) and fluid at steady state, then the plate angular velocity is suddenly changed. How do the dynamical variables characterizing the fluid change in time? What is the spin-up time, i.e., after what time the flow at given distance becomes again steady?

The thickness of the magnetic diffusion region depends on the magnetic properties of the fluid, i.e., on its resistivity. In the two-plate spin-up problem for small magnetic Prandtl number both MDRs quickly reach the thickness of order of the distance between the plates and the current-free region disappears. In the small Prandtl number limit the MDR instantly becomes spatially uniform and infinitely thick even for one bounding plate and the current-free region does not exists at all. Therefore for our MHD Taylor-Couette system in $\mathrm{Pm} \to 0$ we expect that the magnetic diffusion region will dominate majority of the flow, i.e., everywhere but in the Ekman-Hartmann layer, see Fig. 5.3.

5.2.3 Conducting boundaries

Up to this point we considered only insulating plates. However, perfectly conducting boundaries introduce additional currents altering the flow. The Ekman-Hartmann layer itself is not affected by conductivity of the plates as are the Ekman blowing and Hartmann current within this layer. However, additional current 2Φ is induced by the conducting boundaries and the radial Ekman velocity inside MDR is larger by a factor of $2\alpha^2\Phi$ (see Loper, 1970), where

$$\Phi = \frac{\varepsilon\sigma_{\mathrm{plate}}}{\sigma_{\mathrm{fluid}}}\sqrt{\frac{\Omega_{\mathrm{plate}}}{\nu}} = \kappa\sqrt{\frac{\Omega_{\mathrm{plate}}}{\nu}}, \tag{5.4}$$

ε is the thickness of a plate of constant conductivity σ_{plate} and the term $\varepsilon\sigma_{\mathrm{plate}}/\sigma_{\mathrm{fluid}}$ corresponds to κ in our formulation of magnetic boundary conditions (see Section 2.4).

For highly conducting plates the induced Hartmann current drawn into/from the plates is much stronger than the current induced in the layer for insulating boundaries. Figure 5.4 shows how the radial current j_r *in the middle* of the container changes with conductivity of the end-plates. We see that the difference between the perfect insulator and the perfect conductor is almost an order of magnitude.

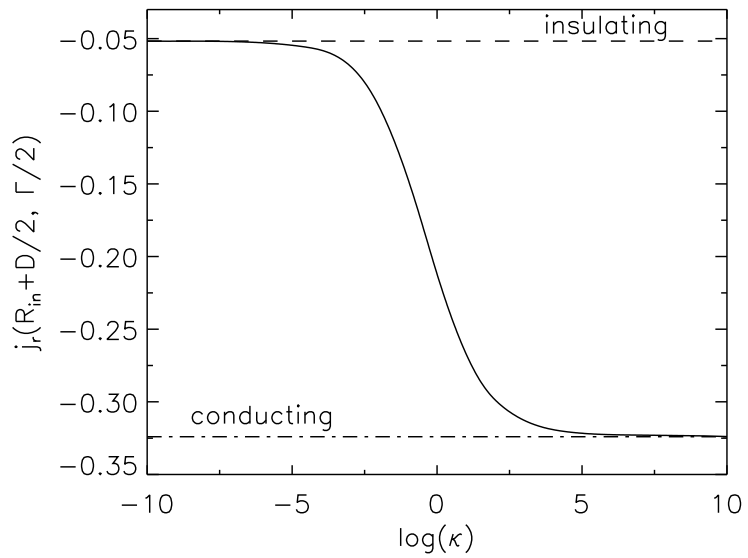

Figure 5.4: *Radial current j_r (——) in the middle of the gap for* $\mathrm{Ha} = 10$, $\mathrm{Re} = 200$, $\Omega_{\mathrm{end}} = 202$. *The upper line represents pseudo-vacuum boundary conditions, the bottom line perfect conductor and in between intermediate case for different values of relative conductance parameter κ.*

5.3 Stability of the MHD Taylor-Dean flow

The induced axial Hartmann current turns into the radial direction in the magnetic diffusion region which fills almost the entire container and then interacts with the externally imposed axial magnetic field B_z giving rise to a body force. Moreover the radial current is rather homogeneous in z in the MDR. The force enters the momentum equation, Eq. (2.11), for u_ϕ and, since the current $j_r \propto r^{-1}$, the flow can be related to a flow driven by azimuthal pressure gradient: Taylor-Dean flow. Let us denote the induced radial electric current at the inner cylinder for $z = H/2$ as j_{r0} then the force is $-\hat{\mathbf{e}}_\phi j_{r0} B_0/(r\rho)$, where B_0 is the strength of the imposed magnetic field. This is identical to a case when $\partial_\phi p \neq 0$, i.e. the term $\hat{\mathbf{e}}_\phi \partial_\phi p/(\rho r)$, does not vanish.[3]

In this section we analyze the idealized Taylor-Dean flow between infinitely long, conducting cylinders with an *explicitly* applied pressure gradient. We search for critical values of the gradient for different strength of the applied magnetic field and different rotation rates. In this way we obtain, for given Ha, necessary value of the radial current which must be induced in order to make the flow unstable. Then, in Section 5.4, we show examples of enclosed MHD Taylor-Couette flows for which indeed such currents are produced by the plates.

5.3.1 The MHD Taylor-Dean flow

Let us now consider infinitely long, conducting cylinders with externally imposed axial magnetic field and non-zero transverse pressure gradient. Its basic stationary solution is a superposition of circular Couette flow Ω_0 and another steady flow (see Dean, 1928; Chandrasekhar, 1961), i.e.,

$$\Omega_{0_\mathrm{D}} = a + \frac{b}{r^2} + e\left(c + \frac{d}{r^2} + \ln(r)\right), \tag{5.5}$$

with

$$e = \frac{1}{\rho\nu} K, \tag{5.6}$$

$$c = \frac{R_{\mathrm{in}}^2 \ln(R_{\mathrm{in}}) - R_{\mathrm{out}}^2 \ln(R_{\mathrm{out}})}{R_{\mathrm{out}}^2 - R_{\mathrm{in}}^2}, \tag{5.7}$$

$$d = \frac{R_{\mathrm{in}}^2 R_{\mathrm{out}}^2 \ln(R_{\mathrm{out}}/R_{\mathrm{in}})}{R_{\mathrm{out}}^2 - R_{\mathrm{in}}^2}, \tag{5.8}$$

$$K = \partial_\phi p, \tag{5.9}$$

and a, b defined in Eq. (2.7). The constant pressure gradient K can be realized by the Lorentz force in an MHD flow or any externally applied pressure, like by a hydrodynamical pump (in which case, of course, it is impossible that $\partial_\phi p$ is constant for $0 \leq \phi < 2\pi$ since the pump must be physically placed somewhere). Naturally when we assume axisymmetric flow all ϕ derivatives are canceled, except that for the pressure p.

We notice that imposing the axial magnetic field and applying an electrostatic potential between the cylinders produces the Lorentz body force $\boldsymbol{j} \times \boldsymbol{B_0}$ acting on the fluid, $\boldsymbol{j}$ being the supplied radial current density. The value of this current is given by Ohm's law $\boldsymbol{j} = \sigma(\boldsymbol{E} + \boldsymbol{u} \times \boldsymbol{B_0})$. Only if currents originating from the term $\boldsymbol{u} \times \boldsymbol{B_0}$ are negligible the motion is decoupled from the electromagnetic variables. In that case the flow can by treated as the Taylor-Dean flow and its rotational profiles is precisely Eq. (5.5), for explicit derivation of value K for this case see e.g. Hong and Wilhelm (1976); Digilov (2007).

[3] Recall that for the cylindrical geometry $\nabla p = \hat{\mathbf{e}}_r \partial_r p + \hat{\mathbf{e}}_\phi r^{-1} \partial_\phi p + \hat{\mathbf{e}}_z \partial_z p$.

If, on the other hand, the applied magnetic field is very strong, $\mathrm{Ha} \gg 1$, the induced currents can not be neglected when compared to the imposed radial current and situation looks rather different. The rotational profile becomes such that $\Omega \propto r^{-2}$, the solution is not trivial, see Khalzov and Smolyakov (2006).

Taylor-Dean flows, as extension to the classical Taylor-Couette problem, form a class of very interesting flows for both hydrodynamical and magnetized liquids. When the two cylinders are at rest the flow is entirely driven only by the pressure gradient (so that $a = b = 0$), an unstable state in such flow is also characterized by Taylor vortices. Stability of the MHD Taylor-Dean flows has been studied for example by Hong and Wilhelm (1976), also by Kurzweg and Khalfaoui (1981); Tabeling and Chabrerie (1981) for thin gap approximation, Chen (1993) studied purely hydrodynamical flow for arbitrary gap width, Stefani and Gerbeth (2004) even suggested a transverse pressure gradient driven MRI experiment (another electrically driven MRI experiment, for large Ha, has been proposed by Khalzov et al., 2006).

Let us now introduce a parameter γ describing Taylor-Dean flows, the ratio of the average pumping velocity to the rotating velocity[4]

$$\gamma = \frac{6V_m}{\Omega_{\mathrm{in}} R_{\mathrm{in}}}, \tag{5.10}$$

where V_m is the average pumping velocity

$$\begin{aligned} V_m &= \frac{1}{D}\int_{R_{\mathrm{in}}}^{R_{\mathrm{out}}} \left[e\left(c + \frac{d}{r^2} + \ln(r) \right) \right] \mathrm{d}r \\ &= -K \frac{R_{\mathrm{out}}}{2\rho\nu} \frac{(1-\hat{\eta}^2)^2 - 4\hat{\eta}^2 (\ln\hat{\eta})^2}{4(1-\hat{\eta})(1-\hat{\eta}^2)}. \end{aligned} \tag{5.11}$$

5.3.2 Linear stability analysis

We consider linear stability of the MHD Taylor-Dean flow governed by the classical MHD equations, Eqs. (1.9). The equations are for general non-axisymmetric case but in this section we will focus only on axisymmetric solutions, i.e., $m = 0$.

The regarded MHD Taylor-Dean flow admits the basic solution $u_\phi = r\Omega_{0_{\mathrm{D}}}$, Eq. (5.5) with $u_r = u_z = b_r = b_\phi = 0$ and the imposed axial magnetic field B_0. The perturbed state is

$$u_r', r\Omega_{0_{\mathrm{D}}} + u_\phi', u_z', b_r', b_\phi', B_0 + b_z. \tag{5.12}$$

After developing disturbances into normal modes we seek solutions of the linearized MHD equations, Eqs. (1.9), in the form

$$\begin{array}{lll} u_r' = u_r(r)e^{i(m\phi+kz+\omega t)}, & u_\phi' = u_\phi(r)e^{i(m\phi+kz+\omega t)}, & u_z' = u_z(r)e^{i(m\phi+kz+\omega t)}, \\ b_r' = b_r(r)e^{i(m\phi+kz+\omega t)}, & b_\phi' = b_\phi(r)e^{i(m\phi+kz+\omega t)}, & b_z' = b_z(r)e^{i(m\phi+kz+\omega t)}. \end{array} \tag{5.13}$$

Non-dimensional equations can be written as a system of ten differential equations (Rüdiger and Shalybkov, 2004)

$$\partial_r u_r' = -\frac{u_r'}{r} - i\frac{m u_\phi'}{r} - iku_z', \tag{5.14a}$$

$$\partial_r u_\phi' = x_2 - \frac{u_\phi'}{r}, \tag{5.14b}$$

[4]Usually in work related to Taylor-Dean flows this parameter is denoted as „β" but here we do not want to confuse it with the other „β", used in previous chapters which measures the ratio of the azimuthal to the axial magnetic field.

$$\partial_r u_z' = x_3, \tag{5.14c}$$

$$\partial_r b_r' = -\frac{b_r'}{r} - i b_\phi' \frac{m}{r} - ik b_z', \tag{5.14d}$$

$$\partial_r b_\phi' = x_4 - \frac{b_\phi'}{r}, \tag{5.14e}$$

$$\partial_r b_z' = i b_r' \left(\frac{m^2}{kr^2} + k\right) - b_r' \frac{\mathrm{Pm}}{k}(\omega + m\mathrm{Re}\Omega_{0_\mathrm{D}}) + u_r' - x_4 \frac{m}{kr}, \tag{5.14f}$$

$$\begin{aligned}\partial_r x_1 = {} & u_r' \left(\frac{m^2}{r^2} + k^2\right) + i u_r'(\omega + m\mathrm{Re}\Omega_{0_\mathrm{D}}) + \\ & + 2i\frac{m}{r^2} u_\phi' - 2\mathrm{Re}\Omega_{0_\mathrm{D}} u_\phi' - ik\mathrm{Ha}^2 b_r',\end{aligned} \tag{5.14g}$$

$$\begin{aligned}\partial_r x_2 = {} & u_\phi' \left(\frac{2m^2}{r^2} + k^2 + i\omega + im\mathrm{Re}\Omega_{0_\mathrm{D}}\right) + u_r' \left(2a\mathrm{Re} - 2i\frac{m}{r^2}\right) + \\ & + u_z' k \frac{m}{r} - b_\phi' ik\mathrm{Ha}^2 - i\frac{m}{r} x_1,\end{aligned} \tag{5.14h}$$

$$\begin{aligned}\partial_r x_3 = {} & u_0' \left(\frac{m^2}{r^2} + 2k^2 + i\omega + im\mathrm{Re}\Omega_{0_\mathrm{D}}\right) + u_\phi' \frac{km}{r} + u_z' k^2 - \\ & - ik\mathrm{Ha}^2 b_z' - \frac{x_3}{r} - ikx_1,\end{aligned} \tag{5.14i}$$

$$\begin{aligned}\partial_r x_4 = {} & b_\phi' \left(\frac{m^2}{r^2} + k^2 + i\mathrm{Pm}\omega + im\mathrm{Re}\Omega_{0_\mathrm{D}}\right) - \\ & - b_r' \left(2i\frac{m}{r^2} + 2\mathrm{PmRe}\frac{b}{r^2}\right) - iku_\phi',\end{aligned} \tag{5.14j}$$

with

$$x_1 = \partial_r u_r' + \frac{u_r'}{r} - p - \mathrm{Ha}^2 b_z'. \tag{5.14k}$$

An appropriate set of ten boundary conditions is needed in order to solve the above system. These are the no-slip boundary conditions for the velocity $u_r' = u_\phi' = u_z' = 0$ and perfectly conducting for the magnetic field $\partial_r b_\phi' + b_\phi' r^{-1} = b_r' = 0$ at the both cylinders (for details on the boundary conditions see Section 2.4). We will only consider marginally stable stationary modes.

The homogeneous set of Eqs. (5.14) together with the boundary conditions for the walls determine an eigenvalue problem of the form $L(\hat{\mu}, \hat{\eta}, k, m, \mathrm{Pm}, \mathrm{Re}, \mathrm{Ha}, \gamma) = 0$. The variables are approximated with finite difference method on a grid typically with 200 points.

5.3.3 Axisymmetric modes

For the current axisymmetric study we set parameters $m = 0, \hat{\eta} = 0.5, \hat{\mu} = 0.27, \mathrm{Pm} = 10^{-6}$, then for given Ha and Re we seek for minimal value of $|\gamma|$ which gives rise to an instability (i.e., the value for which the determinant L is zero). Since γ is directly proportional to the transverse pressure gradient and therefore to the radial electric current for constant Ha, the resulting critical γ_c determines the minimum value of the current for which the flow becomes unstable.

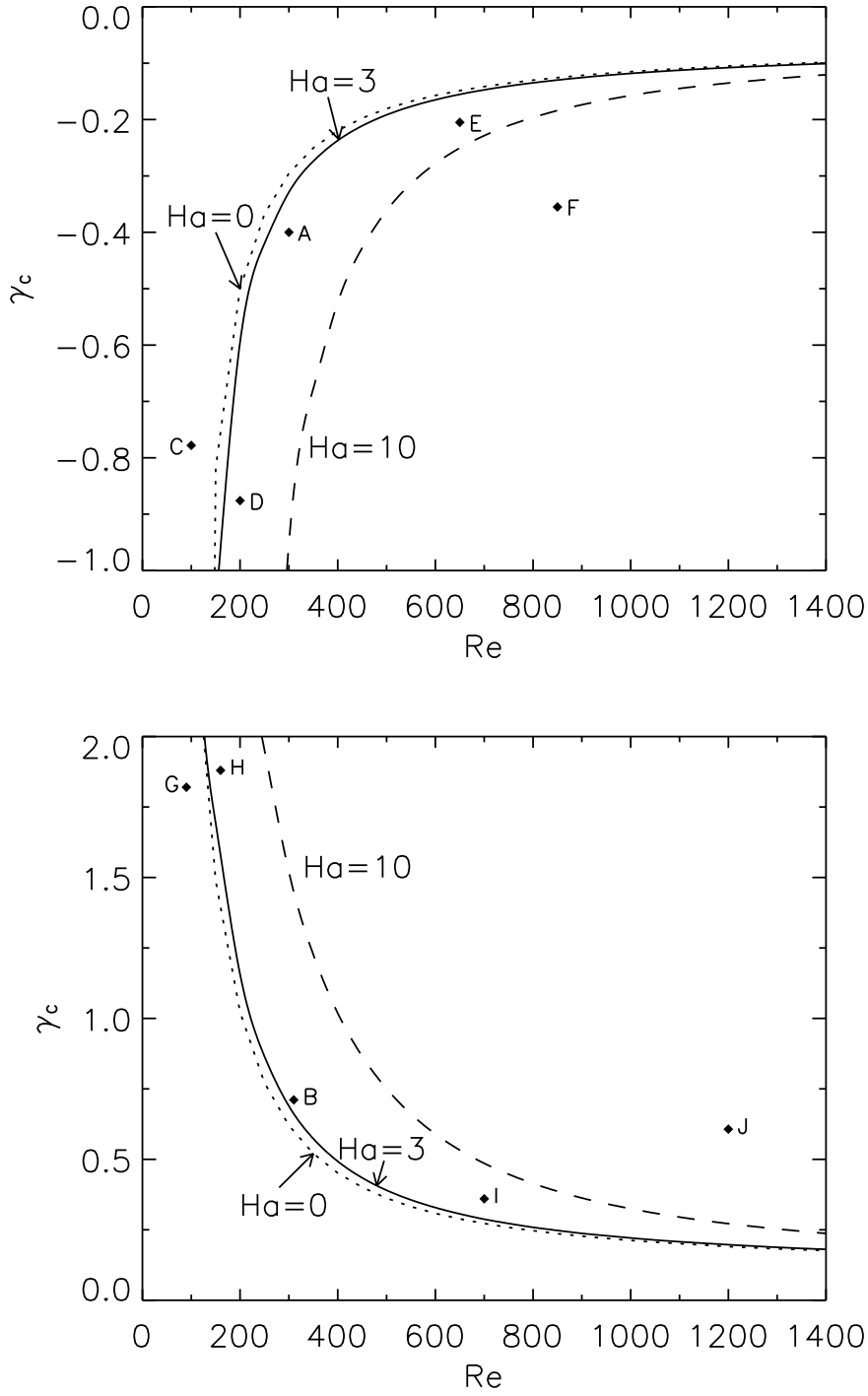

Figure 5.5: *The marginal stability lines for MHD Taylor-Dean flow for infinitely long cylinders for different Hartmann numbers, (· · · · · ·)* $\mathrm{Ha} = 0$*, (——)* $\mathrm{Ha} = 3$*, (– – –)* $\mathrm{Ha} = 10$*. The case for positive (negative)* γ *corresponds to negative (positive) radial currents. In the top (bottom) panel the flow is unstable above (below) the lines. The points labeled with letters represent states displayed in Figs. 5.6–5.12. See the text for the detailed explanation.*

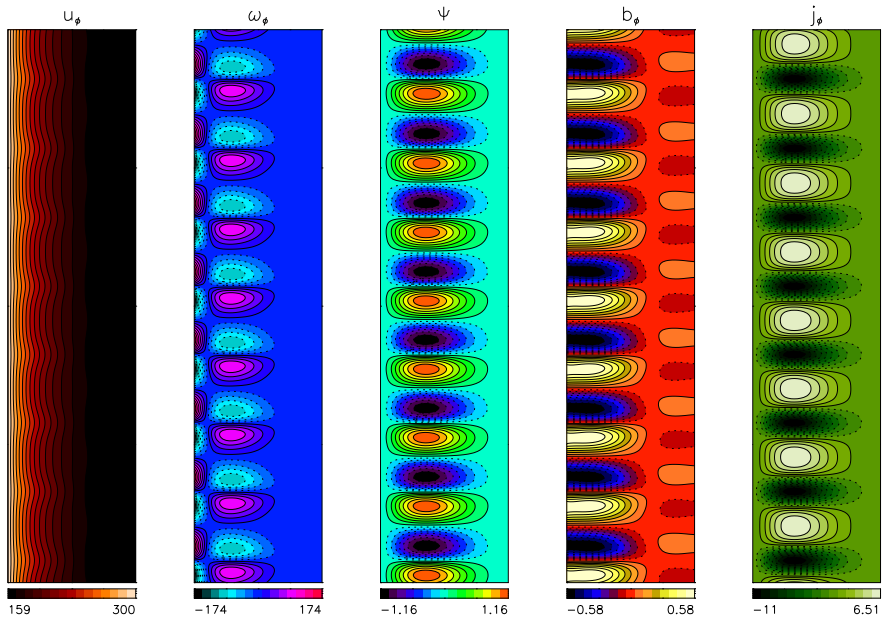

Figure 5.6: *Contour lines of the variables $u_\phi, \omega_\phi, \psi, b_r, j_r$ of the nonlinear fully saturated state for MHD Taylor-Dean flow between cylinders with periodic vertical boundaries. Parameters characterizing this flow correspond to the letter „A" in Fig. 5.5, $\hat{\mu} = 0.27$, $\mathrm{Ha} = 3$, $\mathrm{Re} = 300$ and $\gamma = -0.4$.*

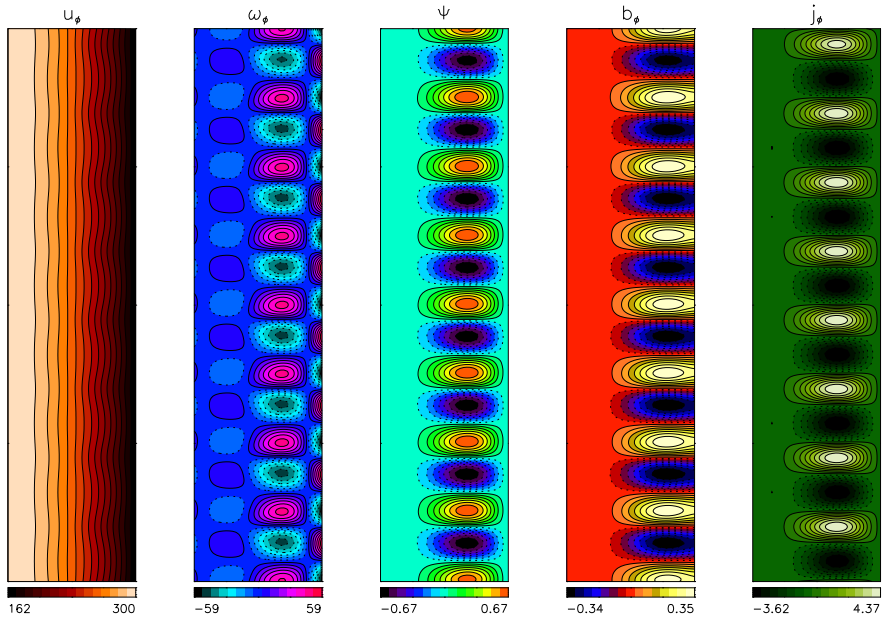

Figure 5.7: *Similarly like Fig. 5.6 but here the flow corresponds to a state labeled with „B" in Fig. 5.5, $\hat{\mu} = 0.27$, $\mathrm{Ha} = 3$, $\mathrm{Re} = 300$ and $\gamma = 0.71$.*

Figure 5.5 shows marginal stability lines for the MHD Taylor-Dean flow for different values of the imposed axial magnetic field[5] for both positive and negative values of γ. The meaning of the points labeled ,,A"-,,J" will be discussed later. We notice that larger value of $|\gamma|$ is needed for stronger axial magnetic field, the reason is that the stronger field stabilizes the flow (at lest for small Pm). Although not shown, the computation indicate that the vertical wavenumber k for the corresponding values of γ changes gradually from $k \approx 4$ for $\mathrm{Re} = 100$ to $k \approx 7$ for $\mathrm{Re} = 1400$.

The results from Fig. 5.5 can serve as yet another test for the nonlinear code described in the Section 2.4, as well as a test for validity of the small $\mathrm{Pm} \to 0$ approximation. In the nonlinear code we have added a term responsible for the transverse pressure gradient to the momentum equation, Eq. (2.21a), so that it became

$$\partial_t u_\phi = (\nabla^2 - r^{-2})u_\phi + [\boldsymbol{u} \times (\mathrm{rot}\, \boldsymbol{u})]_\phi + \mathrm{Ha}^2 \partial_z b_\phi - \frac{K}{r}, \tag{5.15}$$

and K is related to γ by Eqs. (5.10) and (5.11). To test the nonlinear code we apply periodic vertical boundary conditions and for given parameters $\hat{\mu}, \hat{\eta}, \mathrm{Re}, \mathrm{Ha}$ we search for value of K for which the growing rate becomes positive. The agreement between γ_c obtained in this way and γ_c obtained with the linear analysis is pleasing: the difference is not larger than 0.1%.

It is interesting to see how the nonlinearly saturated flow for supercritical values of γ looks like in more details. Figures 5.6, 5.7 display states of the flow just above the critical values of γ corresponding to the points ,,A" and ,,B" in Fig. 5.5. Two cases with different signs of the ratio average pumping/rotation γ are shown.

We notice significant difference for the both flows. Flow labeled ,,A" has the Taylor vortices concentrated close to the inner cylinders, whereas in the flow ,,B" the vortices are found close to the outer cylinder. The azimuthal velocity has significantly different profiles for the both cases.

Let us introduce a non-dimensional vorticity parameter $\zeta \equiv \omega_z / \Omega$

$$\zeta = \frac{1}{r\Omega} \partial_r (r^2 \Omega), \tag{5.16}$$

which serves as a Rayleigh discriminant for stability. The flow is hydrodynamically stable for $\zeta \geq 0$.[6] We notice that for the cases ,,A", ,,B" the criterion is locally violated (see Fig. 5.8).

5.4 The influence of the Hartmann current on the MHD Taylor-Couette flow

We have shown in the Section 5.2 that rotating endplates which enclose any finite Taylor-Couette system introduce similar magnetic effects as, well studied, flow of conducting fluid bounded by an infinite rotating plate (or two such plates). The induced current is turned into radial direction in the magnetic diffusion region which fills majority of the container. For small $\mathrm{Pm} \to 0$ limit it always fills the whole container except boundaries, regardless of the aspect ratio (we stress that we consider only perfectly conducting cylinders here).

In Section 5.3 we have presented a stability analysis of MHD Taylor-Dean flow for an idealized case when the cylinders are infinitely long (or periodic). The azimuthal pressure gradient has been applied explicitly by assuming $\partial_\phi p \neq 0$, critical values of γ_c were calculated.

[5] Naturally we can also consider case when $\mathrm{Ha} = 0$ in which the transverse pressure gradient K is set a priori and is not interpreted as a result of the electromagnetic body force. The flow is then purely hydrodynamical and the ϕ-gradient in the pressure is due to some pumping mechanism.

[6] Moreover, the flow is also magnetohydrodynamically stable for $\zeta \geq 2$. The interesting region is $0 < \zeta < 2$ where MRI can operate and the flow can be unstable (see Ji et al., 2001).

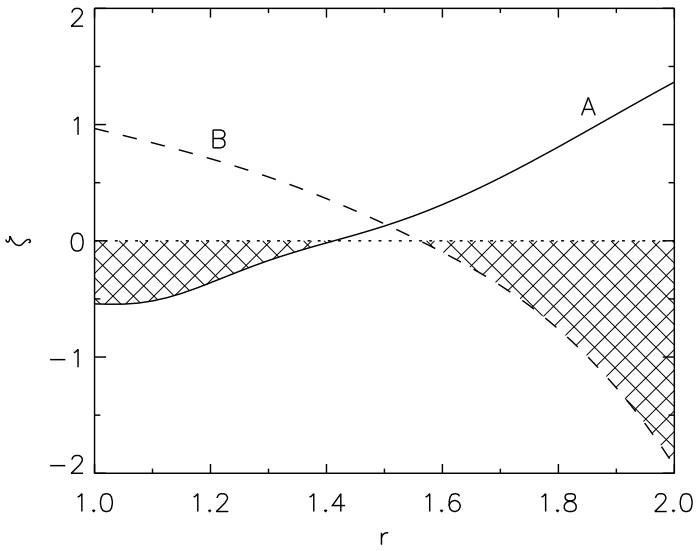

Figure 5.8: *Rayleigh discriminant for stability ζ for the MHD Taylor-Dean flow between periodic cylinders,* $\mathrm{Re} = 300$, $\hat{\mu} = 0.27$, $\mathrm{Ha} = 3$. *(——) „A", $\gamma = -0.4$. (– – –) „B", $\gamma = 0.71$. The Rayleigh line is $\zeta = 0$, the crossed region is centrifugally unstable.*

Consequently, for finite cylinders when the induced current is strong enough, i.e., such that resulting pumping due do the current and the applied axial magnetic field is comparable with critical values γ_c, a possibility of instability should not be ignored. This concerns especially case for conducting endplates for which the current which leaves the Ekman-Hartmann layer is particularly large.

The structure of the Ekman-Hartmann layer changes itself with parameters such as the rotation rates or the strength of the magnetic field. In this section, however, we will concentrate only on flow in the bulk of the container so that only currents and velocities which leave the layer are important.

5.4.1 Endplates rotating with Ω_{out}

First we consider finite cylinders covered with rigid, perfectly conducting endplates rotating with the angular velocity equal to that of the outer cylinder $\Omega_{\mathrm{end}} = \Omega_{\mathrm{out}}$. We choose conducting lids so that the induced current is much stronger (see Section 5.2.3) and its influence on the flow is more evident.

In order to position a specific MHD Taylor-Couette flow on the stability diagram from Fig. 5.5, we run our nonlinear code until a steady solution is obtained. Then γ is computed using the fact that the azimuthal gradient of pressure is $K = \mathrm{Ha}^2 j_{r0}$, as value for the radial current we use j_{r0} from bulk of the fluid (i.e., far from the boundaries, at $z = \Gamma/2$) and close to the inner cylinder. j_r changes with r as $j_r \propto r^{-1}$ so that close to the inner cylinder $|j_r|$ is largest[7].

When the plates rotate with $\Omega_{\mathrm{end}} = \Omega_{\mathrm{out}}$ the Ekman circulation is clockwise and the corresponding Hartmann current has positive sign, i.e., close to the inner cylinder it leaves the Ekman-Hartmann layer with $j_z > 0$, cf. Figs. 5.1, 5.3. Consequently the radial current has also positive sign. Figure 5.9 displays a flow with conducting plates and a weak axial magnetic field applied, $\mathrm{Ha} = 3$. Rotation ratio is $\hat{\mu} = 0.27$ so the flow is hydrodynamically stable, however we notice

[7] We can even say that $|j_r|$ is largest *at* the inner cylinder since the cylinder itself is assumed to be perfectly conducting – the situation would look rather different if insulating cylinders would be considered, however in this work we concentrate only on the conducting ones.

that when the Reynolds number is large enough the flow characteristic changes significantly and set of Taylor vortices can be observed.

The phenomena can be explained as follows: for constant Ha increasing rotation rate leads to stronger Hartmann current drawn into the flow, therefore the corresponding absolute value of γ increases and for certain Re it reaches the critical value γ_c and instability develops. Naturally that kind of instability has nothing to do with MRI since Rayleigh criterion for stability is not fulfilled.

This instability has essentially local character and it is not possible to define any specific critical Reynolds number whose crossing would lead to some exponential grow in the whole container. There exists Re between 100 („C") and 200 („D") for which only part of the container would be filled with the Taylor vortices. However we notice that for small Reynolds number γ_c is very steep (for both positive and negative values of γ) so that when it is crossed in this region the transition between stable flow and flow totally dominated by the vortices is rather sharp.

It is known that stronger axial magnetic field has stabilizing effect even on a hydrodynamically unstable flow. Besides that, the Hartmann current increases with strength of the magnetic field only until certain point is reached. When the magnetic interaction parameter α reaches value ≈ 2.5 increasing Ha does not further increase the Hartmann current (see Gilman and Benton, 1968). For these reasons it is clear that when the imposed magnetic field is strong enough the instability described above will not occur. Indeed it has been checked that for $\mathrm{Re} = 200$ and the magnetic field with $\mathrm{Ha} = 20$ there are no Taylor vortices, although the rotational profile is significantly changed when compared to the non-magnetic situation. This change naturally follows from the $j_r \hat{\mathbf{e}}_r \times \boldsymbol{B_0}$ term which accelerates or decelerates the fluid, nevertheless the strong axial magnetic field suppresses instability in that case.

If the perfectly conducting ends are replaced with insulating ones the induced Hartmann current is much weaker. It is so weak that when the imposed magnetic field has strength such that $\mathrm{Ha} = 3$, absolute value of γ is *always* smaller then γ_c regardless of Re. Therefore such flow is never unstable in the sense described above.

However when the magnetic field is stronger the situation is different. For sufficiently high rotation rates the induced radial current is large enough to generate, together with the field, γ exceeding γ_c. This can be seen in Fig. 5.10. Naturally also for insulating ends when the applied field is too strong the pumping due to the electromagnetic force is too weak to bring the flow into the unstable regime.

5.4.2 Endplates rotating with Ω_in

If rigidly conducting endplates are attached to the inner cylinder, $\Omega_\mathrm{end} = \Omega_\mathrm{in}$, the Ekman circulation is counter-clockwise (Ekman suction) and the corresponding Hartmann current have negative sign, the parameter γ is positive. From Fig. 5.11 we see that, analogously like in the case depicted in Fig. 5.9, when the rotation is sufficiently fast the resulting γ reaches critical value and the flow becomes dominated by the Taylor vortices (the points labeled „G" and „H").

Similarly when the insulating plates are used the axial magnetic field with $\mathrm{Ha} = 3$ is too weak to generate sufficiently large γ. When stronger field is applied, $\mathrm{Ha} = 10$, it is possible to cross γ_c and the flow reaches unstable regime.

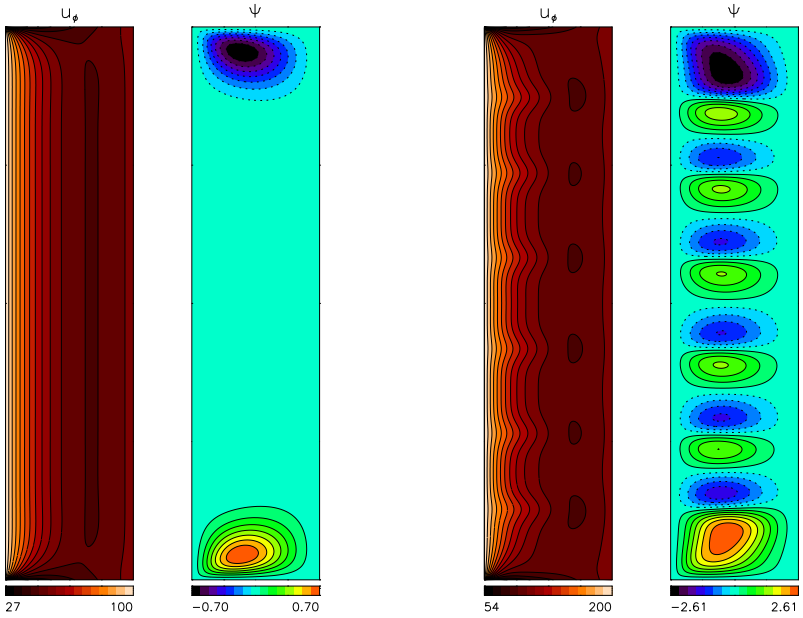

Figure 5.9: *Contour lines of the azimuthal velocity u_ϕ and the stream function ψ. The cylinders are enclosed with perfectly conducting plates rotating as a rigid body with angular velocity $\Omega_{\mathrm{end}} = \Omega_{\mathrm{out}}$. $\hat{\mu} = 0.27, \mathrm{Ha} = 3$. Left: $\mathrm{Re} = 100$, right: $\mathrm{Re} = 200$. On the Fig. 5.5 the both flows are labeled with „C" (the left one) and „D" (the right one). We see that for the flow „D" the corresponding γ is in the region where the MHD Taylor-Dean for infinite cylinders is unstable.*

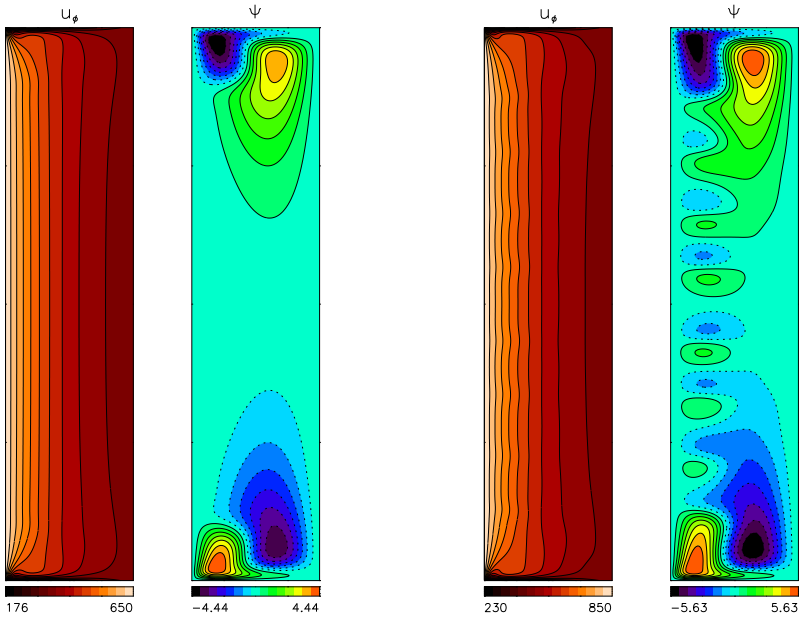

Figure 5.10: *Contour lines of ψ, u_ϕ. The plates are insulating, rotating rigidly $\Omega_{\mathrm{end}} = \Omega_{\mathrm{out}}$, $\hat{\mu} = 0.27, \mathrm{Ha} = 10$. Left: $\mathrm{Re} = 650$, „E". Right: $\mathrm{Re} = 850$, „F". Compare with Fig. 5.5 and Fig. 5.9.*

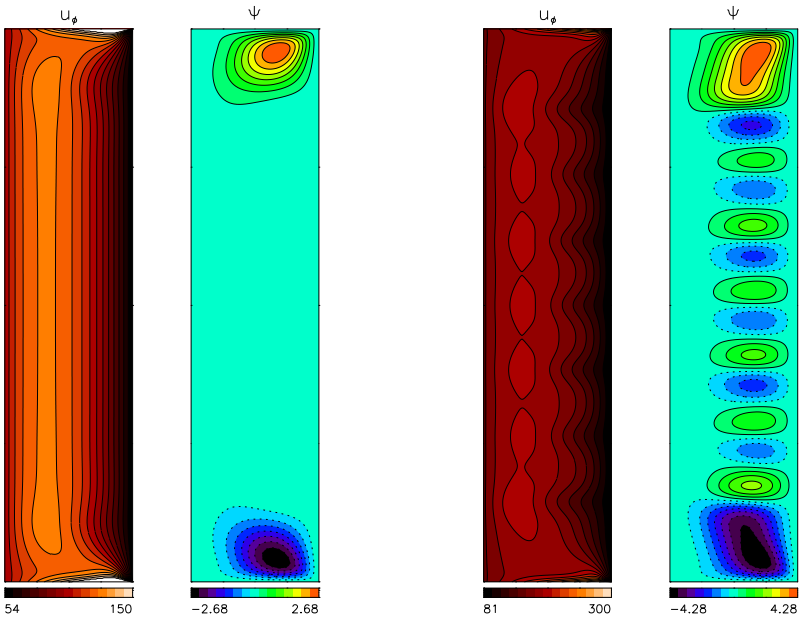

Figure 5.11: *Contour lines of ψ, u_ϕ. The plates are perfectly conducting and rigidly rotating rigidly $\Omega_{\mathrm{end}} = \Omega_{\mathrm{in}}$, $\hat{\mu} = 0.27, \mathrm{Ha} = 3$. Left:* $\mathrm{Re} = 100$ *(„G"), right:* $\mathrm{Re} = 150$ *(„H"). Compare with Fig. 5.5*

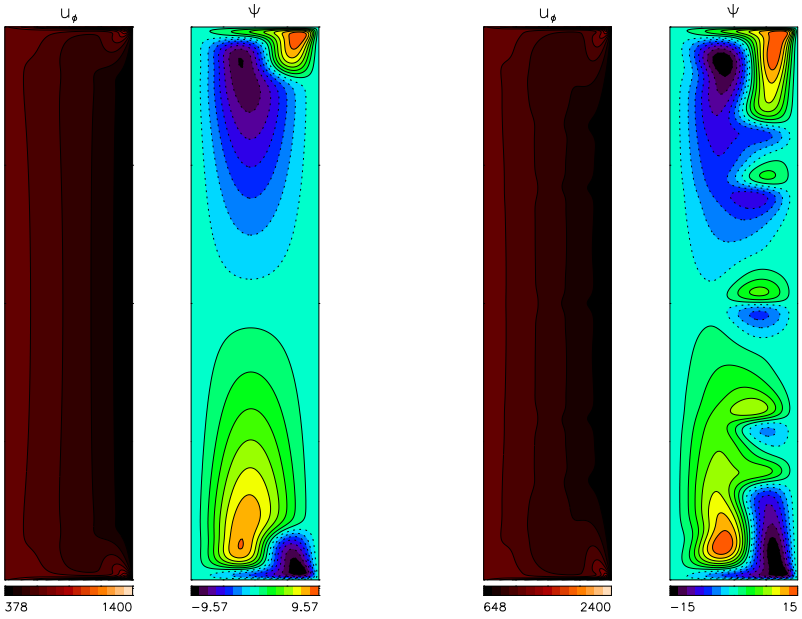

Figure 5.12: *Contour lines of ψ, u_ϕ. The plates are insulating, rotating rigidly $\Omega_{\mathrm{end}} = \Omega_{\mathrm{in}}$, $\hat{\mu} = 0.27, \mathrm{Ha} = 10$. Left:* $\mathrm{Re} = 700$ *(„I"), right:* $\mathrm{Re} = 1200$ *(„J"). Compare with Fig. 5.5*

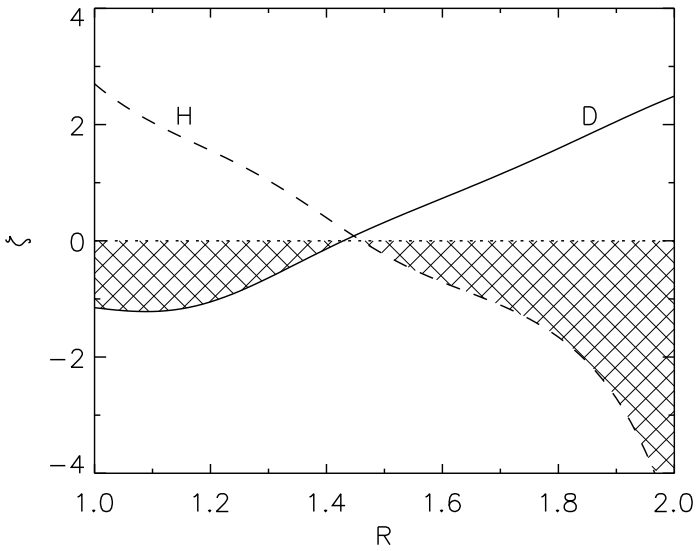

Figure 5.13: *Rayleigh discriminant for stability ζ for the MHD Taylor-Couette flow with $\hat{\mu} = 0.27$,* $\mathrm{Ha} = 3$. *The cylinders are enclosed by perfectly conducting endplates. (——) „D",* $\mathrm{Re} = 200$, $\Omega_{\mathrm{end}} = \Omega_{\mathrm{out}}$. *(– – –) „H",* $\mathrm{Re} = 150$, $\Omega_{\mathrm{end}} = \Omega_{\mathrm{in}}$. *The Rayleigh line is $\zeta = 0$, the crossed region is centrifugally unstable.*

We notice that in the both cases the vortices, as expected, concentrate near the outer cylinder, i.e., in region where $\zeta < 0$ and the Rayleigh criterion is not fulfilled, see Fig. 5.13. Again the effect is clearly more striking when perfectly conducting plates are used, the radial current is much stronger when compared to insulating vertical boundary conditions.

It is not to be forgotten that change of sign of the Hartmann current can also be realized by changing the sign of the applied magnetic field. Obviously in that case the vortices would tend to concentrate near the inner cylinder even if the plates rotate as $\Omega_{\mathrm{end}} = \Omega_{\mathrm{in}}$.

5.4.3 Dependence on the Hartmann number

It has been discussed that in the MDR the induced j_r interacts with $\boldsymbol{B_0}$ and leads to acceleration or deceleration of the fluid azimuthal motion. If B_z and j_r is positive, as is if the plates are attached to the outer cylinder, the flow should be decelerated. Dependence of the azimuthal velocity u_ϕ in the middle of the container ($r = R_{\mathrm{in}} + D/2, z = \Gamma/2$) on strength of the applied magnetic field is shown in Fig. 5.14. Values of the velocity are scaled to cm/s using scales corresponding to the PROMISE setup.

The left panel of the figure refers to a case when the plates are perfectly conducting. Clearly the magnetic field inhibits the angular velocity by almost 50%. If the plates are insulating, the right panel of the figure, it is not the case: the change is noticeable, however much smaller.

The profile of angular velocity in the middle of the gap, for $z = \Gamma/2$, is shown in Fig. 5.15. The change when compared to the Couette solution is dramatic even for relatively weak magnetic field applied. For $\mathrm{Ha} = 10$ the rotation is so much different that relating it to the Couette flow is pointless. However, if the insulating plates are applied the situation is much better in the sense that the profile of Ω is not so profoundly altered. Generally it resembles the Couette solution also for $\mathrm{Ha} = 10$, yet still the Rayleigh criterion for stability is locally violated.

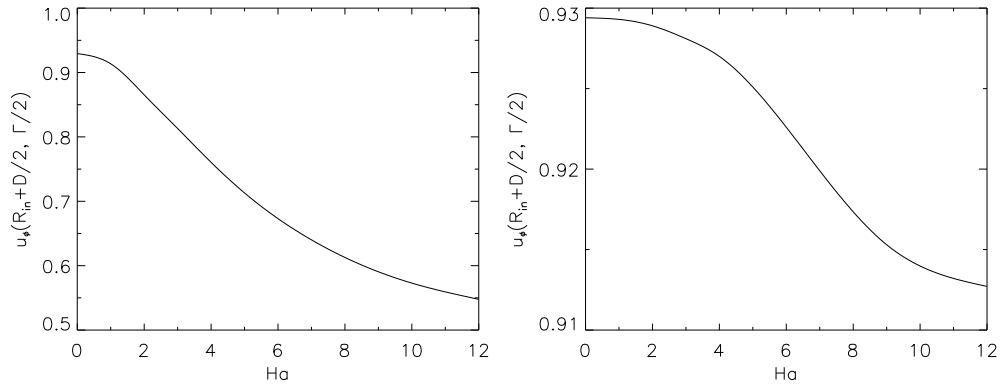

Figure 5.14: *The azimuthal velocity u_ϕ in the middle of the gap for different Hartmann numbers. Left: perfectly conducting endplates. Right: insulating endplates. The Reynolds number is fixed to $\mathrm{Re} = 1775$, $\hat{\mu} = 0.27$, the both plates rotate with the outer cylinder $\Omega_{\mathrm{end}} = \Omega_{\mathrm{out}}$. The velocity is scaled to units of cm/s.*

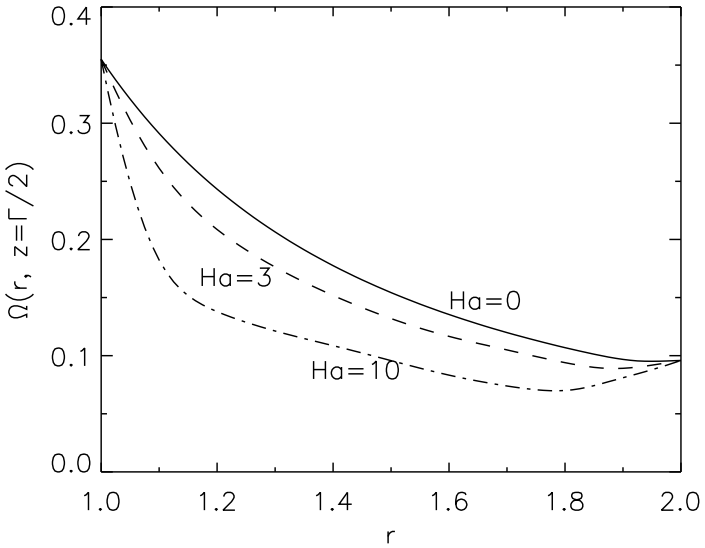

Figure 5.15: *The angular velocity $\Omega(r)$ [Hz] for $z = \Gamma/2$ for different Hartmann numbers. The plates are perfectly conducting, $\Omega_{\mathrm{end}} = \Omega_{\mathrm{out}}$, $\mathrm{Re} = 1775$, $\hat{\mu} = 0.27$.*

5.4.4 Estimation of γ for wide range of Re and Ha

Let us, very roughly, estimate the value of γ – the ratio of average pumping due to the Hartmann current to the rotation velocity, for larger Reynolds and Hartmann numbers. Gilman and Benton (1968) have derived expressions for currents when difference between angular velocity of rotating, insulating, infinite plate and angular velocity of the fluid far from the plate is small (i.e., $\epsilon \ll 1$). Later Benton and Chow (1972) have derived analogous expressions for nonlinear boundary layer and obtained formulae quadratic in ϵ, for example for the ,,blowing" Hartmann current (in the zero Pm limit):

$$\frac{j_z(\infty)}{\frac{B_0}{\mu_0\eta}\sqrt{\nu\Omega_1}} = -\epsilon\frac{2\beta'}{\beta'^2+\beta'^{-2}} + \epsilon^2\frac{4(4\beta'^4-5-\beta'^{-4})}{\beta'(\beta'^2+\beta'^{-2})^8(9\beta'^2+\beta'^{-2})}, \tag{5.17}$$

where $\beta' = [\alpha^2 + (\alpha^4+1)^{1/2}]^{1/2}$ and α is defined by (5.3). If we take value of this current $j_z(\infty)$ and assume that it turns into radial direction $j_{r0} = j_z(\infty)$ (as is for the case where there are two

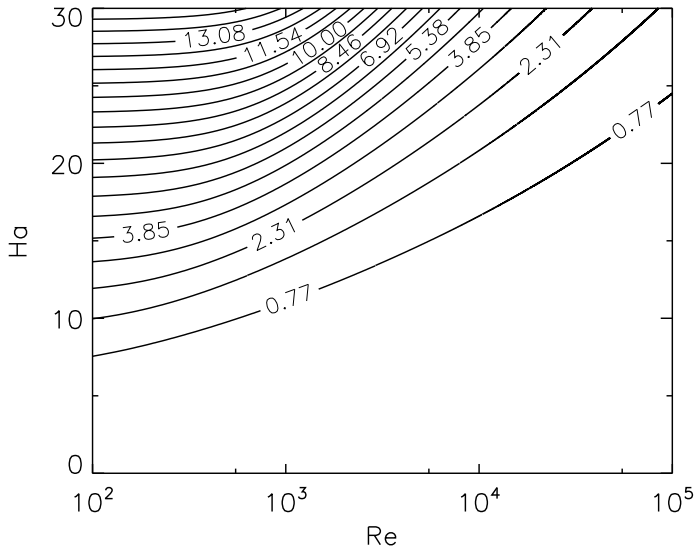

Figure 5.16: *Contour lines of γ' in $(\mathrm{Re}, \mathrm{Ha})$ space. γ' is derived from values of the Hartmann current for rotating plate for different Re and Ha.*

plates and the fluid is confined between them), since $K = j_{r0}\mathrm{Ha}^2$ from (5.10) we can obtain γ' (we use prime to stress that this is computed for theory of infinite rotating plates, not for the Taylor-Couette geometry).

Figure 5.16 shows how γ' derived in such way depends on the rotation rates and the strength of the applied axial magnetic field. We have chosen $\epsilon = 0.3$ which roughly corresponds to our situation for the MHD Taylor-Couette problem if the endplates are attached to the outer cylinder.

Naturally this is rather a crude approximation when related to the MHD Taylor-Couette problem since there are important differences between the idealized case of rotating infinite plates and the flow enclosed between cylinders. One important contradiction can be immediately noticed: for constant value of Ha, $|\gamma'|$ slowly decreases with Re, whereas it was not the case for the Taylor-Couette flow in which increasing rotation led to increasing of $|\gamma|$ and ultimately the flow become unstable.

Nevertheless one can get general picture of importance of the radial currents when the magnetic field is strong or the rotation much faster. For constant Re increasing the axial magnetic field leads to a saturation in which Hartmann current virtually does not increase. This saturation is achieved when $\alpha > 2.5$ (for example for $\mathrm{Re} = 100$ this means $\mathrm{Ha} > 20$). However further increasing of Ha lead to increasing of $K = j_r\mathrm{Ha}^2$ and therefore $|\gamma'|$ (we shall not forget that the critical $|\gamma_\mathrm{c}|$ also increases with Ha, in particular it is clear for small $\mathrm{Re} \lesssim 1000$).

When the magnetic field is kept constant and rotation rates increased then $|\gamma'|$ decreases. This allows us to assume that for reasonable values of $\mathrm{Ha} \approx 10$ and fast rotation, all the effects due to electromagnetic forces induced by the Ekman-Hartmann layer become less important in the sense that $|\gamma'|$ remains small. Of course this is expected since the rotation starts to play the dominant role.

5.5 Summary

Gilman and Benton (1968) have shown, by use of the linear theory, that in vicinity of a rotating plate which serves as a border for rotating conducing fluid there develops an Ekman-Hartmann layer if $\Omega_\mathrm{plate} \neq \Omega_\mathrm{fluid}$ and the axial magnetic field is applied. The most important feature

of the Ekman-Hartmann layers is their ability to induce both mass flux and electric current in the region outside the boundary layer. If $\Omega_{\mathrm{plate}} < \Omega_{\mathrm{fluid}}$ these fluxes are directed outwards the layer („blowing"); when $\Omega_{\mathrm{plate}} > \Omega_{\mathrm{fluid}}$ towards the layer („suction"). Loper (1970) studied conducting plates, it was shown that in that case the mass flux and the current are much stronger.

When the fluid is bounded by two such rotating plates, the induced current eventually turns into radial direction. There exists a region, the magnetic diffusion region, in which all the electric currents have only radial component. They, together with the axial magnetic field, produce electromagnetic body force acting on the fluid.

In this chapter we have seen that similar effects arise for the MHD Taylor-Couette flow in the case when the rotating cylinders are bounded by two rigid plates, rotating with angular velocity of the outer or the inner cylinder. Near the endplates the Ekman-Hartmann layer forms and consequently there exists the Hartmann current which penetrates bulk of the fluid. In the presence of the axial magnetic field such problem can be compared with Taylor-Dean flow – a flow between, possibly rotating, cylinders which is driven by a transverse pressure gradient.

It has been shown that under certain conditions the resulting flow becomes unstable and Taylor vortices can be observed. In particular, this is undesirable phenomena from the point of view of the MRI experiment PROMISE. In such MRI experiment it is necessary to obtain state as close to the standard Couette solution $\mathbf{\Omega}_0$ as possible in major part of the container. Also when the axial field is turned on, therefore the instability develops only after switching on the azimuthal component of the field.

The fluxes induced in the Ekman-Hartmann layer are a direct consequence of shearing close to the boundaries. The layer arises since magnetohydrodynamical variables characterizing the fluid far from the boundaries must match boundary conditions. Exemplary methods of reducing the shearing have been presented in the previous chapter.

Chapter 6

Summary

Magnetorotational instability provides an important and efficient mechanism for transporting angular momentum in wide class of astrophysical objects. In particular it is crucial for accretion disks. The matter in such disks rotates as $\Omega \propto r^{-3/2}$ and, by loosing the angular momentum, falls onto a central compact body. There exist a viscous process which allows the angular momentum to be transported outwards. MRI, if angular velocity decreases outwards and there is a weak magnetic field present, leads to developing of a small scale turbulence which serves as the viscosity. The required conditions for MRI: rotation and magnetic fields are easily fulfilled on astrophysical scales. Naturally, the rotating medium must be conducting which is true for hot ionized plasma but not necessarily true for cold matter like, for example, protostellar disks.

Originally MRI has been discovered for a theoretical flow of ideally conducting liquid between two rotating cylinders in a presence of an axial magnetic field (Velikhov, 1959). Decades later it was realized that the same mechanism can explain the puzzles of angular momentum transport in the disks. Recently the subject became of particular interest for different groups of MHD theoreticians and experimentalists: proving in a laboratory that MRI exists is a significant challenge.

The simplest and most convenient experimental setup for MRI consists of two concentric rotating cylinders with the gap between them filled with a liquid, the Taylor-Couette flow. Usually a liquid metal like gallium or sodium is used. The ratio of the kinematic viscosity to the magnetic diffusivity, i.e., the magnetic Prandtl number, of such liquids is very small, of order 10^{-6}. Since, for the classical MRI with axial magnetic field, the critical Reynolds number associated with the rotation of cylinders scales as Pm^{-1} it is necessary that the rotation is very rapid. This leads to problems of technical nature. Moreover, plates which enclose the cylinders from the top and bottom drive a secondary flow which disturb the flow and make it difficult to excite, observe and properly identify the MRI modes.

The external magnetic field can be easily modified by letting an electric current through a rod placed on the axis of rotation of the cylinders. Therefore an additional azimuthal component of the magnetic field is created and the field takes a helical form, Eq. (2.4). This modification makes it much easier to excite MRI in the sense that much slower rotation is required. It is important to note that the field is steady and current free therefore it does not change the rotational profile (at least in the limit of infinitely long cylinders or for periodic ones). Consequently the instability is driven by the rotation.

The flow with the new configuration of the applied magnetic field has a new property, the solution takes a form of a traveling wave. For an idealized case of infinitely long cylinders it means that the instability manifests itself as moving Taylor vortices in a direction determined by the rotation and the magnetic field. A question was stated whether presence of the endplates would profoundly change, or even destroy, that type of instability. Until now only linear stability results

were known and the question, as well as matter concerning velocity amplitudes of saturated flow, remained unanswered.

In Chapter 3 it has been shown, by use of our nonlinear axisymmetric code, that even if the vertical boundary conditions resemble rotating or stationary endplates, the helical MRI can still be observed (Szklarski and Rüdiger, 2006). The traveling wave, although distracted, could in principle be identified. Amplitudes of all velocity components were presented, theirs values are of order $0.1-1.0$ mm/s and, for parameters of our interest, depend linearly on the Reynolds number. It has also been demonstrated that torque at the cylinders is increased when the flow is unstable, this indicates that the angular momentum is indeed transported outwards. Nevertheless, the plates introduced clear secondary flow which is undesirable and an effort to reduce it should be taken.

Reduction of effects driven by the endplates was discussed in Chapter 4. It has been showed that, for parameters characterizing a stable flow in the limit of infinitely long cylinders, there exists a peculiar instability induced be the plates in the presence of the axial magnetic field. This becomes more evident if perfectly conducting vertical boundaries are applied. That, obviously unwanted, phenomena is a clear result of electric currents induced in a boundary layer close to the endplates. Simple and inexpensive ways of reducing impact of the lids were proposed. It can be done either by allowing to rotate the endplates independently of the cylinders with appropriate angular velocity or by dividing the plates into two rings which can be attached to the both cylinders (Szklarski, 2007). It is crucial that the both plates are made from an insulating material.

The question concerning subcritical excitations has also been addressed. It turns out that the plates can serve as source of viscous perturbations which are then amplified and dragged by the magnetic field resembling frequencies of the traveling wave even for subcritical characteristic values. When the end-effects are reduced this is not an issue, however a special care must be taken concerning vertical wavelengths of the MRI modes. If the cylinders are too short compared with this wavelength it is possible that the instability will not develop.

The classical Ekman layer which arises near the plates enclosing a purely hydrodynamical Taylor-Couette flow is well known. However, magnetic effects induced by the lids are not discussed in details in literature concerning the subject of MHD Taylor-Couette flow. Although the Ekman-Hartmann layer, which develops for a motion of conducting fluid when rotation and a perpendicular magnetic field are present, has already been studied in 60's and 70's. In Chapter 5 of this thesis we have shown how these results are related to the MHD Taylor-Couette flow at finite aspect ratio.

The most important conclusion concerning the Ekman-Hartmann layer is its ability to induce electric current which leave the layer and penetrated the flow. The current turns in radial direction and, acting in concert with the axial magnetic field, increases or decreases the azimuthal fluid velocity. In our Taylor-Couette setup this can be viewed as a additional force representing an azimuthal pressure gradient and it makes possible to relate the flow to a Taylor-Dean flow. If the induced currents are strong enough, the rotational profile can be significantly changed and instability can set it (Szklarski and Rüdiger, 2007). This, however, has nothing to do with MRI since for that case the Rayleigh local criterion for centrifugal stability is not fulfilled. All these effects can be significantly reduced by minimizing vertical shears with the methods described earlier.

The existence of the helical MRI has been proved in the PROMISE experiment (Stefani et al., 2006; Rüdiger et al., 2006; Stefani et al., 2007). The traveling wave has been observed, its frequency and direction matching theoretical predictions. Also the agreement for velocity amplitudes was quite good, see Appendix A. However, the vertical boundaries introduced clear problems and there is some space for improvement. In the first place the vertical boundaries

were not symmetric, moreover one of the plates were made from copper which led to induction of additional undesirable electric currents. Therefore, from the experimental point of view, a new version of PROMISE would provide more clear and more evident results.

When it comes to the Ekman-Hartmann layer and its influence on the flow there is more work which can be done. How the flow would behave for much faster rotation and much stronger magnetic field? How insulating radial boundary conditions would change the presented results? The helical MRI introduces the traveling wave, how the flow would behave for different height of the cylinders and different strength of the azimuthal field? What about non-axisymmetric modes? It is known that these modes in a Taylor-Dean flow can be fairly easy excited. Moreover, there exists an instability only due to the toroidal magnetic field which operates only for non-axisymmetric flows.

Theory of Taylor-Couette flow and its MHD version is an extremely reach and exciting field of science. It is surprising that conceptually so simple system can provide so much interesting questions still waiting to be answered.

Appendix A

The PROMISE Facility

The PROMISE experiment has been conducted by MHD group at Forschungszentrum Dresden-Rossendorf. Here we briefly describe this facility, more details about the experiment and its results can be found in Stefani et al. (2006); Rüdiger et al. (2006); Stefani et al. (2007).

The PROMISE setup consists of a cylindrical copper vessel placed on a precision turntable, its outer wall has thickness of 15 mm and extends from 80 mm to 95 mm, serving as the outer cylinder for the MHD Taylor-Couette flow. The inner cylinder is also made of copper and is attached to an upper turntable, so that it is immersed into the fluid from above. Its thickness is 4 mm and extends in radius from 36 mm to 40 mm. The fluid confined between the cylinders can be filled up to 410 mm and it corresponds to a Taylor-Couette flow with $D = R_{\rm out} - R_{\rm in} = 40$ mm and $H = 400$ mm, $\Gamma = 10$ (see Fig. A.1).

The upper endplate, made of plexiglas and hence insulating, was attached to the frame and therefore stationary, $\Omega_{\rm top} = 0$. The bottom endplate was part of the rotating copper vessel so it was conducting and $\Omega_{\rm bot} = \Omega_{\rm out}$. This particular setup introduced asymmetry to the problem: vertical boundary conditions were different for the velocity and the magnetic fields as well.

The fluid itself is an alloy of GaInSn which is liquid at room temperatures. The physical properties are: the density $\rho = 6.36$ g cm^{-3}, the kinematic viscosity $\nu = 3.40 \times 10^{-3}$ cm^2/s, the electric conductivity $\sigma = 3.27(\Omega{\rm m})^{-1}$ so that the magnetic Prandtl number is ${\rm Pm} = 1.40 \times 10^{-6}$.

The axial magnetic field was created by a coil through which currents up 200 A were delivered, Fig. A.2. The created field could be up to $B_0 = 20.35$ mT which corresponds to ${\rm Ha} = 31.7$. The azimuthal component of helical field was due to flowing current through a central rod $J_{\rm rod}$. The flowing current was up to 8 kA and it was necessary to cool the rod, since undesirable temperature gradients could interfere the flow. The relation between the current and β is

$$\beta = \frac{J_{\rm rod}}{5 B_0 R_{\rm in}} \tag{A.1}$$

where $J_{\rm rod}$ is in Ampère, B_0 in Gauss and $R_{\rm in}$ in cm.

Naturally it was impossible to measure the velocity with standard optical techniques.[1] Instead two ultrasonic transducers, mounted at the top stationary endplate, were used. The sensors using high frequency sound waves (4 MHz) were able to deliver information about the vertical component of the velocity with resolution 1.84 s in time and 0.685 mm in z direction with accuracy ~ 0.05 mm/s. Two of such devices were used in order to determine if the observed modes are symmetric with $m = 0$ or nonsymmetric $m = 1$. It should be noted that $m = 1$ were observed for certain range of parameters.

[1] Normally when the rotating fluid is transparent it is possible to eject into it „tracers" (for example tiny pieces of some metal). Then by means of Doppler shift techniques it is possible to measure theirs velocity with a laser beam.

Figure A.1: *The PROMISE setup as for December 2005.* Left: *The both cylinders mad of copper with radii* $R_{\mathrm{in}} = 4$ *cm,* $R_{\mathrm{out}} = 8$ *cm are presented. Electric motor driving the cylinder also can be seen.* Right: *Later in the central hole a copper rod was placed through which an electric current of up to* 8000 *A could flow. Since such large currents can heat the device it was necessary to cool the rod with water constantly flowing around it.* Photos by R. Arlt.

In Fig. A.3 comparison between experimental and numerical data is presented. The simulation was performed with use of the code described in Section 2.4. Although in the computations treatment of the magnetic boundary conditions was simplified, the agreement for the velocity amplitudes and the traveling wave frequency is quite good. Fore more detailed comparison with the experimental data the reader can refer to Stefani et al. (2007).

Acknowledgments The above information is given on basis of the cited articles. I thank to Frank Stefani for providing me the experimental data and to Rainer Arlt for the photos.

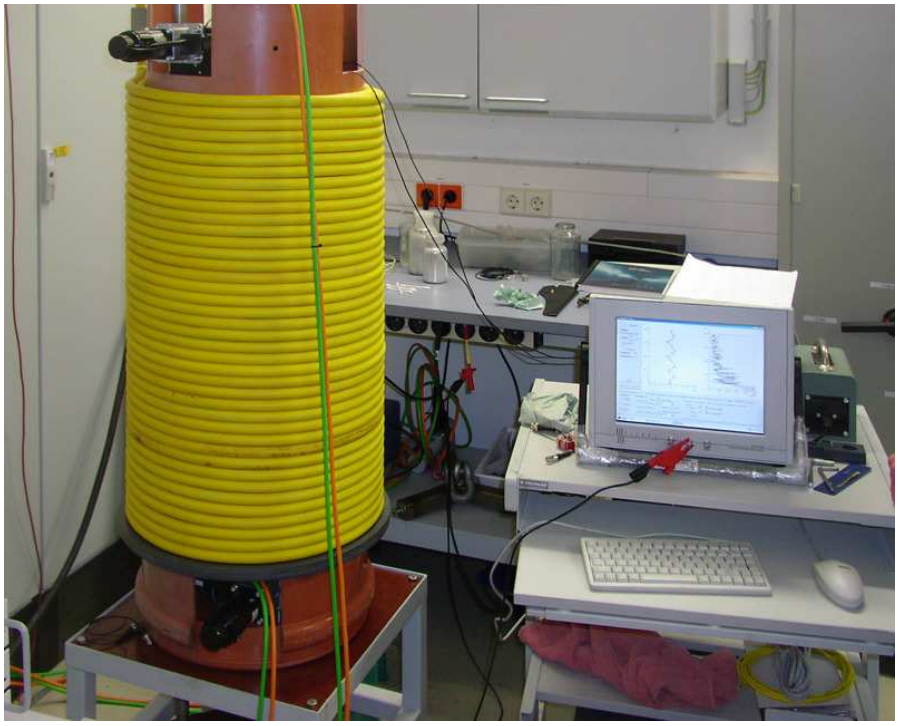

Figure A.2: *The experiment at work, July 2006. The rotating cylinders were enclosed in the coil which generated the axial magnetic field.* Photo by R. Arlt.

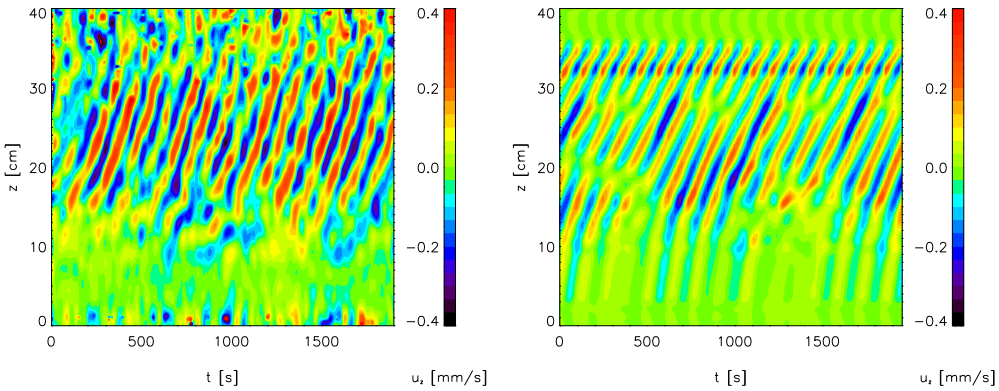

Figure A.3: *Comparison of the data collected from the experiment (left) and results of our nonlinear simulations (right) for* $\mathrm{Re} = 1480, \hat{\mu} = 0.27, \mathrm{Ha} = 9.5, \beta = 6.0$. *The boundary conditions for the velocity in the simulation are the same like in the experiment, i.e.,* $\Omega_{\mathrm{bot}} = \Omega_{\mathrm{out}}$, $\Omega_{\mathrm{top}} = 0$. *However, for the magnetic field in the simulation both endplates are assumed to be insulating, whereas in the experiment the bottom one is made of copper. In this figure* $z = 0$ *corresponds to the lower plate, we notice that the vortices travel upwards. This is expected since in the experiment product* $B_0 \times \beta \times \Omega_{\mathrm{in}}$ *has negative sign.*

Appendix B

MHD parameters

The characteristic scales for our MHD Taylor-Couette flow are: for the magnetic field $\mathcal{B}$ it is the strength of the applied axial magnetic field B_0, for the length scale $\mathcal{L}$ it is the gap width $D = R_{\rm out} - R_{\rm in}$. As the time scale we use hydrodynamic diffusion time $\mathcal{L}^2/\nu$ and as the velocity scale $\mathcal{U}$ we have $\nu/\mathcal{L}$. Radii of the rotating cylinders are denoted by $R_{\rm in}, R_{\rm out}$, theirs height by H, theirs angular velocity by $\Omega_{\rm in}, \Omega_{\rm out}$.

All the principal parameters used in the thesis can be summarized in the Table B.1.

Table B.1: *MHD parameters*

Symbol	Description	General definition	MHD Taylor-Couette definition
ν	Kinematic viscosity		
η	Magnetic diffusivity		
ρ	Fluid density		
μ_0	Magnetic permeability		
σ	Conductivity	$\sigma = 1/\mu_0\eta$	
Pm	Magnetic Prandtl number	ν/η	
$\hat{\mu}$	Rotation ratio		$\hat{\mu} = \Omega_{\rm out}/\Omega_{\rm in}$
$\hat{\eta}$	Radius ratio		$\hat{\eta} = R_{\rm in}/R_{\rm out}$
Γ	Aspect ratio		$\Gamma = H/D$
V_a	Alfvén velocity	$\mathcal{B}/\sqrt{\mu_0\rho}$	$B_0/\sqrt{\mu_0\rho}$
Re	Reynolds number	$\mathcal{U}\mathcal{L}/\nu$	$\Omega_{\rm in}R_{\rm in}D/\nu$
Ha	Hartmann Number	$V_a\mathcal{L}/\sqrt{\nu\eta}$	$B_0\sqrt{R_{\rm in}D/\mu_0\rho\nu\eta}$
Rm	Magnetic Reynolds number	$\mathcal{U}\mathcal{L}/\eta$	$\Omega_{\rm in}R_{\rm in}D/\eta \equiv \mathrm{RePm}$
$d_{\rm E}$	Ekman depth	$\sqrt{\nu/\Omega}$	$\sqrt{\nu/\bar{\Omega}}$
$d_{\rm H}$	Hartmann depth	$\sqrt{\nu\eta}/V_a$	D/Ha
β	Azimuthal/axial field		$\boldsymbol{B_0} = \hat{\mathbf{e}}_\phi B_0 \beta R_{\rm in} r^{-1} + \hat{\mathbf{e}}_z B_0$

Acknowledgments

In the first place I would like to thank my supervisor, Prof. Günther Rüdiger, for guiding me through the exciting field of magnetohydrodynamics. At the beginning of our cooperation we both thought that the vertical boundaries in the discussed problem are of much less importance. Fortunately the nature of science is such that there is always place for interesting surprises.

I also thank to other members of the MHD group at AIP: Detlef Elstner and Manfred Schultz for discussions concerning the subject, Prof. Detlef Schönberner who carefully edited some of my texts. I thank to[1] Oliver, Stavro, Aniket, Pavel, Udo, André, Marcus and Rainer for every-day contact, common lunch time, interesting talks concerning every possible topic (photography in the first place), for spending some nightlife together in Potsdam and Berlin. Additional thanks goes to the only women in our MHD building, Mrs. Andrea Hans, the only person who always remembers about everyone's birthday.

I thank to the rest of AIP stuff, to the administration which did not make any problems and actually was very helpful with all the bureaucratic work; to the library stuff, especially to Mrs. Regina v. Berlepsch who delivered every paper I asked for; to Karl-Heinz for solving hardware-related problems and occasional chat in my native language. I thank to Antony Youd from University of Newcastle for providing me his version of the numerical code and fruitful discussions about Taylor-Couette flows.

The very personal thanks goes to members of my family for continuous support during my time in Potsdam, especially to my mother and brother. I am also grateful to all real friends in my hometown. The warmest ,,Thank You" goes, however, to Monika.

Jacek Szklarski
Potsdam
August 2007

[1] In an increasing desktop-walking-distance order!

List of Figures

List of Tables

Bibliography

J. Abshagen, K. A. Cliffe, J. Langenberg, T. Mullin, G. Pfister, and S. J. Tavener. Taylor Couette flow with independently rotating end plates. *Theoretical and Computational Fluid Dynamics*, 18: 129, 2004.

D. J. Acheson and R. Hide. Hydromagnetics of rotating fluids. *Reports of Progress in Physics*, 36: 159, 1973.

C. D. Andereck, S. S. Liu, and H. L. Swinney. Flow regimes in a circular Couette system with independently rotating cylinders. *Journal of Fluid Mechanics*, 164:155, 1986.

O. Andreev, Y. Kolesnikov, and A. Thess. Experimental study of liquid metal channel flow under the influence of a nonuniform magnetic field. *Physics of Fluids*, 18:5108, 2006.

S. A. Balbus. Enhanced Angular Momentum Transport in Accretion Disks. *Annual review of astronomy and astrophysics*, 41:555, 2003.

S. A. Balbus and J. F. Hawley. A powerful local shear instability in weakly magnetized disks. I - Linear analysis. II - Nonlinear evolution. *Astrophys. J.*, 376:214, 1991.

S. A. Balbus and J. F. Hawley. Instability, turbulence, and enhanced transport in accretion disks. *Reviews of Modern Physics*, 70:1, 1998.

E. R. Benton and D. E. Loper. On the spin-up of an electrically conducting fluid. Part 1. The unsteady hydromagnetic Ekman-Hartmann boundary-layer problem. *Journal of Fluid Mechanics*, 39:561, 1969.

Edward R. Benton and Julianna H. S. Chow. Steady Nonlinear Ekman-Hartmann Boundary Layers. *Physics of Fluids*, 15:2174, 1972.

A. Brandenburg and K. Subramanian. Astrophysical magnetic fields and nonlinear dynamo theory. *Phys. Rep.*, 417:1, 2005.

A. Brandenburg, A. Nordlund, R. F. Stein, and U. Torkelsson. Dynamo-generated Turbulence and Large-Scale Magnetic Fields in a Keplerian Shear Flow. *Astrophys. J.*, 446:741, 1995.

M. J. Burin, H. Ji, E. Schartman, R. Cutler, P. Heitzenroeder, W. Liu, L. Morris, and S. Raftopolous. Reduction of Ekman circulation within Taylor-Couette flow. *Experiments in Fluids*, 40:962, 2006.

S. Chandrasekhar. The Stability of Non-Dissipative Couette Flow in Hydromagnetics. *Proceedings of the National Academy of Science*, 46:253, 1960.

S. Chandrasekhar. *Hydrodynamic and hydromagnetic stability*. International Series of Monographs on Physics, Oxford: Clarendon, 1961.

F. Chen. Stability of Taylor-Dean flow in an annulus with arbitrary gap spacing. *Phys. Rev. E*, 48:1036, 1993.

M. M. Couette. Sur un nouvel appareil pour l'etude du frottement des fluids. *Compt es Rendus*, 107:388, 1888.

O. Czarny, E. Serre, P. Bontoux, and R. M. Lueptow. Ekman vortices and the centrifugal instability in counter-rotating cylindrical Couette flow. *Theoretical and Computational Fluid Dynamics*, 18:151, 2004.

W. R. Dean. Fluid Motion in a Curved Channel. *Royal Society of London Proceedings Series A*, 121:402, 1928.

R. M. Digilov. Making a fluid rotate: Circular flow of a weakly conducting fluid induced by a Lorentz body force. *American Journal of Physics*, 75:361, 2007.

W. Dobler, A. Shukurov, and A. Brandenburg. Nonlinear states of the screw dynamo. *Phys. Rev. E*, 65(3):036311, 2002.

P. G. Drazin and W. H. Reid. *Hydrodynamic stability*. Cambridge University Press, 1981.

B. Dubrulle and F. Hersant. Momentum transport and torque scaling in Taylor-Couette flow from an analogy with turbulent convection. *European Physical Journal B*, 26:379, 2002.

B. Dubrulle, L. Marié, C. Normand, D. Richard, F. Hersant, and J.-P. Zahn. An hydrodynamic shear instability in stratified disks. *Astron. & Astrophys.*, 429:1, 2005.

V.W. Ekman. *Ark. Mat. Astr. Fys*, 2:1, 1905.

K. Fricke. Stability of Rotating Stars II. The Influence of Toroidal and Poloidal Magnetic Fields. *Astron. & Astrophys.*, 1:388, 1969.

H. Furukawa, T. Watanabe, Y. Toya, and I. Nakamura. Flow pattern exchange in the Taylor-Couette system with a very small aspect ratio. *Phys. Rev. E*, 65(3):036306, 2002.

A. Gailitis, O. Lielausis, S. Dement'ev, E. Platacis, A. Cifersons, G. Gerbeth, T. Gundrum, F. Stefani, M. Christen, H. Hänel, and G. Will. Detection of a Flow Induced Magnetic Field Eigenmode in the Riga Dynamo Facility. *Physical Review Letters*, 84:4365, 2000.

A. Gailitis, O. Lielausis, E. Platacis, S. Dement'ev, A. Cifersons, G. Gerbeth, T. Gundrum, F. Stefani, M. Christen, and G. Will. Magnetic Field Saturation in the Riga Dynamo Experiment. *Physical Review Letters*, 86:3024, 2001.

Peter A. Gilman. Instabilities of the Ekman-Hartmann Boundary Layer. *Physics of Fluids*, 14:7, 1971.

Peter A. Gilman and Edward R. Benton. Influence of an Axial Magnetic Field on the Steady Linear Ekman Boundary Layer. *Physics of Fluids*, 11:2397, 1968.

J. F. Hawley, C. F. Gammie, and S. A. Balbus. Local Three-dimensional Magnetohydrodynamic Simulations of Accretion Disks. *Astrophys. J.*, 440:742, 1995.

R. Hollerbach and A. Fournier. End-effects in rapidly rotating cylindrical Taylor-Couette flow. In *AIP Conf. Proc. 733: MHD Couette Flows: Experiments and Models*, page 114, 2004.

R. Hollerbach and G. Rüdiger. New Type of Magnetorotational Instability in Cylindrical Taylor-Couette Flow. *Physical Review Letters*, 95(12):124501, 2005.

S. H. Hong and H. E. Wilhelm. Magnetohydrodynamic instability of a cylindrical liquid-metal brush. *Journal of Applied Physics*, 47:906, 1976.

H. Ji, J. Goodman, and A. Kageyama. Magnetorotational instability in a rotating liquid metal annulus. *Mont. Not. Astron. Soc.*, 325:L1, 2001.

H. Ji, J. Goodman, A. Kageyama, M. Burin, E. Schartman, and W. Liu. Magnetorotational Instability in a Short Couette Flow of Liquid Gallium. In R. Rosner, G. Rüdiger, and A. Bonanno, editors, *AIP Conf. Proc. 733: MHD Couette Flows: Experiments and Models*, page 21, 2004.

H. Ji, M. Burin, E. Schartman, and J. Goodman. Hydrodynamic turbulence cannot transport angular momentum effectively in astrophysical disks. *Nature*, 444:343, 2006.

A. Kageyama, H. Ji, J. Goodman, F. Chen, and E. Shoshan. Numerical and Experimental Investigation of Circulation in Short Cylinders. *Journal of the Physical Society of Japan*, 73:2424, 2004.

E. Kersalé, D. W. Hughes, G. I. Ogilvie, S. M. Tobias, and N. O. Weiss. Global Magnetorotational Instability with Inflow. I. Linear Theory and the Role of Boundary Conditions. *Astrophys. J.*, 602:892, 2004.

I. V. Khalzov and A. I. Smolyakov. On the calculation of steady-state magnetohydrodynamic flows of liquid metals in circular ducts of a rectangular cross section. *Technical Physics*, 51:26, 2006.

I. V. Khalzov, V. I. Ilgisonis, A. I. Smolyakov, and E. P. Velikhov. Magnetorotational instability in electrically driven flow of liquid metal: Spectral analysis of global modes. *Physics of Fluids*, 18:4107, 2006.

E. Knobloch. Symmetry and instability in rotating hydrodynamic and magnetohydrodynamic flows. *Physics of Fluids*, 8:1446, 1996.

D. Krasnov, E. Zienicke, O. Zikanov, T. Boeck, and A. Thess. Numerical study of instability and transition to turbulence in the Hartmann flow. *APS Meeting Abstracts*, A10+, 2003.

D. S. Krasnov, E. Zienicke, O. Zikanov, T. Boeck, and A. Thess. Numerical study of the instability of the Hartmann layer. *Journal of Fluid Mechanics*, 504:183, 2004.

F. Krause and K.-H. Rädler. *Mean-field magnetohydrodynamics and dynamo theory*. Oxford, Pergamon Press, Ltd., 1980.

U. H. Kurzweg. The stability of Couette flow in the presence of an axial magnetic field. *Journal of Fluid Mechanics*, 17:52, 1963.

U. H. Kurzweg and A. H. Khalfaoui. Current-induced instabilities in rotating hydromagnetic flows between concentric cylinders. *Physics of Fluids*, 25:440, 1981.

W. Liu, J. Goodman, I. Herron, and H. Ji. Helical magnetorotational instability in magnetized Taylor-Couette flow. *Phys. Rev. E*, 74(5):056302, 2006a.

W. Liu, J. Goodman, and H. Ji. Simulations of Magnetorotational Instability in a Magnetized Couette Flow. *Astrophys. J.*, 643:306, 2006b.

W. Liu, J. Goodman, and H. Ji. Traveling waves in a magnetized Taylor-Couette flow. *Phys. Rev. E*, 76(1):016310, 2007.

M. Livio and G. Shaviv. On the Stability of Accretion Disks. *Astron. & Astrophys.*, 55:95, 1977.

D. E. Loper. Steady Hydromagnetic Boundary Layer near a Rotating Electrically Conducting Plate. *Journal of Fluid Mechanics*, 13:2999, 1970.

D. E. Loper and E. R. Benton. On the spin-up of an electrically conducting fluid. Part 2. Hydromagnetic spin-up between infinite flat insulating plates. *Journal of Fluid Mechanics*, 43:785, 1970.

J. M. Lopez and F. Marques. Small aspect ratio Taylor-Couette flow: Onset of a very-low-frequency three-torus state. *Phys. Rev. E*, 68(3):036302, 2003.

A. Mallock. Determination of the viscosity of water. *Royal Society of London Proceedings Series A*, 48:322, 1888.

M. J. Molemaker, J. C. McWilliams, and I. Yavneh. Instability and Equilibration of Centrifugally Stable Stratified Taylor-Couette Flow. *Physical Review Letters*, 86:5270, 2001.

Banibrata Mukhopadhyay. Description of pseudo-newtonian potential for the relativistic accretion disk around kerr black holes. *The Astrophysical Journal*, 581:427, 2002.

T. Mullin, Y. Toya, and S. J. Tavener. Symmetry breaking and multiplicity of states in small aspect ratio Taylor-Couette flow. *Physics of Fluids*, 14:2778, 2002.

K. Noguchi and V. I. Pariev. Magnetorotational Instability in a Couette Flow of Plasma. In M. Schauer, T. Mitchell, and R. Nebel, editors, *AIP Conf. Proc. 692: Non-Neutral Plamsa Physics V*, page 285, 2003.

K. Noguchi, V. I. Pariev, S. A. Colgate, H. F. Beckley, and J. Nordhaus. Magnetorotational Instability in Liquid Metal Couette Flow. *Astrophys. J.*, 575:1151, 2002.

G. Pfister, H. Schmidt, K. A. Cliffe, and T. Mullin. Bifurcation phenomena in Taylor-Couette flow in a very short annulus. *Journal of Fluid Mechanics*, 191:1, 1988.

Y. B. Ponomarenko. *J. Appl. Mech. Techn. Phys.*, 14, 1973.

J. E. Pringle. Accretion discs in astrophysics. *Annual review of astronomy and astrophysics*, 19: 137, 1981.

L. Rayleigh. On the Dynamics of Revolving Fluids. *Royal Society of London Proceedings Series A*, 93:148, 1917.

P. H. Roberts. *An Introduction to Magnetohydrodynamics*. Longmans, Greeen and Co. Ltd., 1967.

R. Rosner, G. Rüdiger, and A. Bonanno, editors. *MHD Couette Flows: Experiments and Models*, 2004.

G. Rüdiger. Linear theory of MHD Taylor-Couette flow. In *AIP Conf. Proc. 733: MHD Couette Flows: Experiments and Models*, page 71, 2004.

G. Rüdiger and R. Hollerbach. Comment on "Helical MRI in magnetized Taylor-Couette flow". *ArXiv e-prints* 0705.0883, 2007.

G. Rüdiger and D. Shalybkov. Linear instability of magnetic Taylor-Couette flow with Hall effect. *Phys. Rev. E*, 69(1):016303, 2004.

G. Rüdiger, M. Schultz, and D. Shalybkov. Linear magnetohydrodynamic Taylor-Couette instability for liquid sodium. *Phys. Rev. E*, 67(4):046312, 2003.

G. Rüdiger, R. Hollerbach, M. Schultz, and D. A. Shalybkov. The stability of MHD Taylor-Couette flow with current-free spiral magnetic fields between conducting cylinders. *Astronomische Nachrichten*, 326:409, 2005.

G. Rüdiger, R. Hollerbach, F. Stefani, T. Gundrum, G. Gerbeth, and R. Rosner. The Traveling-Wave MRI in Cylindrical Taylor-Couette Flow: Comparing Wavelengths and Speeds in Theory and Experiment. *Astrophys. J. Lett.*, 649:L145, 2006.

N. I. Shakura and R. A. Sunyaev. Black holes in binary systems. Observational appearance. *Astron. & Astrophys.*, 24:337, 1973.

F. Stefani and G. Gerbeth. MRI in Taylor-Dean flows. In R. Rosner, G. Rüdiger, and A. Bonanno, editors, *AIP Conf. Proc. 733: MHD Couette Flows: Experiments and Models*, page 100, 2004.

F. Stefani, T. Gundrum, G. Gerbeth, G. Rüdiger, M. Schultz, J. Szklarski, and R. Hollerbach. Experimental Evidence for Magnetorotational Instability in a Taylor-Couette Flow under the Influence of a Helical Magnetic Field. *Physical Review Letters*, 97(18):184502, 2006.

F. Stefani, T. Gundrum, G. Gerbeth, G. Rüdiger, J. Szklarski, and R. Hollerbach. Experiments on the magnetorotational instability in helical magnetic fields. *New Journal of Physics*, 9:295, 2007.

J. Szklarski. Reduction of boundary effects in spiral MRI experiment PROMISE. *Astronomische Nachrichten*, 328:499, 2007.

J. Szklarski and G. Rüdiger. Nonlinear simulations of magnetic Taylor-Couette flow with current-free helical magnetic fields. *Astronomische Nachrichten*, 327:844, 2006.

J. Szklarski and G. Rüdiger. The Ekman-Hartmann layer in MHD Taylor-Couette flow. *Sumbitted to Phys. Rev. E*, 2007.

P. Tabeling and J. P. Chabrerie. Magnetohydrodynamic Taylor vortex flow under a transverse pressure gradient. *Physics of Fluids*, 24:406, 1981.

R. Tagg. The Couette-Taylor problem. *Nonlinear Science Today*, 3:1, 1994.

G. I. Taylor. Stability of a Viscous Liquid Contained between Two Rotating Cylinders. *Royal Society of London Philosophical Transactions Series A*, 223:289, 1923.

E. P. Velikhov. Stability of an Ideally Conducting Liquid Flowing Between Cylinders Rotating in a Magnetic Field. *Sov. Phys. JETP*, 36:1398, 1959.

B. von Rekowski and A. Brandenburg. Outflows and accretion in a star-disc system with stellar magnetosphere and disc dynamo. *Astron. & Astrophys.*, 420:17, 2004.

T. Watanabe and H. Furukawa. Mode formation and bifurcation in decelerating taylor vortex flow. *Proceedings of the 3rd ASME/JSME Joint Fluid Engineering*, 1999.

F. Wendt. Turbulente Strömungen zwischen zwei rotierenden konaxialen Zylindern. *Archive of Applied Mechanics (Ingenieur Archiv)*, 4:577, 1933.

A. P. Willis and C. F. Barenghi. Hydromagnetic Taylor Couette flow: numerical formulation and comparison with experiment. *Journal of Fluid Mechanics*, 463:361, 2002a.

A. P. Willis and C. F. Barenghi. A Taylor-Couette dynamo. *Astron. & Astrophys.*, 393:339, 2002b.

A. J. Youd. *Bifurcations in Forced Taylor-Couette Flow*. PhD thesis, University of Newcastle, 2005.

A. J. Youd and C. F. Barenghi. Hydromagnetic Taylor-Couette flow at very small aspect ratio. *Journal of Fluid Mechanics*, 550:27, 2006.

A. J. Youd and C. F. Barenghi. Reversing and nonreversing modulated Taylor-Couette flow at finite aspect ratio. *Phys. Rev. E*, 72(5):056321, 2005.

O. Zikanov and A. Thess. Direct numerical simulation of forced MHD turbulence at low magnetic Reynolds number. *Journal of Fluid Mechanics*, 358:299, 1998.